Clear Water Temporal Scour around Cylindrical Pier with Circular and Airfoil Collars Fixed on Bed

A thesis submitted towards partial fulfilment of the requirements for the degree of

Master of Engineering

in

Water Resources and Hydraulic Engineering

Submitted by

PURBI ALI

Examination Roll No.: M4WRE24016

Registration No.: 163869 of 2022-23

Under the guidance of

Dr. SUBHASISH DAS

Associate Professor and Joint Director

School of Water Resources Engineering, Jadavpur University

School of Water Resources Engineering

M.E. (Water Resources & Hydraulic Engineering)

*Course affiliated to **Faculty Council of Engineering & Technology***

Jadavpur University

Kolkata-700032, West Bengal, India

2024

Declaration of Originality and Compliance of Academic Ethics

I hereby declare that this thesis contains literature survey and original research work by the undersigned candidate, as part of my **Master of Engineering** in **Water Resources and Hydraulic Engineering** in the Faculty Council of Interdisciplinary Studies, Law & Management, Jadavpur University during academic session 2023-24.

All information in this document has been obtained and presented in accordance with academic rules and ethical conduct.

I also declare that, as required by these rules and conduct, I have fully cited and referenced all material and results that are not original to this work.

Name	:	**PURBI ALI**
Exam Roll Number	:	**M4WRE24016**
Thesis Title	:	**Clear Water Temporal Scour around Cylindrical Pier with Circular and Airfoil Collars Fixed on Bed**
Signature with Date	:	

M.E. (Water Resources & Hydraulic Engineering)
Course affiliated to
Faculty Council of Engineering & Technology
Jadavpur University
Kolkata, India

Certificate of Recommendation

This is to certify that the thesis entitled "**Clear Water Temporal Scour around Cylindrical Pier with Circular and Airfoil Collars Fixed on Bed**" is a bonafide work carried out by **Ms. Purbi Ali** under my supervision and guidance for partial fulfilment of the requirement for the Post Graduate Degree of Master of Engineering in Water Resources and Hydraulic Engineering during the academic session 2023-24.

THESIS ADVISOR
Dr. Subhasish Das
Associate Professor and Joint Director
School of Water Resources Engineering
Jadavpur University

DIRECTOR
Prof. (Dr.) Asis Mazumdar
School of Water Resources Engineering
Jadavpur University

DEAN
Prof. (Dr.) Joydeep Mukherjee
Faculty Council of Interdisciplinary Studies, Law & Management
Jadavpur University

M.E. (Water Resources & Hydraulic Engg.) course affiliated to
Faculty Council of Engineering & Technology
Jadavpur University
Kolkata, India

CERTIFICATE OF APPROVAL **

This foregoing thesis is hereby approved as a credible study of an engineering subject carried out and presented in a manner satisfactory to warrant its acceptance as a prerequisite to the degree for which it has been submitted. It is understood that by this approval the undersigned do not endorse or approve any statement made or opinion expressed or conclusion drawn therein but approve the thesis only for the purpose for which it has been submitted.

Committee of

Final Examination

for the evaluation

of the thesis

_____

_____

_____

_____

** Only in case the thesis is approved.

ACKNOWLEDGEMENT

*I express my sincere gratitude to my supervisor, **Dr. Subhasish Das**, Associate Professor and Joint Director of the School of Water Resources Engineering, Jadavpur University, under whose supervision and guidance this work has been carried out. It would have been impossible to carry out this thesis work with confidence without his wholehearted involvement, advice, support, and endless encouragement throughout. He has not only helped me in carrying out my thesis but also has given valuable advice to proceed further in my life.*

*I would also like to express my sincere gratitude to **Prof. (Dr.) Asis Mazumdar**, Director of the School of Water Resources Engineering, Jadavpur University, **Prof. (Dr.) Arunabha Majumder**, Emeritus Professor; **Prof. (Dr.) Pankaj Kr. Roy**, **Dr. Rajib Das**, and **Dr. Gourab Banerjee**, Faculty members of the School of Water Resources Engineering, Jadavpur University for their valuable suggestions.*

*I would like to express my sincere thanks to **Mr., Buddhadev Nandi**, a Research Scholar of School of Water Resources Engineering, Jadavpur University for his unwavering support and encouragement throughout my work. I would also like to thank **Mr. Saikat Mondal**, **Mr. Plabon Sen**, and **Mr. Tanmoy Das**, Research Scholars, for their support and affection during my work. Also, thanks to my classmates **Ms. Tania Sultana**, **Ms. Shubhashree Laha**, **Ms. Tryasa Roy**, and **Mr. Binoy Banik** for their help.*

Thanks, are also to all staff of the School of Water Resources Engineering and the Regional -cum-Facilitation Centre (RCFC), NMPB, Jadavpur University for their help and support.

*Lastly, I would like to express my heartfelt gratitude to my family (**Amina Ali**, Mother; **Farhad Ali**, Father; **Paraz Ali**, Brother). Their constant support and encouragement have been invaluable throughout this journey.*

Date : 29 August, 2024

Place : Jadavpur University

Ms. Purbi Ali

(Exam Roll No: M4WRE24016)

ABSTRACT

Scouring around the bridge pier is a critical issue in hydraulic engineering as it affects the structural stability and safety of bridges. This natural and complex phenomenon is a leading cause of hydraulic bridge failures, resulting in public safety hazards, and economic losses. Therefore, implementing effective countermeasures to prevent scour around bridge piers is essential. An increase in scour resistance or flow alteration are two major countermeasure techniques. The goal is to counteract the erosive forces of scour-inducing mechanisms using durable engineering materials or, to shift the scour formation away from the immediate vicinity of the pier. The downflow that is responsible for clear water scour can be mitigated by using a collar plate. The present study focuses on the application of the collar as a scour countermeasure technique. This study investigates the temporal development of scour around a circular pier with circular and airfoil collars and also without any such protection. This study also aims to analyze the scour morphology, along with a new predictive model based on the nonlinear regression formula and Classification and Regression Tree (CART), a machine learning model to estimate temporal scour depth in the presence of a collar. The predictive ability has been compared with established empirical equations given in the works of literature. A total of 11 experiments are conducted under clear water scour conditions using cohesionless, uniform sand bed material to investigate the effects of collar shape and size on scour development around a pier. The study uses a fixed pier diameter and examines five different circular collars and five different airfoil collars, varying in diameter and length. The experiments aim to assess the effectiveness of these collars in preventing scour and to understand the time-dependent scour patterns at various points around the pier. All tests are conducted with collars fixed at bed level, with a constant flow depth, discharge, and flow intensity. Simultaneously, from the literatures as many as possible, similar experimental inputs and outputs have been collected or extracted for comparative analysis. The results reveal that the temporal development of the scour hole at the pier depends on whether the pier is protected with a collar or not. In the presence of a collar, the development of the scour hole is significantly delayed. It is observed that the larger sized circular collars ($b_c = 3b$-$3.5b$) are more effective in reducing scour where b_c and b are the collar and pier diameters, respectively. In the case of an unprotected pier and for smaller-sized circular collars ($b_c = 1.5b$-$2b$), the maximum scour depth (D_{scm}) is observed at the upstream face of the pier (0°) but for the larger sized collars ($b_c = 2.5b$-$3.5b$), it is found downstream of the pier (135°). On the other hand, for smaller and larger airfoil collars, D_{scm} is observed at the side (90°) and the downstream (135°) of the pier, respectively. A significant variation in protection efficiencies is observed when comparing circular collars to an unprotected pier, ranging from 26.23% to 84.96% at the upstream face of the pier and from 4.94% to 74.13% (collar diameter = $3.5b$) at the

side of the pier, depending on collar dimensions. On the other hand, airfoil collars demonstrated higher protection efficiencies, ranging from 83.29% to 89.20% at the upstream face of the pier and from 32.67% to 82.80% (collar diameter $= 3.5b$) at the side of the pier. For both the circular and airfoil collars, maximum protection efficiency is observed for the larger collars ($3.5b$). It is also observed that for an unprotected pier, the scour length (l_s) is less than the scour width (w_s), and for a circular collar of $1.5b$ diameter, they are almost the same. However, for the remaining collars $l_s > w_s$. Based on the error analysis and statistical analysis, the CART model and the equation proposed in this study show a better fit with the observed data than the equations derived in previous literatures. This study may aid in protecting bridge pier designs globally under clear water scour conditions, but the predictive efficiency is limited by the use of fixed sediment types, flow conditions, and pier geometry and collar geometry.

CONTENTS

Declaration			iii
Certificate of Recommendation			v
Certificate of Approval			vii
Acknowledgment			ix
Abstract			xi-xii
Chapter 1	Introduction		1-7
	1.1	Background	1
	1.2	Scour	5
	1.3	Types of Scours at Bridges	5
		1.3.1 Clear-water and Live-bed Scour	6
	1.4	Scour Countermeasures	7
Chapter 2	Literature Survey		8-17
	2.1	Literature Review	8
	2.2	Previous Research and Findings on the Use of Collars	8
	2.3	Literature Formulas to Predict Equilibrium and Temporal Scour Depths around Pier with Collar	15
	2.4	Research Gap	17
	2.5	Aim of the Present Study	17
Chapter 3	Scour Mechanism and Scour Countermeasures		18-41
	3.1	Scour Countermeasures	18
	3.2	Types of Scour Countermeasures	18
		3.2.1 Hydraulic Countermeasures	18
		3.2.2 Structural Countermeasures	19
		3.2.3 Monitoring	20
	3.3	Flow-altering Countermeasures	21
	3.4	Collars	22
	3.5	Local Scour Mechanism with and without Collar	23
		3.5.1 Horseshoe Vortex and Downflow	24
		3.5.2 Wake Vortex	25
		3.5.3 Bow Wave	26
		3.5.4 Flow Mechanism in the Presence of a Collar	27
	3.6	Factors Affecting Local Scour at Pier	28
		3.6.1 Pier Diameter	30
		3.6.2 Pier Shape	30
		3.6.3 Collar Diameter	31
		3.6.4 Collar Elevation	31
		3.6.5 Flow Depth	32
		3.6.6 Median Sediment Size	32
		3.6.7 Angle of Repose	33
		3.6.8 Flow Intensity	33
		3.6.9 Flow Shallowness	34
		3.6.10 Sediment Coarseness	35
		3.6.11 Contraction Ratio	36

		3.6.12	Sediment Nonuniformity	36
		3.6.13	Froude Number	36
		3.6.14	Time	37
	3.7		Dimensional Analysis	37
Chapter 4	Objectives and Methodology			42-51
	4.1		Objectives	42
	4.2		Methodology	42
		4.2.1	Methods for Flow Conditions	42
		4.2.2	Methods for selection of pier dimension	44
		4.2.3	Methods for selection of collar dimensions	45
		4.2.4	Instruments Used for Measurements	47
		4.2.5	Method for Predictive Modelling of Scour Depth: CART	48
		4.2.6	Statistical Indices for Model Evaluation	49
Chapter 5	Experimental Procedure			52-60
	5.1		Experimental Setup	52
		5.1.1	Tilting Flume	54
		5.1.2	Pump	55
		5.1.3	Circular pier	55
		5.1.4	Circular and Airfoil Collars	56
		5.1.5	Pier-collar arrangement	57
		5.1.6	Sand Bed	58
	5.2		Experimental Procedure	59
Chapter 6	Results and Discussion			61-94
	6.1		Results	61
	6.2		Experiments Conducted	61
		6.2.1	Experiment Number 1	61
		6.2.2	Experiment Number 2	62
		6.2.3	Experiment Number 3	63
		6.2.4	Experiment Number 4	64
		6.2.5	Experiment Number 5	65
		6.2.6	Experiment Number 6	66
		6.2.7	Experiment Number 7	67
		6.2.8	Experiment Number 8	68
		6.2.9	Experiment Number 9	69
		6.2.10	Experiment Number 10	70
		6.2.11	Experiment Number 11	71
	6.3		Temporal Variation of Scour Depth	72
		6.3.1	Circular Pier without Collar	72
		6.3.2	Circular Pier with Circular Collars	73
		6.3.3	Circular Pier with Airfoil Collar	75
	6.4		Influence of Collar Diameter on Temporal Development of Scour Depth	77
	6.5		Reduction of Temporal Scour Depth with Circular and Airfoil Collars	79

	6.6	Morphological Geometry of Scour for Pier with and without Collar	80
	6.7	Longitudinal Scour Hole Profile	86
	6.8	Scour Dimensions	87
	6.9	Influence of Collar Shape on Scour Protection Efficiency	90
	6.10	Overall Discussion	93
Chapter 7	Predictive Model and New Empirical Equation		95-112
	7.1	Predictive Model of Temporal Scour Depth using CART Regression	95
	7.1.1	Modelling of Scour Depth for Pier with Circular Collars	95
	7.1.2	Modeling of Scour Depth for Pier with Airfoil Collars	102
	7.2	A New Empirical Equation for Temporal Variation of Scour Depth around a Pier with Circular Collar	107
	7.2.1	Error Analysis	110
	7.2.2	Statistical Analysis	111
	7.2.3	Limitations of Proposed Equation	112
Chapter 8	Conclusions and Recommendations		113-116
	8.1	Conclusions	113
	8.2	Limitations of Present Study	114
	8.3	Scopes of Future Study	115
Notations			117-118
References			119-126
Appendices			127-128

CHAPTER – 1

INTRODUCTION

1.1 Background

Bridges are essential to society as they provide quick access across rivers and other water bodies. They facilitate the transport of goods and people, thereby significantly contributing to the development of a region. Overall, bridges play a pivotal role in enhancing connectivity, supporting economic activities, and improving the quality of life for communities. Designing and constructing bridges has always been a complex process, especially when they span over water. A significant majority of bridges in the USA, nearly 83% of the 5,83,000 bridges recorded in the U.S. National Bridge Inventory (NBI) in 2007, were constructed over water (Lagasse et al., 2007). In many cases, it is unavoidable to place piers in the water due to the large distances being spanned, which exposes the bridge to a significant failure mechanism known as scour. The failure of bridges is a serious issue because of the high investment costs, safety risks, and adverse effects on the economy of the affected region.

Scour is one of the leading causes of bridge failure. "Men who overlook water under the bridge will find the bridge underwater" (Neill, 1973). Scour has been responsible for about 60% of bridge failures in the USA (Lagasse et al., 2007). Scour is defined as the erosion of streambed sediment around an obstruction in a flow field (Chang, 1988). It is the erosion of bed material occurring around the base of bridge piers and is driven by the movement of water around these piers (Arneson et al., 2012). This erosion is problematic because it can undermine the foundations, threatening the structural integrity of the bridges and hydraulic structures. This issue not only endangers infrastructure but also poses a significant risk to public safety. Hoffmans and Verheij (1997) noted that local scour around bridge piers and foundations due to flood flows is a major cause of bridge failure.

Scour was identified as the main cause of the 1987 Schoharie Creek Bridge failure in New York (Fig. 1.1a), which resulted in the deaths of 10 people (Ting et al., 2001; Wardhana and Hadipriono, 2003). In 1989, the catastrophic collapse of the U.S. Route 51 bridge over the Hatchie River in Tennessee killed eight people (Lagasse and Richardson, 2001). Another incident described by Lagasse and Richardson (2001) involved the collapse of the twin (southbound and northbound) bridges carrying Interstate 5 over the Arroyo Pasajero (Los Gatos Creek) in California during a major flood, causing four vehicles to plunge into the creek and resulting in seven deaths. Chiew and Lim (2003) and Chiew (2004) reported the failure of the Kaoping Bridge in Southern Taiwan in August 2000. Dey and Barbhuiya (2004) also referenced the collapse of Bulls Bridge over the Rangitikei River in New Zealand. Kumar et al. (2023) reported the bridge collapse due to scouring in Taiwan in 2008 (Fig. 1.1b).



Fig. 1.1 (a) Schoharie Creek Bridge failure in New York, 1987; **(b)** Collapse of Hou-Fong Bridge due to the causes of scouring in Taiwan, 2008

Beyond the human toll, bridge failures due to scour result in substantial financial costs, including direct expenditures for replacement and restoration and indirect costs related to transportation disruptions (Lagasse and Richardson, 2001). A study by Cheremisinoff et al. (1988) reported that the Federal Highways Administration claimed damages to bridges and highways from major floods in 1964 and 1972 amounted to about $100 million (₹838.85 crores) per event. According to a survey by Macky (1990) cited by Melville and Coleman (2000), scour in New Zealand rivers results in annual expenditures of NZ$36 million (₹188.10 crores). Thus, significant amounts are spent annually on repairing or reconstructing bridges whose piers have been destroyed by scour (Dey, 1997).

The potential losses from bridge failures and the necessity of preventing them have spurred efforts to better understand the scour process and improve scour prediction methods and equations. Underestimating pier scour depth can lead to bridge failure, while overestimating it can result in excessive construction costs (Ting et al., 2001). Numerous experimental and numerical studies have aimed to quantify the equilibrium depth of scour in

various soil materials. Researchers such as Raudkivi and Ettema (1983), Ahmed and Rajaratnam (1998), Chiew and Melville (1987), Breusers et al. (1977), Lança et al. (2013), Franzetti et al. (2022), Nandi and Das (2023), Nandi et al. (2024*a*) and Nandi et al. (2024*b*) have contributed to the understanding of pier scour considering equilibrium as well as the temporal evolution of scour. Breusers et al. (1977) provided a comprehensive review of local scour around circular piers.

Despite the extensive research on scour processes, some aspects remain unresolved, as reported by various contradictions in the literature. Raudkivi and Ettema (1983) pointed out that while the scientific foundation for bridge structural design is well established, there is currently no unifying theory that allows designers to confidently estimate scour depth at bridge piers. Cheremisinoff et al. (1988) and Hoffmans and Verheij (1997) supported Raudkivi and Ettema's claims. According to several authors, this issue arises not only from the extreme complexity of the problem but also because stream characteristics, bridge constriction geometry, and soil water interactions vary for each bridge and each flood. Federico et al. (2003) also indicated that a reliable assessment of general and local erosion of pier foundation soil cannot be safely calculated using the empirical correlations available in the technical literature. Hoffmans and Verheij (1997) emphasized that scour analysis should be integral to the design of new bridge substructures to ensure they can withstand high flows during floods.

Many existing bridges were not designed to handle the scour they are now facing, as the full potential for scour may not have been evident at the time of their construction. Discrepancies between predicted and actual scour depths can be attributed to factors such as changes in flood magnitudes and frequencies, evolving channel geometries, or additional influences like the presence of ice cover (Arneson et al., 2012; Lagasse et al., 2007). The U.S. Federal Highway Administration (FHWA) mandates that both new and existing bridges adhere to a bridge inspection program specified in the National Bridge Inspection Standards (NBIS). This program includes evaluations for pier scour and underwater inspections. A key component of the program is identifying bridges that are at risk of failure due to scour in the event of a significant flood. Such bridges are categorized as scour-critical. In 2011, the FHWA reported that more than 23,000 bridges in the USA were classified as scour-critical (Arneson et al., 2012). A specific example occurred in 1994 in Georgia, USA, when tropical storm Alberto produced extensive and destructive flooding, causing damage to over 500 bridges due to scour. Of these bridges, 31 were deemed unsafe and required rebuilding because the scour reached depths of 4 to 6 meters (Arneson et al., 2012). This incident clearly demonstrates that scour is a widespread issue and has consistently resulted in significant damage.

Once a bridge is identified as scour-critical, a Plan of Action (POA) must be developed as specified by the National Bridge Inspection Standards (NBIS). A POA includes site-specific actions aimed at enhancing public safety and reducing the risk of bridge failure. At a minimum, a POA typically involves monitoring programs to track scour progression and alert bridge owners. In many cases, additional actions are necessary to ensure the bridge is no longer scour critical. These actions often include the installation of accepted scour countermeasures. However, in extreme cases where scour has progressed beyond the effectiveness of countermeasures, the bridge may require replacement or significant rehabilitation (Lagasse et al., 2009; Arneson et al., 2012) (from Valela, 2021).

Local scour at a bridge pier primarily occurs due to the downflow along the upstream face of the pier, which generates a horseshoe vortex at the pier's base that contributes to the phenomenon (Kumar et al., 1999). One method to reduce pier scour is to armor the riverbed with hard engineering materials like stone riprap. Another approach is to weaken or inhibit the formation of downflow and the horseshoe vortex using flow-altering devices (Chiew and Lim, 2003; Melville and Coleman, 2000). Devices used to protect piers against local scour include sacrificial piles, Iowa vanes, slots through the pier, and flow deflectors such as collars. The use of collars has been studied by several researchers, including Chabert and Engeldinger (1956), Laursen and Toch (1956), Thomas (1967), Tanaka and Yano (1967), Chiew (1992), Kumar et al. (1999), Zarrati et al. (2006), Alabi (2006), Moncada-M et al. (2009), Garg et al. (2005), Izadinia et al. (2012), Tafarojnoruz et al. (2012), Jahangirzadeh et al. (2014), Pandey et al. (2020), Pandey et al. (2022), Kassem et al. (2023) and others. Results generally show collars are effective in reducing scour depth at bridge piers.

While the primary interest in scour studies is the scour depth, the time required to reach a particular scour depth is also crucial, as scour holes take time to develop. Under clear water scour conditions, the depth of a scour hole approaches an equilibrium condition asymptotically with time (Breusers, 1977). Thus, time is an important factor in scour studies. Researchers like Melville and Chiew (1999), Moncada-M et al. (2009), Mashahir et al. (2009), and Pandey et al. (2020) have studied the temporal development of scour in the presence of collar and without a collar. The rate of local scour around a bridge pier is significant for scheduling mitigation measures and understanding scour under time-varying flows (Gosselin and Sheppard, 1995). Adequate representation of temporal scour development and the effectiveness of a collar in model studies depend on the definition of time to equilibrium, which determines test duration.

Many definitions of equilibrium scour depth exist, but most equations for local scour provide equilibrium depth and are conservative regarding temporal effects (Melville and Coleman, 2000). Peak flood flows may last only a few hours or days, insufficient for achieving equilibrium scour depth. Consequently, the actual scour depth may be a small percentage of the equilibrium depth, which could take weeks to develop fully.

Using a collar can mitigate pier scour by preventing direct downflow impact on the riverbed, reducing both the depth and rate of scour (Mashahir et al., 2004; Pandey et al., 2020; Gupta et al., 2024). This reduction in scour rate limits the risk of pier failure during short-duration floods. Zarrati et al. (2004) observed that the time to reach equilibrium scour depth depends on whether a pier is protected with a collar, impacting the validity of results from tests with fixed durations. Therefore, it is crucial to critically review the results of the literature based on short testing times. Different shapes of collars can be used to prevent the scour at the upstream face of the pier (Khodashenas et al., 2018; Gupta et al., 2023; Kassem et al., 2023; Gupta et al., 2024).

In the present study, two different collar shapes have been considered for the temporal evaluation of the scour at the upstream face of the pier. The constant flow discharge of 25.5 l/s was considered for all the experiments. The effect of the width of the collar (circular) as well as the effect of width and length (airfoil collar) has been analyzed in the present study.

1.2 Scour

Scour is a natural phenomenon caused by the flow of water in rivers and streams (Breusers et al., 1977). It is most pronounced in alluvial materials, but deeply weathered rock can also be vulnerable in certain circumstances. It is the consequence of the erosive action of flowing water, which removes and erodes material from the bed and banks of streams and also from the vicinity of bridge piers and abutments. Cheremisinoff et al. (1988) defined scour as the lowering of the river bed level by water erosion, which can potentially expose the foundations of riverine structures such as bridges.

Scouring occurs naturally as part of the morphological changes of rivers and as the result of man-made structures. Scour can either be caused by normal flow or flood events. Normal flow can lower the channel bed but the rate of scouring is much higher during peak flow conditions when the flow velocity is higher.

Scour Depth is the vertical distance by which the riverbed is lowered due to erosion, measured from the original bed level before the scour occurred. A scour hole is defined as the depression or void in the riverbed formed as sediment is eroded and washed away by the flowing water.

1.3 Types of Scours at Bridges

Scour can be broadly classified into two major types - general scour and localized scour. Some other sub-divisions of scour are shown in Fig. 1.2. The types of scours that may occur at bridge sites can be categorized as follows:

- **General scour** occurs in a river or stream as the result of natural processes irrespective of whether a bridge is there or not.
- **Constriction scour** occurs due to the narrowing of the waterway and the alteration of flow patterns caused by the bridge.
- **Local scour** occurs around bridge piers, abutments, or other structures that obstruct the flow. These obstructions result in an acceleration of the flow and create vortices that erode sediments from the immediate vicinity of the obstruction. Local scour, which varies with the type of structure, is generally more severe than general or constriction scour and adds to their effects. As local scour is a key focus of this study, it is explored in greater detail in the upcoming chapters (Chapter 3).

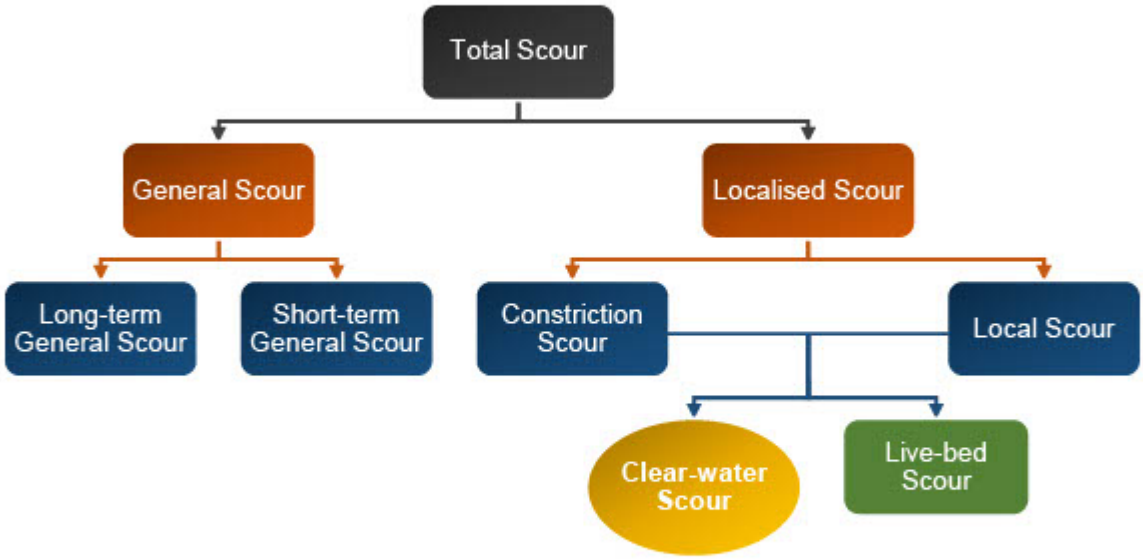


Fig. 1.2 Classification of Scour

1.3.1 Clear-water and Live-bed Scour

Local and constriction scour can occur in two ways: clear-water scour and live-bed scour. Local scour can occur in addition to both general and localized scour. Clear-water scour happens when the bed material upstream of the scour area remains stationary. In this situation, the shear stresses away from the scour area are either equal to or less than the critical shear stress needed to initiate particle movement. Maximum scour depth in clear-water scour is reached when the flow is no longer able to move particles from the scour hole.

Live-bed scour, also known as scour with sediment transport, occurs when the stream is transporting a bed load. Equilibrium scour depths are achieved when, over time, the amount of sediment removed from the scour hole by the flow equals the amount of sediment entering the hole from upstream. Distinguishing between clear-water and live-bed scour is crucial because they influence both the development of the scour hole over time and the relationship between scour depth and approach flow velocity differently. These relationships are shown in the schematic diagram below (Fig. 1.3). In live-bed conditions, scour depth initially increases rapidly with time and then fluctuates around a mean value, known as the equilibrium scour depth. This equilibrium scour depth is generally less than the maximum scour depth observed under clear-water conditions. The present study focuses on experimental results for clear-water scour at cylindrical piers with collars attached in a steady flow condition.

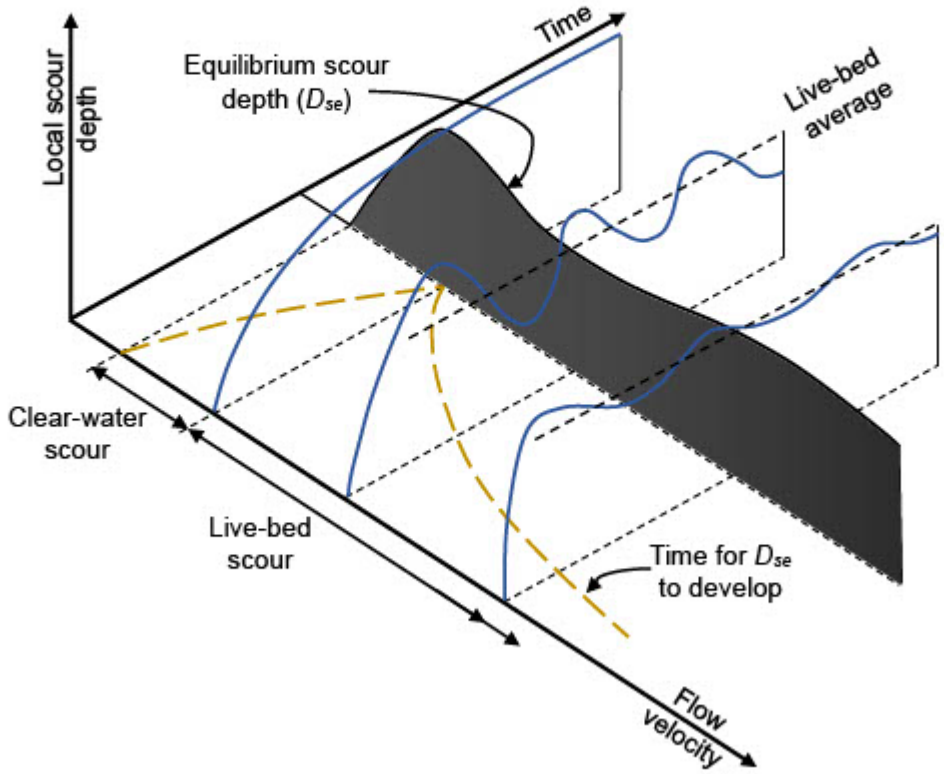


Fig. 1.3 Variation of local scour depth with flow velocity and time

1.4 Scour Countermeasures

Scour countermeasures, as defined by the Hydraulic Engineering Circular No. 23 (HEC-23), are techniques designed to prevent, delay, or mitigate the severity of scour (Lagasse et al., 2009). While numerous countermeasures are available today, each comes with its own advantages and disadvantages. Currently, no single countermeasure is ideal for eliminating scour under all conditions while also being cost-effective, easy to maintain, and simple to install. This complexity makes selecting an appropriate countermeasure challenging and often requires the expertise of a specialist in the field. Therefore, further research into scour countermeasures is essential, as they are a primary solution to the widespread scour issue that ultimately endangers public safety.

In the present analysis, we tried to evaluate the effectiveness of two different collar shapes (circular and airfoil). As it is the main focus of the study, scour countermeasures are discussed in much more detail in Chapter 3.

CHAPTER – 2

LITERATURE SURVEY

2.1 Literature Review

Numerous studies have been conducted and published on the development of local scour around bridge piers. It is crucial to accurately predict the scour depth around the bridge pier experimentally, and numerically as well as using machine learning techniques. There are a significant number of studies available for isolated bridge piers and a combination of bridge piers. The study on isolated pier scour depth computation formula was conducted by Melville and Chiew (1999), Oliveto and Hager (2002), Aksoy et al. (2017), Franzetti et al. (2022), etc. The study of eccentric multiple piers was conducted by several researchers (Das et al., 2014*a*; Das et al., 2014*b*; Das et al., 2016; Das and Mazumdar, 2018; Das et al., 2019; Nandi and Das, 2023*b*). The flow characteristics near a pier have been studied by Das et al. (2013), Das et al. (2014*c*), Das et al. (2017), Jaman et al. (2017), Das et al. (2019), and others. Scouring around the bridge pier is a crucial issue. Hence, many researchers aimed to study different scour countermeasures (e.g., riprap, slot, sacrificial piles, vanes, etc.) to protect the bridge pier. Quite a few researches have been published to understand the effectiveness of a collar as a scour countermeasure (Kumar et al., 1999; Moncada-M et al., 2009; Jahangirzadeh et al., 2014; Pandey et al., 2020; Pandey et al., 2022; Gupta et al., 2023; Gupta et al., 2024; Kassem et al., 2023; etc.).

This chapter aims to summarize the current understanding of local scour, the temporal development of scour, and the effectiveness of different shapes of collars in mitigating scour around a bridge pier. It is intended to familiarize readers with relevant terminologies and enhance their understanding of scour and scour countermeasures.

2.2 Previous Research and Findings on the Use of Collars

In this section previous research done in the field of collar as a scour countermeasure is presented in detail. Different studies done investigating circular and airfoil collars are discussed below.

Laursen and Toch (1956) were among the first to study the use of a collar-like device to avoid scouring at piers. This study suggested that these devices could be effective for scour mitigation. However, they did not provide information on the feasibility of using collars in the field (Alabi, 2006).

Chabert and Engeldinger (1956) found that placing a circular plate $0.4b$ (where b = pier diameter) below the original bed elevation and with a diameter of $3b$ could significantly reduce scour depth by 60% (Alabi, 2006).

Tanaka and Yano (1967) also investigated the use of a collar to reduce scouring. It was found that reducing the size of the plate decreased its effectiveness in reducing scour

depth and vice versa. Increasing the plate elevation relative to the bed surface also led to an increased scour depth (Alabi, 2006).

The schematic of the pier-collar arrangement adopted for the different literature studies is illustrated in Fig. 2.1.

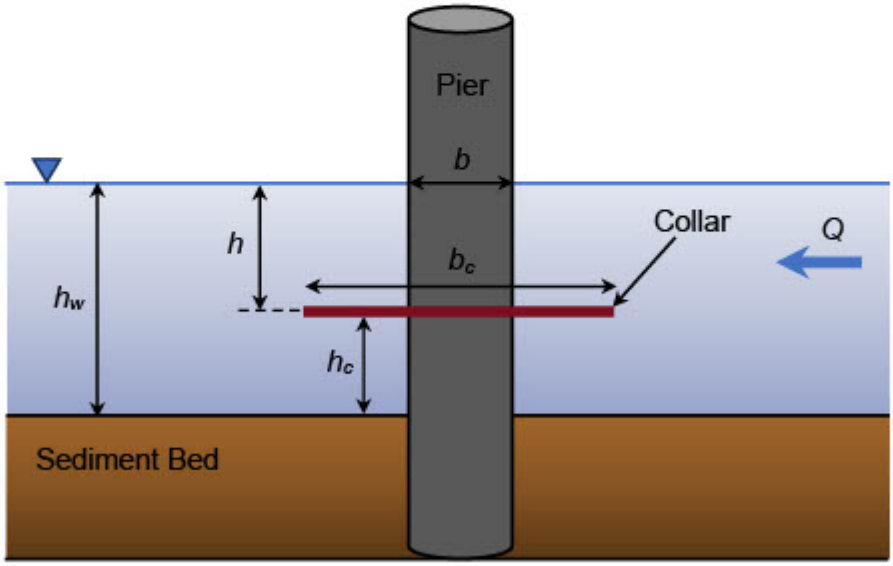


Fig. 2.1 Schematic diagram of Pier-Collar arrangement

Ettema (1980) conducted a series of experiments to determine the feasibility of using a collar to reduce local scour around a circular bridge pier. It was found that, when a collar of diameter of b_c equaling $2b$ is installed at an elevation of $h_c = b/2$ above the channel bed, the collar is not effective in reducing the scour depth. However, installing a collar at the channel bed significantly reduces scour. The general conclusion was that the width of the collar has a greater impact on scour as the collar elevation decreases (Alabi, 2006).

Dargahi (1990) investigated how a collar can reduce local scour by influencing the horseshoe vortex system. To study the impact of collar shape on performance, a circular collar and a collar with a Joukowski profile were tested. It was observed that the collar did not effectively prevent the formation of the horseshoe vortex. It was reported that regardless of collar position or shape, the scour mechanism was similar to that of a circular pier without a collar. For a circular collar, at an elevation of $h_c/h_w = -0.015$ (h_w = flow depth), the maximum reduction of scour depth occurred and, in this case, the upstream and downstream scour depths were reduced by 50% and 75% compared to the maximum scour depth for the cylinder without a collar. The collar position, $h_c/h_w = 0.25$, had no significant effect on scouring. The comparison of the scour profile with profiles measured for the Joukowski case showed that changing the collar design had no meaningful impact on local scouring around the cylinder. It was found that the collars can efficiently reduce the strength of the horseshoe vortices when placed within the separated boundary layer. It was also reported that if t_c/b (t_c = collar thickness) increases, the effective pier diameter will increase, causing an increase in the scour depth. However, Dargahi (1990) pointed out that further research is required before practical implementations.

Chiew (1992) also examined the effect of a collar in minimizing the local scour around a pier. He observed that a collar can reduce the scour depth by 20%.

Fotherby and Jones (1993) studied how effective are the collars in reducing scour. They found that the width and thickness of collars and the elevation of the collar above the bed level affect their scour mechanism. It was concluded that larger collars are more effective at reducing scour, but their efficiency decreases when positioned at higher elevations above the channel bed. Fotherby and Jones also pointed out that a collar is a hypothetical scour countermeasure technique that has not been employed in practice. Later it was supported by Alabi (2006).

Kumar et al. (1999) investigated the use of pier slots and collars to reduce local scour at bridge piers. They examined how placing circular collars of various sizes at various elevations affects scour reduction. Generally, it is observed that the deepest scour occurs at the upstream face of the pier when smaller collars are placed at higher elevations. In contrast, larger collars positioned at lower elevations lead to deeper scour in the wake of the pier. They also found that with a collar of $2.5b$ diameter at bed level, there is significantly less scour in front of the pier compared to the sides and rear of the collar. Conversely, another collar $4b$ diameter resulted in no scour at the front or sides but caused considerable scour at the rear of the pier. By analyzing the experimental data alongside information from previous research, a formula was developed to predict the maximum scour depth around circular bridge piers equipped with collars. This formula is applicable to local scour in uniform sediment and clear-water flow.

Singh et al. (2001) also worked on a collar as a scour protection device around a circular pier. They believed that the growth of a vortex can be arrested by keeping it on a rigid surface, such as a collar plate. It was observed that the width and vertical placement of a collar affect its effectiveness in preventing scour and a larger collar plate size reduces scouring. Using collar plates with sizes $b_c = 1.5b$, $2b$, and $2.5b$ on the channel bed reduced scour by 50%, 68%, and 100% respectively, compared to an unprotected pier. It was also found that placing collar plates of $b_c = 2b$ at $0.1b$ depth below the bed resulted in a 91% reduction in scour depth. However, placing the same collar plate $0.5b$ height above the bed resulted in a 25% reduction in scour depth (Alabi, 2006).

Mashahir et al. (2004) aimed to analyze the effect of a collar on the scouring rate and the time of equilibrium. In this study temporal development of scouring around a circular pier with and without collar was measured and compared. A point gauge was used to measure the scour depth in the flume, while a periscope inside the pier monitored the growth of the scour hole along the perimeter of the pier. They found that using a collar significantly affects the time development of scouring. It was observed that the scouring of an unprotected circular pier starts simultaneously at the downstream due to wake vortices and upstream face due to downflow. Then horseshoe vortex influences the development of the scour hole upstream of the pier. The experiment lasted 44 hours, with the final 8 hours showing a fluctuation in scour depth of less than 2% of the pier diameter. The maximum depth of the scour hole was gauged 92 mm for the unprotected pier. On the other hand, when the collar was attached, they observed that initial scouring occurred downstream due to powerful wake vortices, resulting in a 2 cm deep scour hole within 30 minutes. Meanwhile, no scouring was seen at the upstream face due to the downflow and horseshoe vortex. The scouring rate at the upstream face of the

circular pier was significantly slower during the first 30 hours, with just 30% of maximum scouring occurring, as opposed to 98% at the unprotected pier over the same period. The maximum scour depth was 67.5 mm after 90 hours, with a fluctuation of less than 5% of the pier diameter in the last 24 hours. It was also seen that scouring at the upstream face of the pier was zero after about 4 hours from the start of the experimentation. However, scouring accelerated after 30 hours. During that period, the flow penetrated below the collar. After this time, scouring developed similarly to an unprotected pier but with a milder slope. They concluded that not only scour depth, but collars considerably reduce the scouring rate as well. It was reported that the circular pier has a much lower rate of scouring at the upstream face of the pier compared to unprotected piers during the first 30 hours. It was also reported that collars are more effective in reducing the scour rate than wider foundations of similar width and elevation.

Garg et al. (2005) focused on mitigating the scour by employing collar plates to restrict the growth of the primary vortex, emphasizing the role of a rigid surface in this preventative measure. The objective of the study was to minimize scour around a bridge pier through experiments with various sizes and configurations of collar plates. The study aimed to find the most effective collar size and elevation for significant scour reduction. Experiments were conducted under clear water scour conditions for uniform flow velocity corresponding to the incipient motion of sediment. To reduce flow depth-related effects on scouring, the ratio, h_w/b was kept above 2.5, as recommended by Ettema (1980) and Chiew (1984). They observed that b_c and h_c have the greatest impact on scour depth at a pier protected with a collar. It was found that at a specific location, larger collars were more effective than smaller collars. Increasing the size of the collar plate from 1.5b to 3b reduced the maximum scour depth from 37% to nearly 100%. They also found that shifting the elevation of a collar from 0 (average bed level) to 0.5b results in an increase in maximum scour depth from 0.36b to 0.9b. This indicated a performance potential of 66% and 16%, respectively. They concluded that a collar with a size of 3b or above, placed at bed level, offers total protection against scour.

Zarrati et al. (2006) conducted an experimental study to investigate the efficiency of collars in controlling local scour around the bridge pier. The experimental findings were compared to previous investigations on single piers with collars. Comparing the maximum scouring depth with calculations from Melville and Sutherland (1988) for a single unprotected pier, a 27% reduction in scouring with a collar was observed. Importantly, in addition to reducing scour depth, the application of a collar significantly decreases the rate of scouring. Also, there was a delay in scouring around the pier when collars were used.

Mashahir et al. (2009) examined the effectiveness of single collars in lowering scour rate and depth around cylindrical bridge piers through experimental methods. The scour hole was monitored on the upstream face of the pier, where it was predicted to reach its maximum depth. The depth of the scour holes at both sides and rear side of the pier was measured. Tests were conducted at the threshold of sediment motion where maximum scouring was expected. They found that after 2 hours from the start of the experiment, scouring began at the upstream face of the pier, and by 8 hours, the collar was entirely undermined. The rate of scouring increased when flow penetrated beneath the collar's upstream edge. After 90 hours, at the upstream face of the pier, the maximum scour depth was 71 mm. At this time, the scour hole downstream of the pier was 55 mm deep. This test resulted in a 23% reduction in maximum

scour depth compared to the unprotected pier. Tanaka et al. (1967) observed a maximum reduction of 25%, which was consistent with this study's finding. They observed that the temporal variation of scouring in the case of a pier with a collar was due to the extension of scouring below the collar. They concluded that the use of a collar significantly reduced both the scour depth and the rate of scouring.

Moncada-M et al. (2009) also conducted an experimental investigation to study the effect of a collar on scour depth by varying collar size, collar elevation, and flow depth. A total of 8 experiments for an unprotected pier, 29 experiments for a collar of diameter $2b$, and 21 experiments for a collar of diameter $3b$ were carried out. The relationship between the collar efficiency and the collar location for different flow depths was addressed. They found that the collar is the most effective when it is placed at the bed level and efficiency becomes lower when it is placed above the bed level. However, in some cases, efficiency is also found to be significant when the collar is positioned below the bed level. It was also observed that the efficiency (E%) of the collar is inversely related to the flow depth.

Zarrati et al. (2010), in their experimental study, conducted two experiments in the presence of collars to examine their efficiency for scour reduction. They observed that the scour depth was approximately 20% and 26% less than that of the unprotected pier for collar widths of $2b$ and $3b$, respectively. These results agreed with results reported by Tanaka and Yano (1967) and Ettema (1980).

Izadinia et al. (2012) studied the effectiveness of using collars experimentally to prevent local scouring at a circular bridge pier close to the threshold flow conditions of initiation of uniform sediment motion. For all the experiments conducted by them, the temporal scour depths were measured at the upstream of the pier. It was observed that during the experiment, the scour depth of a single pier was higher than that of a pier with a collar. This was because the collar reduced the strength of the downflow to excavate the bed. On the other hand, the scouring began quickly at the upstream of single piers due to the downflow impinging on the bed. They also observed that as the scour around the pier with a collar started with a delay, the equilibrium time was longer than those without a collar. The scour depth upstream of the single pier was 7 cm. The scour depth upstream of the collar protected pier was 5.6 cm and the collar resulted in a 20% reduction in scour depth.

Tafarojnoruz et al. (2012), in their study, experimentally evaluated six different types of flow-altering countermeasures (submerged vanes, bed sill, transverse sacrificial piles, collar, threading, and pier slot) against local scour at bridge piers. They conducted experiments in clear water scour conditions and found that the efficiency of a $3b$-wide collar was equal to 28.7%.

Jahangirzadeh et al. (2014) used experimental and numerical approaches to study the effectiveness of circular collars and rectangular collars with various dimensions and levels of installation relative to the streambed in mitigating scour around a bridge pier in clear water scour conditions. Approximately 80% of the scouring occurred within the first 20% of the equilibrium time. The highest rate of scouring was observed during the initial hours of the experiments, with the rate gradually decreasing over time. They found that the percentage reduction of scour only changed by 1.7% as the width of the circular collar exceeded $3.5b$. They suggested that the optimal and most cost-effective collar dimensions for maximizing scour reduction were within the range of $b_c = 3b$ to $3.5b$. They also developed two new

equations using both experimental and numerical data, to predict the effect of a collar on the percentage reduction of scour.

Khodashenas et al. (2018) also aimed to investigate the application of circular collars around a cylindrical pier at various elevations from the bed. They found that installing a collar of diameter 2.5b at the bed level could reduce scour depth by up to 24% and the reductions were 5% and 18% for the collars of diameter 1.5b and 2b, respectively. The rate of scour depth was found to be significantly decreasing, with circular collars showing 50% reductions, when compared to a single pier without a collar.

Tabarestani and Zarrati (2019) also examined the development of scour holes around a circular bridge pier with a collar under both steady and unsteady flow conditions. In this study, the flow intensity parameter i.e., the ratio of shear velocity to critical shear velocity (U_*/U_{*c}) was shown to be the most important factor for collar efficiency in delaying scour development. Reducing U_*/U_{*c} from 0·99 to 0·8 in a steady flow state reduced the time it takes to undermine the collar by approximately 26 times. Therefore, they concluded that the collar would protect the pier properly at lower flow intensities.

Wang et al. (2019), in their experimental study, addressed the crucial issue of local scour around bridge piers, which is a danger to bridge damage. Their goal was to assess the preventive efficacy of an "anti-scour collar" for cylindrical bridge piers in erodible sediment beds. All the experiments were carried out under live-bed conditions. This study found that when the collar is placed above the riverbed, closer proximity results in better protection, with increased effectiveness observed as the installation height decreased and the maximum scour depth occurred at the front of the pier, which was consistent with the model without a collar. During the first 120 minutes of testing, there was no scour while the collar was on the bed surface. They concluded that a collar of diameter of 3b can minimize scour depth by more than 50% compared to piers without protection.

Pandey et al. (2020), in their experimental study, investigated the influence of a collar on the temporal development of scour depth at the collar-protected circular pier. The effectiveness of collars of various diameters and at different elevations was explored through flume experiments under clear-water scour conditions. In addition to temporal scour depth profiles analyzed over various time intervals up to equilibrium scour conditions, variations in scour depth along flume length and flume width were also investigated around non-protected and collar-protected piers. Results of this study showed that a collar worked efficiently when it was provided at bed level and the rate of scour depth reduction decreased with an increase in collar elevation. Also, it was found that in the presence of a collar, the maximum reduction in time-dependent scour depth around a circular pier was observed when the collar diameter was 2.3b. In this work, a new relationship for the temporal variation of the scour depth around the pier with a collar was proposed. This study concluded that collars could effectively reduce scour around circular piers, but collar diameter and collar elevation were the two most important factors in deciding the protective efficiency of collars.

Pandey et al. (2022) assessed the effectiveness of collars with different diameters and depth positions in reducing scour around circular piers. Utilizing both previous and newly collected data, the study aimed to propose and validate an empirical equation for computing maximum scour depth. The maximum equilibrium scour depths were measured in the absence of any appurtenances around the pier and in the presence of a circular collar under clear-water

scour conditions. The study revealed that a larger-diameter collar ($b_c \geq 2.5$) effectively reduced scour depth when positioned at bed level. The results also indicated that the best position for collar deployment was at bed level with a collar diameter range of 1.5b–2.5b. In this work, a new equation to compute the maximum scour depth around the pier in the presence of a collar has been derived by non-linear regression using an extensive range of datasets. They validated their experimental study waith a fair accuracy of the equation of Kumar et al. (1999) for estimating maximum scour depth when $1.5b \leq b_c \leq 2.5b$, and the collar was positioned near the bed. Furthermore, it was reported that the newly proposed equation of this paper gave a better and more widely applicable estimation of maximum scour depth around the pier with collar compared to the equation of Kumar et al. (1999).

Gupta et al. (2023*a*) aimed to assess the efficiency of airfoil-shaped collars in reducing scour around circular bridge piers. Along with experimental investigations on scour reduction, morphological changes in the sediment bed were also studied through experimental and numerical analyses. Experiments were conducted with and without airfoil-shaped collars under clear water conditions. If the change in scour depth was less than 0.05b in 24 h, then it was defined as an equilibrium scour depth. Results of the present study showed that the four collars (2b, 2.5b, 3b, 3.5b) had scour reduction percentages of 46%, 86%, 100%, and 100% at bed level, respectively. Notably, no scour was observed around the pier with collars of sizes 3b and 3.5b. When collars were kept at a height of h_w/4, percentages of scour reduction were 53%, 59%, 61%, and 56% respectively. The percentages of scour reduction were 37%, 48.14%, 45.67%, and 16% when the collars were kept at a height of h_w/2, and 22%, 19.75%, 32.01%, and 16% when kept at a height of 3h_w/4. It was also seen from the profiles of the scour hole that the length of the transverse scour hole was greater than that of the longitudinal one. It was concluded that airfoil-shaped collars placed at the bed level were the most efficient in reducing scour. Specifically, collars with diameters of 2b, 2.5b, and 3b demonstrated the highest effectiveness, resulting in scour reduction ranging from 86% to 100%. Initially, the efficiency of the collar was found to be rapidly reduced because of the fast rate of scouring around the pier. However, that efficiency was increased later due to the weakening of the horseshoe vortex and the protection provided by the airfoil-shaped collar. It was observed that scour reduction percentages decreased as the collars were elevated, with the highest reductions occurring at bed level. In both the experiment and the simulation, it was confirmed that there was no scour around the pier when a collar of diameter 3b was placed on the bed.

Gupta et al. (2023*b*) experimentally investigated the effectiveness of four different airfoil collars in reducing scour around the circular bridge pier. Airfoil collars, varying in diameter and placed at four different locations from the uniform sediment bed, were introduced to understand their influence on scouring. Experiments were conducted under clear water scour conditions. They compared scenarios with and without the airfoil collar. A total of 69 experiments were conducted. From the experimental results, it was seen that the scour depths at the pier with airfoil collars of diameters 2.5b and 3b when placed on the bed level were found almost zero. When the collar was placed at bed level, h_w/4, h_w/2, and 3h_w/4 above the bed level, the protection efficiencies were found to range between 65–100%, 40–53%, 23–38%, and 8–29% for the collars of diameter of 1.5b, 2b, 2.5b, and 3b, respectively. They concluded that increasing the pier diameter and flow intensity led to greater scour depth while increasing the collar diameter minimized scour at the pier. It was seen that larger collar

and pier diameters resulted in increased scour around the pier at threshold velocity. It was also reported that the collar placed on the bed reduced the volume of the scour hole by reducing the scour hole's length, width, and depth. An empirical relationship was proposed for the temporal variation of scour depth. Statistical sensitivity analyses were performed and it was found that the most and least sensitive parameters were h/h_w and T_c, where h and T_c were the collar's location from the water surface and dimensionless time, respectively.

Kassem et al. (2023) conducted a clear water scour experimental investigation that examined the impacts of circular and novel hexagonal collar shapes on scouring around circular piers embedded in a uniform sand bed. They analysed the scour geometry for both protected and unprotected piers, with an evaluation of the percentage reductions in the scour hole dimensions and volume. They found that using collars notably altered the scour mechanism around the pier, changing the topography, shifting the maximum depth, and decreasing both the volume and dimension of the scour. While the unprotected pier exhibited its greatest scour depth directly in front of it, the collared pier experienced three deep scour holes, one in front and two behind. They also found that nondimensional scour depth increased as Fr and U/U_c increased for all tested groups. In the presence of a circular collar, within the range of Froude number (0.10-0.33), the maximum scour depth was reduced by approximately 42-37% compared to an unprotected pier. They proposed empirical prediction formulas for scour dimensions. To incorporate a novel consideration for estimating scour depth at collared piers, common prediction equations were updated by adding the newly developed collar shape coefficient. The proposed and upgraded formulas were compared and validated, showing robust consistency in the findings.

Gupta et al. (2024) experimentally evaluated the performance of circular and octagonal collars in reducing scour around the pier. A total of 33 experiments with and without collars were carried out under steady uniform flow and clear water conditions. The efficiency of four different-sized circular collars at four different elevations was studied. They found that the maximum scour depth for an unprotected pier was $1.58b$ and with circular collars ($b_c = 2.5b$) it was $0.37b$, $1.28b$, $1.39b$, and $1.47b$ when placed at a height (h_c) of 0, $0.25h_w$, $0.5h_w$, and $0.75h_w$ respectively. The scour reduction percentages were 76.8, 18.9, 12.6, and 7.3% at those four heights. When placed at bed level, the percentage reductions in scour were 16.84, 36.84, 76.9, and almost 100% for collars of diameter $1.5b$, $2b$, $2.5b$, and $3b$ respectively. They found the collar of diameter $3b$ to be the most effective one. Relationships for temporal and maximum scour depth at a pier with a collar (given in the following section) were proposed. From statistical and sensitivity analysis they observed that the location of the collar followed by the collar width were the most influential parameters.

2.3 Literature Formulas to Predict Equilibrium and Temporal Scour Depths around Pier with Collar

Some empirical equations have been developed in the previous literatures for estimating temporal and equilibrium scour depths at the pier in the presence of a collar. These formulas are listed in the Table 2.1. The conditions at which these predictive equations can be applied as described in the literatures are also mentioned in the table.

Table 2.1 Equations proposed in previous literatures to predict the scour depth around a circular pier with collar of different shapes

Shape	Scour	Literature	Equation	Conditions	Notes
Circular Collar	Equilibrium	Kumar et al. (1999)	$\frac{D_{se}-D_{sce}}{D_{se}}=0.057\left(\frac{b_c}{b}\right)^{1.612}\left(\frac{h}{h_w}\right)^{0.837}$	▪ Should be used only for $h < h_w + D_{se}$.	b = pier diameter b_c = collar diameter l_c = collar length h = location of the collar from the water surface h_w = flow depth D_{st} = temporal scour depth around pier without collar D_{se} = equilibrium scour depth for pier without collar D_{sct} = temporal scour depth around the pier with collar D_{sce} = equilibrium scour depth around the pier with collar K_1 and K_2 = shape factor for circular collar (= 0.105 and 0.048) K_c = collar shape coefficient (= 0.623) $A_C = \pi/4\times(b_c^2-b^2)$ $A_T = \pi/4\times b_c^2$ $T_c=\frac{\sqrt{(S-1)gd_{50}}}{\left(b_c^{\,2}h_w\right)^{\frac{1}{3}}}t$
Circular Collar	Equilibrium	Jahangirzadeh et al. (2014)	$\frac{D_{se}-D_{sce}}{D_{se}}\times 100=0.57e^{4.71A_C/A_T}e^{-0.96h_c/b}$	▪ Can be effectively applied to a typical river experiencing flood conditions with fine gravel as bed sediment. ▪ Collar must be fixed on the bed or above. ▪ Valid under non-contracted and clear-water scour conditions ($U/U_c < 1$).	
Circular Collar	Temporal	Pandey et al. (2020)	$\frac{D_{sct}}{D_{st}}=0.23\left(\frac{b_c}{b}\right)^{-0.82}\left(\frac{h}{h_w}\right)^{-0.58}\log T_c$		
Circular Collar	Maximum	Pandey et al. (2022)	$\frac{D_{se}-D_{sce}}{D_{se}}=0.20\left(\frac{b_c}{b}\right)^{0.17}\left(\frac{h}{h_w}\right)^{0.48}$	▪ Applicable for any collar location (below, at, or above the bed level).	
Circular Collar	Maximum	Kassem et al. (2023)	$\frac{D_{sm}}{b}=7.50(\mathrm{Fr})^{1.549}K_c$	▪ $U/U_c < 1$, $\mathrm{Fr} \le 0.33$, $h_w/b < 2.60$, uniform sand bed with $b/d_{50} > 50$, and $\sigma_g < 1.50$.	
Airfoil Collar	Temporal	Gupta et al. (2023*b*)	$\frac{D_{st}-D_{sct}}{D_{st}}=0.84\left(\frac{b_c}{b}\right)\left(\frac{l_c}{b}\right)^{-0.52}\left(\frac{h}{h_w}\right)^{3.28}(\log T_c)^{-0.173}+0.21$	▪ Collar must be fixed on the bed or above. ▪ $U/U_c < 1$, uniform sand, steady and uniform flow, no contraction effect.	
Airfoil Collar	Maximum	Gupta et al. (2023*b*)	$\frac{D_{se}-D_{sce}}{D_{se}}=2.22\left(\frac{b_c}{b}\right)^{2.98}\left(\frac{l_c}{b}\right)^{-2.28}\left(\frac{h}{h_w}\right)^{1.21}$	▪ Same as the previous one.	
Circular Collar	Temporal	Gupta et al. (2024)	$\frac{D_{st}-D_{sct}}{D_{st}}=K_2\left(\frac{b_c}{b}\right)^{1.67}\left(\frac{h}{h_w}\right)^{3.32}\log T_c$	▪ Circular collar must be located on or above the bed under clear-water conditions in steady and uniform flow. ▪ Sand should be uniform and wall interference should not be present.	
Circular Collar	Maximum	Gupta et al. (2024)	$\frac{D_{se}-D_{sce}}{D_{se}}=K_1\left(\frac{b_c}{b}\right)^{2}\left(\frac{h}{h_w}\right)^{3}$	▪ Same as the previous one.	

2.4 Research Gap

Bridge pier scour has been extensively studied over the years, but is still the leading cause of bridge failures (Lagasse et al., 2007). This indicates that, despite the advances made in understanding scour, there are still critical gaps that need further exploration. Based on the review of literatures performed above, three key areas stand out where research is either insufficient or could be significantly enhanced: (1) Flow mechanism, temporal development of clear water scour around a pier in the presence of a collar, (2) Influence of collar shapes on scour reduction, and (3) Temporal scour depth prediction formula.

- It is observed from the literatures that a few studies addressed the flow mechanism and the temporal scour depth was measured only at the upstream face of the pier with a collar. However, it is necessary to understand the flow pattern and temporal scour depth at the sides and downstream of the pier also as the collar alters the flow pattern around the pier.
- Very few researchers studied the influence of different collar shapes on scour reduction. It is essential to understand the impact of collar shapes on protection efficiency.
- Accurate estimation of temporal scour depth around the pier with a collar is very important for the safety and stability of the bridge pier. From the literatures, it is seen that only a few equations are available to calculate temporal scour depth around the pier in the presence of a collar and also, they are not widely applicable. Additionally, to calculate D_{sct} from those equations D_{st} is first needed to be determined either through experimentation or by using existing formulas.

2.5 Aim of the Present Study

The present study aims to contribute to the areas mentioned above. The aim is to:

- Investigate the temporal scour depth around a pier with and without a collar at four different important locations.
- Study two different collar shapes (circular and airfoil) to understand the influence of collar shapes in reducing scour.
- Develop an equation to more accurately predict the temporal scour depth around a circular pier with a collar directly without knowing the scour depth around the same pier without collar.

CHAPTER – 3

SCOUR MECHANISM AND SCOUR COUNTERMEASURES

3.1 Scour Countermeasures

Scouring is an issue that may not always be anticipated during the design phase but can develop later. Due to the potential damage and safety risks associated with scour, implementing retrofit solutions is crucial. According to HEC-23, these solutions are known as countermeasures, which are defined as methods used to "…monitor, control, inhibit, change, delay, or minimize stream instability and bridge scour problems" (Lagasse et al., 2009). Countermeasures are highly useful as they can address existing scour issues or prevent future ones. Each countermeasure has its own advantages and disadvantages, making it challenging for engineers to choose the most appropriate one for a specific situation.

3.2 Types of Scour Countermeasures

HEC-23 classifies countermeasures into three categories: hydraulic, structural, and monitoring (Lagasse et al., 2009) as shown in Fig. 3.1. Countermeasures have been classified based on how they address scour and stream instability. The following sections will delve into these categories, providing examples and discussing the benefits and drawbacks of each.

3.2.1 Hydraulic Countermeasures

Hydraulic countermeasures focus on altering the flow path through the use of river training structures or riverbed armoring (Lagasse et al., 2009). This approach modifies the surrounding environment rather than the bridge itself. The advantages of this method include cost-effectiveness, reduced impact on the bridge, and potentially easier installation.

River Training Structures

River training structures are employed to alter the flow behavior upstream or around a bridge pier to reduce potential scour caused by the flow. These structures can be made from various materials, including wood, metal, or concrete. However, their orientation in the flow is crucial. They can be positioned perpendicular (e.g., groins) to the flow, parallel (e.g., guide banks) to it, or spread across (e.g., sacrificial piles and vanes) the river, with each arrangement offering distinct benefits (Lagasse et al., 2009).

Armoring Countermeasures

Armoring methods are more commonly used as scour countermeasures compared to river training structures. In the armoring method, a protective layer is placed over the riverbed to help the underlying erodible material withstand the increased forces from the flowing water (Lagasse et al., 2009). Typically, armoring can be applied to large areas, including riverbanks, or it can be focused on protecting specific areas like around bridge piers, which is the primary focus of this research. Armoring countermeasures generally do not significantly alter the flow behavior, nor do they vary in function, but they differ considerably in terms of materials and construction. These countermeasures can be divided into two categories based on their flexibility - flexible and rigid. Armoring techniques include riprap, partially grouted riprap, cable-tied blocks, grout-filled containers, gabions, etc.

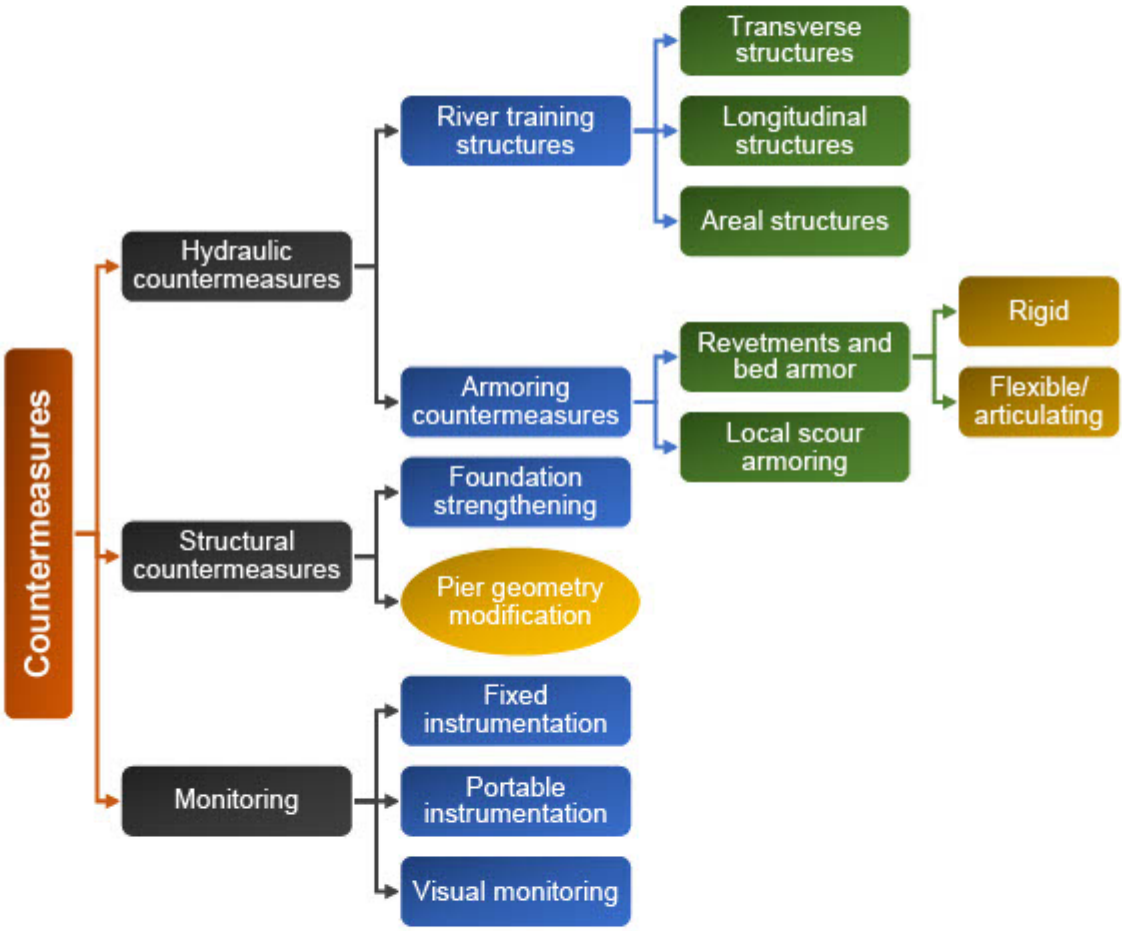


Fig. 3.1 Classifications of Scour Countermeasures (modified from Lagasse et al., 2009)

3.2.2 Structural Countermeasures

Structural countermeasures offer an alternative to hydraulic methods by modifying the bridge piers to help reduce scour. These countermeasures are categorized based on which part of the

pier is being adjusted. Foundation strengthening addresses the portion of the pier below the riverbed, while pier geometry modifications focus on the part of the pier above the riverbed (Lagasse et al., 2009).

Foundation Strengthening

Foundation strengthening is one of the most comprehensive and resource-intensive methods for mitigating scour-related failures. This approach involves enhancing the existing pier foundation, either by increasing reinforcement or expanding its size to improve the pier's stability and thus prevent failure if the riverbed lowers due to scouring (Lagasse et al., 2009). Common foundation strengthening techniques include enlarging the footing with additional concrete, filling scour-induced voids beneath the footing, or installing piles under the footing.

Pier Geometry Modifications

Pier geometry modifications focus on the portion of the pier above the riverbed, aiming to influence the flow behavior. By altering components such as the shape, texture, and overall geometry of the pier (Pier slot, Collars), the intensity of the horseshoe vortex, the increased velocity along the sides of the pier, and the wake vortices can be diminished. This is advantageous because these flow characteristics directly impact the scour depth.

3.2.3 Monitoring

The final group of countermeasures is monitoring, which differs from the others as it is a reactive approach. Instead of physically altering the pier site to prevent scour, monitoring alerts relevant personnel when scour is occurring. Once notified of scour, actions can be taken to stop or mitigate further damage before failure occurs. Monitoring is valuable because it addresses the uncertainty associated with pier scour, as predicting exact scour depths can be challenging.

There are three monitoring techniques. Fixed instrumentation involves monitoring devices installed at specific locations on the bridge. Fixed instrumentation is beneficial for providing real-time data on scour depths and, in some cases, tracking the scour process over time (Conaway, 2006). However, the main limitation is that installing monitors on every pier may not be practical, so typically only a few piers are selected for monitoring (Lagasse et al., 2009). Portable instrumentation refers to monitoring devices that are not permanently attached to the bridge. These devices can be used on multiple piers of a single bridge and then moved to other bridges as needed. Visual inspection involves monitoring the bridge using standard methods without advanced instrumentation. This includes regular site visits, as well as inspections before and after significant flow events, to record the riverbed height around the piers (Lagasse et al., 2009).

3.3 Flow-altering Countermeasures

Engineering solutions for reducing scour at bridge piers can be broadly classified into two categories, namely flow-altering countermeasures and armoring countermeasures. Flow-altering countermeasures aim to disrupt the flow field around the pier, thereby weakening the erosive power of downflow and horseshoe vortex system, which are the primary causes of pier scour (Parker et al., 1998; Chiew and Lim, 2003). These devices can break up vortices and reduce velocity near the piers (Lauchlan, 1999). Parker et al. (1998) reviewed the literature on both types of countermeasures. Since then, new experiments have been conducted on flow-altering methods such as collars, slots, and sacrificial piles, along with various combinations of countermeasures. Flow-altering countermeasures are further divided into four categories based on shape and performance: (1) openings through piers, (2) pier attachments, (3) bed attachments, and (4) other devices (Fig. 3.2).

Armoring methods might not effectively protect the local scour around bridge piers due to riprap failure mechanisms like shear, winnowing, edge failure, and bed form undermining. This also highlights the need for flow-altering devices, as they significantly modify the flow field, reducing the impinging downflow, which in turn weakens the strength of horseshoe vortices. Additionally, flow-altering devices may be a more cost-effective solution, especially when riprap stones are either scarce or too expensive.

Opening through piers: The intensity of the downflow and horseshoe vortex is diminished by permitting some of the incoming flow to pass through openings within a pier or among smaller piers. Three primary configurations have been suggested to achieve this, namely internal connecting tubes, pier groups, and slots (Tafarojnoruz et al., 2010). Vittal et al. (1994) suggested replacing a solid pier with three smaller piers in two configurations: partial and full pier groups. Slots were studied by many researchers including Chiew (1992), Kumar et al. (1999), and Moncada-M et al. (2009).

Pier-attachments: In this type of flow-altering countermeasures, the downflow and horseshoe vortex are weakened by attaching suitable devices to the piers. These devices include threading, collars or horizontal plates, and pier-attached plates. Dey et al. (2006) suggested that threading was economical and easy-to-install countermeasure. The collar was found to be an effective countermeasure by several authors and it is discussed in the next section.

Bed-attachments: This type of countermeasure diverts or weakens the approach flow and modifies the boundary layer. Melville and Hadfield (1999) described sacrificial piles as piles placed upstream of a bridge pier to protect it from local scour. These piles, which may experience significant scour themselves, protect the pier by deflecting high-velocity flows and creating a wake region behind them. Chang and Karim (1972) and Paice and Hey (1993) conducted both laboratory and field studies on sacrificial piles. Vanes and sills were studied by Odgaard and Wang (1991), and Lauchlan (1999).

Johnson and Niezgoda (2004) identified two main types of flow-altering devices. The first type breaks up vortices and reduces high flow velocities, particularly upstream of a pier. Common examples include sacrificial piles such as sill, sheet, or cylindrical piles. The second

type realigns the flow to prevent local and contraction scour, as well as bank widening and lateral migration. Examples include vanes and guide banks.



Fig. 3.2 Classification of flow-altering countermeasures against pier scour (modified from Tafarojnoruz et al., 2010)

According to Johnson and Niezgoda (2004), "the feasibility of and confidence in each of the various countermeasures depend on many variables, including effectiveness, cost, maintenance, and the ability to detect failure." Therefore, the type of protection applied to a bridge pier depends on the specific nature of the problem. In the present study, we tried to explore collars.

3.4 Collars

Melville and Coleman (2000) defined collars as devices attached to the pier, typically near the bed. A collar is a thin protective disc designed to protect the bed from the scouring effects

of downflow at the pier and the associated vortex action around the base of the pier (Chiew, 1992). A collar extends around the outside edge of the pier, aiming to reduce scour by inhibiting and deflecting local scour mechanisms. It should not be so thick that it obstructs the flow and promotes scour (Whitehouse, 1998).

The effectiveness of the collar largely depends on its diameter and position on the pier. Chiew (1992) found that larger collar diameters lead to greater reductions in scour. However, engineers typically aim to keep the collar as small as possible to minimize environmental impact, simplify fabrication, reduce material use, and lower costs. Figure 3.3 illustrates typical collars (circular and airfoil) and their arrangement for circular piers.

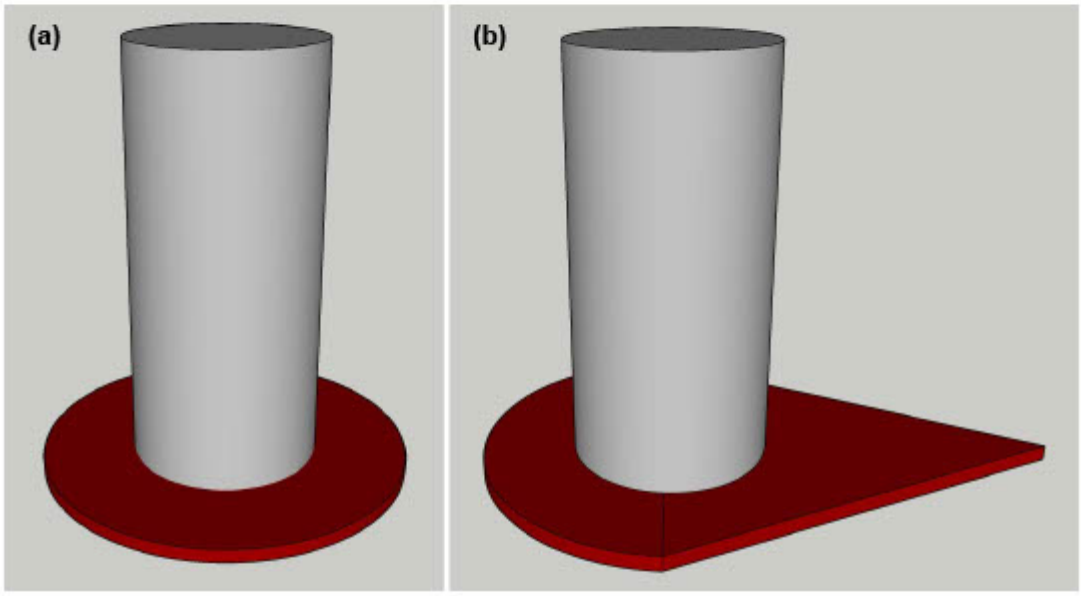


Fig. 3.3 Collars and their arrangement for circular piers **(a)** circular collar; **(b)** airfoil collar.

One notable issue with collars is the risk of undermining beneath them, especially under live-bed conditions where passing bed forms with troughs can expose the edges of the collar to the flow. This can lead to scour beneath the collar, eventually exposing the pier and rendering the collar ineffective (Chiew, 1992). However, if erosion underneath the collar can be effectively managed, collars could serve as an excellent countermeasure, as they have been found effective in reducing scour by over 50%. Due to the potential shown by collars, this is an active area of research.

3.5 Local Scour Mechanism with and without Collar

The flowing pattern of a normal flow comes to a sudden change when it encounters a pier on its path. The basic mechanism creating the local scour around a bridge pier has been identified as the system of vortices that develops around the pier. The vortex system is generally composed of three components as discussed below.

3.5.1 Horseshoe Vortex and Downflow

The presence of a pier in flowing water obstructs the flow and creates a pressure field on the upstream face of the pier that causes the approach flow to separate around the pier. The boundary layer flow past a circular pier undergoes a three-dimensional separation (Figs. 3.4-3.5). This separation results in a portion of the flow being drawn downwards immediately in front of the pier. The downward flow then travels to the riverbed, where it is redirected upstream for a short distance before being carried back downstream by the passing flow. This motion creates a continuous 360-degree flow path, causing the flow to circulate repeatedly as it propagates around the front and down the sides of the pier until it merges with the main flow. This phenomenon is known as the horseshoe vortex because if viewed from the top, this vortex system has the characteristic shape of a horseshoe (Fig. 3.4). Raudkivi and Sutherland (1981) described the horseshoe vortex in local scour as "resembling a very thick rope caught by the pier with its ends trailing downstream…". The formation of the horseshoe vortex and the associated downflow around the circular pier results in increased shear stress (Melville and Coleman, 2000) which consequently results in the sediment transport capacity of the flow in that area. This process leads to the creation of a deep scour hole around the pier and that is why the horseshoe vortex is known as one of the primary contributors to pier scour (Chiew, 1992).

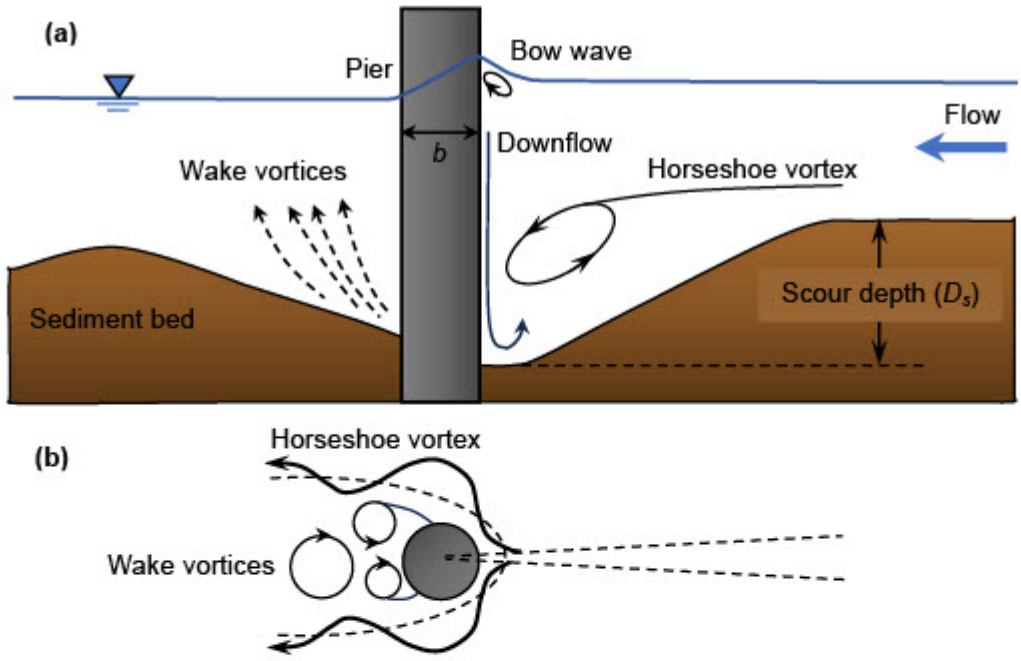


Fig. 3.4 Flow structure at the circular pier without collar **(a)** side view; **(b)** top view.

The downflow in front of the pier is the main cause of the erosion of local scour around bridge piers. It acts somewhat like a vertical jet in eroding the bed material. Ettema (1980) commented that "the velocity of the downflow, impinging on the base of the scour hole, increases as the scour hole forms and deepens. At a certain depth of scour, the downflow

attains a peak strength and thereafter it gradually decreases as the scour hole deepens." (from Chiew, 1984). The temporal variation of scour and the maximum depth of scour at bridge elements therefore mainly depend on the characteristics of flow, pier, and river-bed material.

Melville (1975) described the development of the horseshoe vortex and the scour hole as follows (from Chiew, 1984):

- Initially, the horseshoe vortex is small and comparatively weak, with a roughly circular cross-section.
- With the formation of the scour hole, the vortex grows rapidly in both size and strength, as more fluid attains a downward component, and the strength of the downflow intensifies.
- The horseshoe vortex descends into the developing scour hole and expands as the hole widens.
- As the scour hole continues to grow, the circulation associated with the horseshoe vortex increases due to the enlarging cross-sectional area, but at a decreasing rate.

The portion of the flow that is not drawn down to the riverbed but remains influenced by the pier, alongside the horseshoe vortex, experiences an increase in velocity as it moves past the sides of the pier (Ettema et al., 2017). This happens because the flow must travel a farther distance to bypass the pier, therefore resulting in a flow contraction and, ultimately, an increase in velocity. The increased velocity leads to higher shear stress on the bed on either side of the pier, which directly contributes to scouring in these areas (Arneson et al., 2012).

3.5.2 Wake Vortex

In addition to the horseshoe vortex and downflow, wake vortex is another significant cause of scour around bridge piers. Wake vortices are the result of flow separation at the sides of the pier. When the flow passes along the sides of the pier, the shear layers next to the pier generate vortices with a vertical axis (Fig. 3.5). These vortices, formed along the sides of the pier, are unstable and shed alternately from both downstream edges in an oscillatory manner. The frequency of vortex shedding is directly proportional to the approach velocity and inversely proportional to the pier diameter. Once they are shed, they create a trail of vortices that move downstream, gradually losing energy as they travel farther from the pier. Due to their vertical orientation, the revolving flow within each vortex creates a low-pressure region at the center, which draws sediment off of the riverbed and up into the vortex. They act as little tornadoes lifting the sediment from the bed and generating an independent scour hole downstream of the pier (Zarrati et al., 2006). To describe the scouring action, Melville (1975) wrote "Each of the concentrated vortices acts with its low-pressure center as a vacuum cleaner," picking up material from the bed, which is then transported downstream. Known as wake vortices, these structures contribute, to a lesser extent, to the scour occurring along the sides and rear of the pier (Marris, 1964; Stevens et al., 1991; Ettema et al., 2006).

Wake vortex scour occurs downstream of the pier and it has little or no destructive potential. As the horseshoe vortex scour occurs at the face of the pier and threatens to undermine the pier, this type of scour has been given considerable theoretical thought by

Bruesers et al. (1977) and is well-documented with model studies by Raudkivi (1986) and other researchers. However, information on wake vortex scour at bridge piers is particularly scanty, and the knowledge about the same has come mainly from a few laboratory tests of Melville (1975).

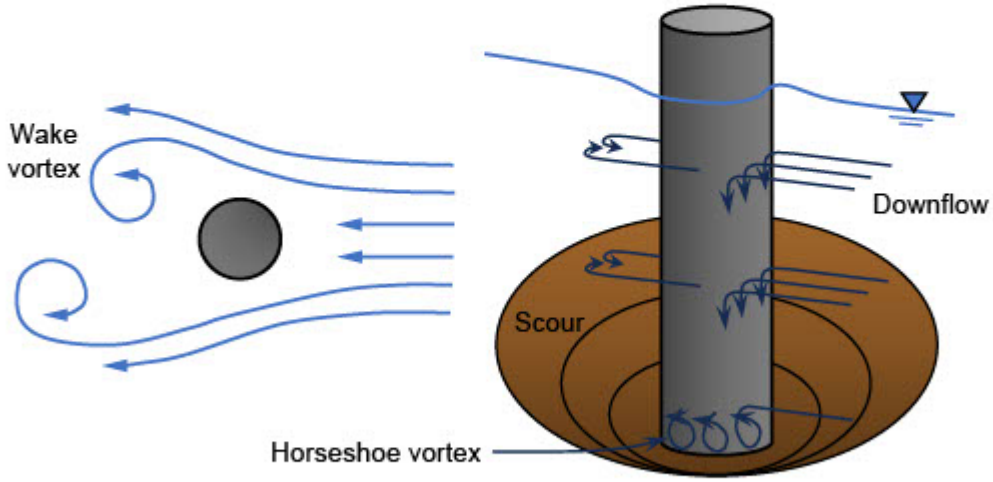


Fig 3.5 Flow structure at the circular pier without collar case.

At most bridges, wake vortex scour is insignificant and confluence scour does not exist. In clear-water rivers flowing on fine sand, these two forms of local scour can be very large. The deep scour holes downstream from the large circular piers (10 and 15 m in diameter) at the Tahrir and Imbaba Bridges over the Nile River in Cairo, Egypt were produced by the conflicting velocity fields at the intersection of the wake vortex streams from adjacent piers. The depths of scour due to these wake vortices are now 8 to 11 m where the normal depth of flow is approximately 8 m. Confluence scour where the main and side channel join upstream from the Imbaba Bridge was 9 m in 1981 and 1987 and was aligned with the bisector of the intersection angle of the two channels. These depths of scour can be considered nearly clear-water scour as the bridges are in the backwater of the Delta Barrages, the velocity is less than 1 m/s and sediment transport is very low. There is concern that the holes may enlarge or move upstream endangering the piers and the bridges. We have made observations in the vicinity of the scour holes and have come to the conclusion that, in each case, the scour was caused by two streams of wake vortices from adjacent piers intersecting downstream. The vortices that result from the two conflicting velocity fields create local scour. At one bridge, the scour is enhanced by the vortices that occur at the confluence of the main channel and its side channel. This is known as confluence scour.

3.5.3 Bow Wave

The presence of a pier generates a surface roller around it, similar to a bow wave created by a boat, and a horseshoe vortex at the base of the pier. These two rollers rotate in opposite directions. In principle, as long as the rollers do not interfere with one another, the local scour depth remains unaffected by the flow depth. However, as the flow depth decreases, the surface

roller becomes more dominant and eventually suppresses the horseshoe vortex, causing the vortex at the base of the pier to reverse its direction of rotation in very shallow conditions (Raudkivi and Ettema, 1983).

3.5.4 Flow Mechanism in the Presence of a Collar

When a collar is attached to the pier, it alters the flow pattern around the pier and disrupts the formation of the horseshoe vortex and downflow. The collar prevents the direct impact of vortices on the sediment bed (Fig. 3.6). As a result, the increased shear stress typically caused by the horseshoe vortices is mitigated, reducing the extent of local scour around the pier. The collar divides the flow into two regions above and below the collar as shown in Fig. 3.7. For the region above it, the collar acts as an impenetrable barrier against the downflow, and hence the downflow loses its strength on impingement at the collar. In the region below the collar, the strength of downflow and therefore the horseshoe vortex is reduced (Kumar et al., 1999). The collar also modifies the flow separation, which is responsible for the formation of wake vortices. Larger-sized collars ($2.5b - 4b$) increase the intensity of wake vortices by altering the flow dynamics. This results in a deeper scour in the wake region. The absence of scour at the front and sides prevents sediment from being deposited in the wake for larger collars, and thus the higher scour in the wake is understandable (Kumar et al., 1999).

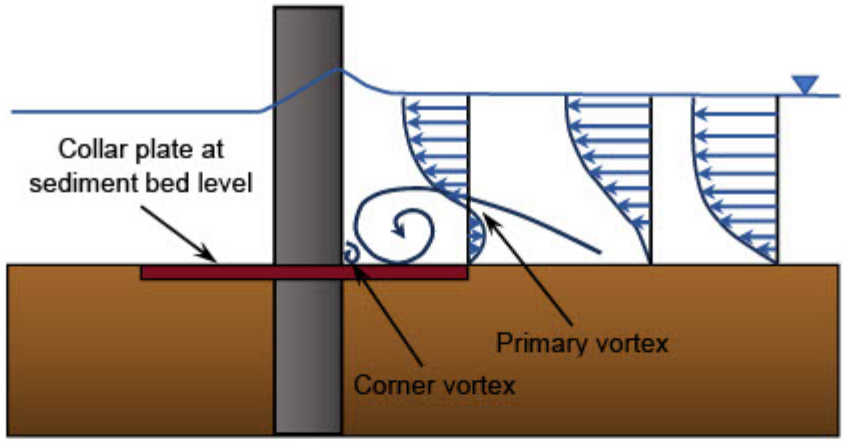


Fig. 3.6 Schematic view of flow mechanism upstream of a pier with a collar just before scouring starts to develop.

The scouring processes described above lead to the removal of sediment from around the pier, which must be relocated. This sediment is typically transported a short distance downstream, where it is deposited once the flow has no longer enough energy to keep it suspended. Near the pier, the flow velocity increases due to the pier-induced flow behaviors, but it returns to the mean velocity downstream, causing sediment to be removed from the area around the pier and deposited slightly downstream. While scouring is recognized as a problem, sediment deposition also presents issues, such as significantly reducing water depth (Ettema et al., 2006). This is particularly concerning in areas with active boat traffic, as the risk of vessels running aground increases, making dredging necessary to address the issue.

Therefore, both scour and the resulting sediment deposition are undesirable, highlighting the need for an effective solution to this complex problem.

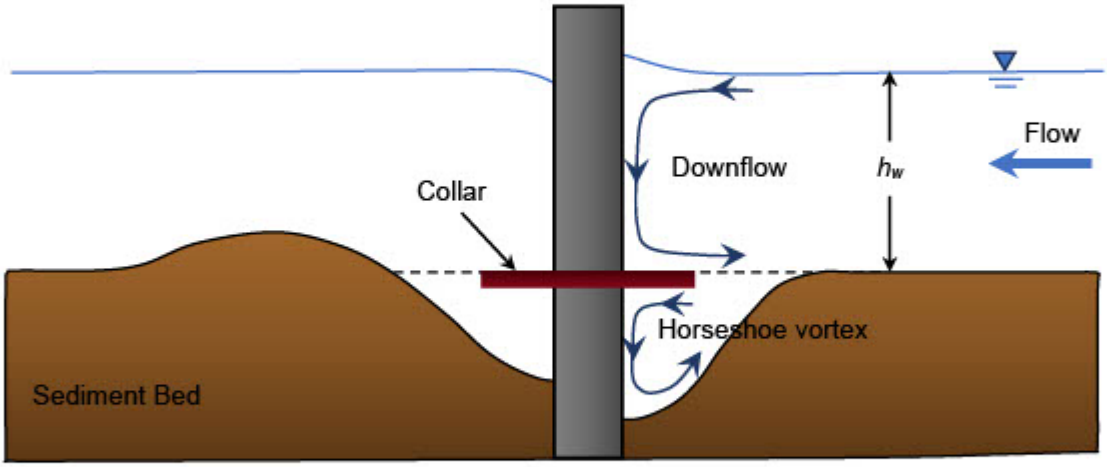


Fig. 3.7 Schematic view of scour and deposition around a pier in the presence of collar (diagram is not to scale).

3.6 Factors Affecting Local Scour at Pier

Local scour around bridge piers is influenced by several interrelated parameters according to Raudkivi and Ettema (1983), Richardson and Davies (1995), Dey (1997), Lagasse et al. (2001) and others. This interdependence means that the effect of one specific parameter on the depth of the scour hole may be overshadowed by others. The complexity of these interactions limits the effectiveness of mathematical analysis, as it would require simplifying assumptions for a solution. To understand the impact of each parameter, they can be primarily grouped into different categories as follows:

Scour depth = f (fluid, flow and sediment properties, pier and collar geometry, time)

Fluid properties: In fluid mechanics, a fluid is characterised by its density (ρ) and kinematic viscosity (ν), both of which depend on temperature. In laboratory settings, the temperature can be controlled, and the data typically pertain to a constant temperature. However, in real-world conditions, temperature may affect scour depth by influencing fluid properties. Currently, no data are available to quantify this influence.

Flow properties: The flow of a fluid is characterised by its depth (h_w), flow velocity (U), slope of the channel (S_o), gravitational acceleration (g), critical velocity (U_c), bed roughness, etc.

Time: Dey et al. (1997) included the time of scouring as an additional parameter. Scouring is a gradual process where the scour geometry of the sediment bed approaches a new equilibrium shape. This takes time and it is particularly important during a flood. The duration of the flood determines if the peak conditions last long enough to achieve maximum scour depth. The early stages of flood recession are especially crucial, as the maximum scour

depth can occur when the bed elevation is at its lowest due to general scour. As the flood decreases, general sediment transport is reduced to such an extent that clear water scour conditions could prevail. At this time, the rate of scour development can significantly impact the maximum scour depth.

Pier geometry: The effects of a pier are primarily determined by its diameter (b), although other significant factors include the shape of the pier, the number of piers, the angle of attack of the flow with respect to the pier axis, the ratio of channel width to pier width (B/b), also known as the aspect ratio, the surface condition of the pier, blockage of the flow channel by ice or debris accumulating at the pier, etc.

Collar geometry: The effects of collars are determined by their width (b_c), length (l_c), thickness (t_c), shape, position of the collar on the pier, number of collars, etc.

Sediment properties: Sediment can be characterized by its specific gravity (S) or mass density (ρ_s) and the grain size distribution. The uniformity of particle size distribution is defined by its standard deviation (σ_g). Other important factors include the cohesiveness of the sediment, shape factor, angle of repose, etc.

The list of variables affecting the clear water temporal scour in the presence of a collar is very long. Limiting the study to the case of the pier with a collar in a river whose flow is assumed to be steady and uniform, there are many parameters that may influence the scouring phenomenon as shown in Table 3.1. A brief summary of how each parameter influences scour at the pier with collar is provided below.

Table 3.1 Parameters influencing local scour at the pier with collar

Attribution	Variable name	Symbol	Dimension
Pier	Pier diameter	b	[L]
	Pier shape	–	–
Collar	Collar diameter	b_c	[L]
	Length of the collar	l_c	[L]
	Collar thickness	t_c	[L]
	Collar shape	–	–
	Elevation of the collar from bed level	h_c	[L]
Flow	Approach flow depth	h_w	[L]
	Flow velocity	U	$[LT^{-1}]$
	Critical flow velocity	U_c	$[LT^{-1}]$
Flume	Flume width	B	[L]
	Channel bed slope	S_0	$[M^0L^0T^0]$
Fluid	Acceleration due to gravity	g	$[LT^{-2}]$
	Density of fluid	ρ_f	$[ML^{-3}]$
	Kinematic viscosity of fluid	v	$[L^2T^{-1}]$
Bed material	Sediment density	ρ_s	$[ML^{-3}]$
	Geometric standard deviation	σ_g	$[M^0L^0T^0]$
	Median size of sediment	d_{50}	[L]
Time	Instantaneous time	t	[T]
	Run duration	t_m	[T]

3.6.1 Pier Diameter (b)

Experiments have demonstrated that scour depth is related to the size of the pier (Breusers et al., 1977). This can be physically explained by the fact that scour is caused by the horseshoe vortex system, whose dimensions depend on the pier's diameter. Additionally, the horseshoe vortex, one of the primary scouring agents, is proportional to the pier Reynolds number (Re_p) which is a function of the pier diameter. Therefore, for a given mean approach flow velocity, scour depth is proportional to the width of the pier.

Under clear-water scour conditions, the size of the pier primarily affects the time required to reach the equilibrium scour depth but does not significantly impact the relative magnitude of scour depth (D_s/b), provided that the effects of relative flow depth (h_w/b) and relative grain size (b/d_{50}) on the local scour depth are not considered according to Breusers and Raudkivi (1991). They also illustrated that the volume of the local scour hole formed around the upstream half of the perimeter of the pier is proportional to the cube of the pier diameter. The larger the pier the larger the scour hole volume and also the longer the time taken for the development of the scour hole for a given shear stress ratio.

3.6.2 Pier Shape

Bridge piers are built in a variety of shapes. The most common are circular, rectangular, square, rectangular with chamfered ends, oblong, lenticular, and Joukowski. Figure 3.8 illustrates some of these pier shapes. Research has shown that the shape of the pier affects scour depth, as reported by numerous studies (e.g., Breusers, 1977; Breusers and Raudkivi, 1991; Dey, 1997; Melville and Coleman, 2000). Generally, blunter piers tend to cause deeper local scour. The front nose of the pier plays an important role in determining maximum scour depth whereas the shape of the downstream end of the pier is less significant.

A shape factor is often used to account for the influence of pier shape. Melville and Coleman (2000) referenced the work of Mostafa (1994), who proposed shape factors for uniform piers — those with a constant section throughout their depth. Mostafa's measurements indicated that circular piers resulted in the least scour, while rectangular piers with blunt ends caused the most. In practice, shape factors are most relevant when axial flow is maintained, as even a slight angle of attack can negate the advantages of a streamlined shape (Melville and Coleman, 2000).

Non-uniform piers, such as those with piled foundations, caissons, slab footings, and tapered designs, also affect scour depth. For tapered piers with sloping upstream and downstream faces, the angle of the taper influences scour depth. Specifically, downward-tapered piers induce deeper scour compared to a circular pier of the same width.

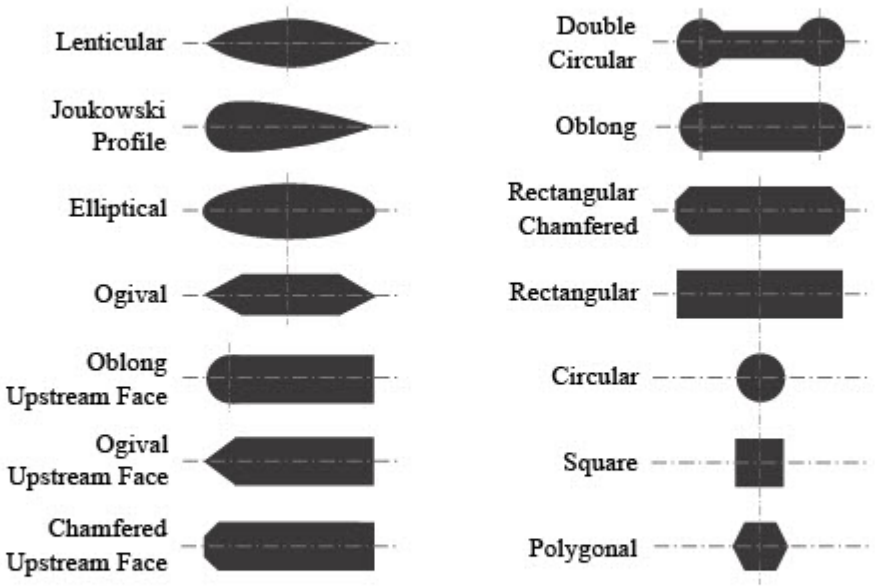


Fig. 3.8 Schematic illustrations of some conventional pier shapes.

3.6.3 Collar Diameter (b_c)

Studies have shown that collar size has a significant effect on maximum scour depth. A larger diameter collar can reduce scour depth sufficiently (Pandey et al., 2022). A collar of diameter, $b_c = 3b$ was found to be more effective than the collar of diameter $2b$. It indicates that the larger the collar diameter, the smaller the scour depth (Moncada-M et al., 2009). When the size of the collar is large, it can protect the larger area of the bed in front of the pier from impingement by the downflow, thus reducing scour.

3.6.4 Collar Elevation (h_c)

Collars can be positioned at different elevations relative to the sediment bed – on the sediment surface, above it, or buried below. Each placement influences the interaction between the pier and the flow dynamics differently, altering the effectiveness of scour reduction.

When placed on the sediment bed, the collar acts as an immediate barrier to the horseshoe vortex and downflow right at the sediment interface, directly preventing sediment removal around the pier base. This position is generally most effective in reducing scour (Moncada et al., 2009; Pandey et al., 2020; Gupta et al., 2023a; etc.) because it directly obstructs the erosive flow and vortex activity at the point of initial impact.

When the collar is located below the bed, it does not obstruct the initial erosive forces acting at the pier base, allowing the horseshoe vortex and downflow to remove sediment until the collar is eventually exposed. Once exposed, it starts to mitigate further scour, but by this time, significant sediment loss may have already occurred. Few previous studies (Moncada-M et al., 2009; Khodashenas et al., 2018) claim that this collar position is also effective and,

in some cases, the efficiency is even greater compared to other elevations. However, a proper explanation for the underlying reasons is missing.

When the collar is fixed at any level above the bed, it divides the flow into two regions above and below the collar. As a result, the strength of the downflow and horseshoe vortex is reduced to some extent but scour develops due to the flow beneath the collar. This position is the least effective and does not provide significant protection.

3.6.5 Flow Depth (h_w)

The impact of flow depth on scour depth has been studied by various researchers (Breusers and Raudkivi, 1991; Melville and Coleman, 2000; etc.). The presence of a pier in a channel creates a surface roller around the pier and a horseshoe vortex at its base. Flow depth influences local scour depth by affecting the interaction between the surface roller (or bow wave) at the pier's leading edge and the horseshoe vortex. These two rollers rotate in opposite directions, and as long as they do not interfere with each other, local scour depth is primarily determined by the pier diameter rather than flow depth. In such cases, commonly referred to as deep flow conditions, local scour is typically observed around narrow piers. When flow depth decreases, the surface roller becomes more prominent, reducing the effectiveness of the horseshoe vortex in sediment entrainment. Consequently, in shallower flows, the local scour depth decreases. In very shallow flows, local scour becomes dependent on flow depth, and the scour is typically associated with wider piers.

In summary, observations indicate that at shallow flow depths, local scour around piers increases with flow depth. However, at larger water depths (i.e., deep flow), scour depth becomes independent of flow depth but depends on the pier diameter.

3.6.6 Median Sediment Size (d_{50})

The impact of the grain size and the density of the sediment material are often characterized as a function of the critical flow velocity for the initiation of sediment motion. Breusers and Raudkivi (1991) reviewed the work of Raudkivi and Ettema (1977*a*, *b*), which investigated how sediment size influences the local depth of scour around a bridge pier. It was observed from their experiments, conducted under clear-water scour conditions using a pier with a diameter of 10.2 cm and a flume of 1.5 m width, that sediment size of $d_{50} < 0.7$ mm leads to the formation of ripples, while sediment of $d_{50} \geq 0.7$ mm does not. The study also found that the scour results differed significantly between these two sediment size categories.

According to Raudkivi and Ettema, for sediments of $d_{50} \geq 0.7$ mm where ripples do not form, the experiments can be conducted successfully under a flow condition, $U_*/U_{*c} \simeq 0.95$, without causing disturbances in the upstream bed by the approaching flow. However, for finer sands ($d_{50} < 0.7$ mm), it is not possible to maintain a flatbed under the same flow conditions due to ripple formation. In such cases, a flatbed cannot be sustained near the threshold shear stress condition because ripples will develop, leading to some sediment transport and replenishment of the sand scoured at the pier. Therefore, true clear-water scour conditions cannot be achieved with sediments smaller than 0.7 mm.

3.6.7 Angle of Repose (φ_r)

The angle of repose, also referred to as the angle of friction, is an engineering property of granular materials. The angle of repose is the maximum angle of a stable slope determined by friction, cohesion, and the shapes of the particles. When bulk granular materials are poured onto a horizontal surface, a conical pile will form. The internal angle between the surface of the pile and the horizontal surface is known as the angle of repose (Fig. 3.9) and is related to the density, surface area, and coefficient of friction of the material. Material with a low angle of repose forms flatter piles than material with a high angle of repose.

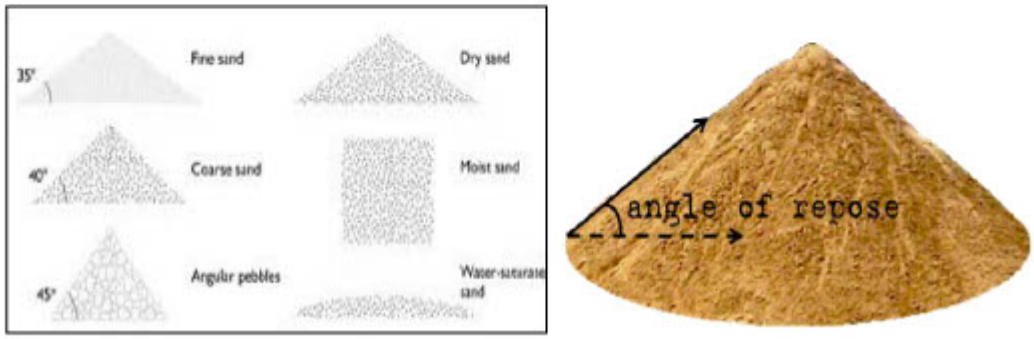


Fig. 3.9 Schematic diagram of Angle of repose

The angle of repose is the steepest angle that the surface of a mass of loose particulate matter makes with the ground. The angle of repose is affected by the size, mass, angularity, and dampness of the particles and by the force of downward acceleration, but it is consistent for a given material. Knowing the angle of repose of a material in various circumstances is vital for engineers and landscapers, for example.

The way in which most people are familiar with the angle of repose is sand castles. Dry sand generally has an angle of repose of about 30°, so piled dry sand forms shallow inverted cones. When sand is dampened, the surface tension of the water binds the grains together, and the angle of repose is increased to more than vertical so that walls, towers, and sea caves can be made. However, when sand is too wet, the water lubricates the grains instead of sticking them together, and the angle of repose is decreased to nearly zero. This should be required knowledge for anyone who is thinking of buying a house built on a sandbar.

3.6.8 Flow Intensity (U/U_c or U_*/U_{*c})

Flow intensity is defined as the ratio of the approach mean velocity (U) to the critical mean velocity (U_c) or the ratio of the shear velocity (U_*) to the critical shear velocity (U_{*c}). Under clear-water conditions, the local scour depth in uniformly graded sediment increases almost linearly with increasing flow intensity until reaching a maximum known as the threshold peak, which occurs at the threshold velocity (Melville and Chiew, 1999). The maximum scour depth (D_{sm}) is reached when the ratio $U_*/U_{*c} = 1$. For non-uniform sediments, the maximum scour depth is referred to as the armor peak and the live-bed peak.

When the flow velocity exceeds this threshold, the scour depth initially decreases before increasing again to a second peak termed the live-bed peak. This second peak is observed around the transition to a flatbed stage of sediment transport. However, the threshold peak remains the highest scour depth in uniform sediment. The variation of local scour depth with flow intensity, as evident from previous studies (Chabert and Engeldinger, 1956; Ettema, 1980; Raudkivi and Ettema, 1983; Chiew, 1984; etc.) and is shown in Fig. 3.10.

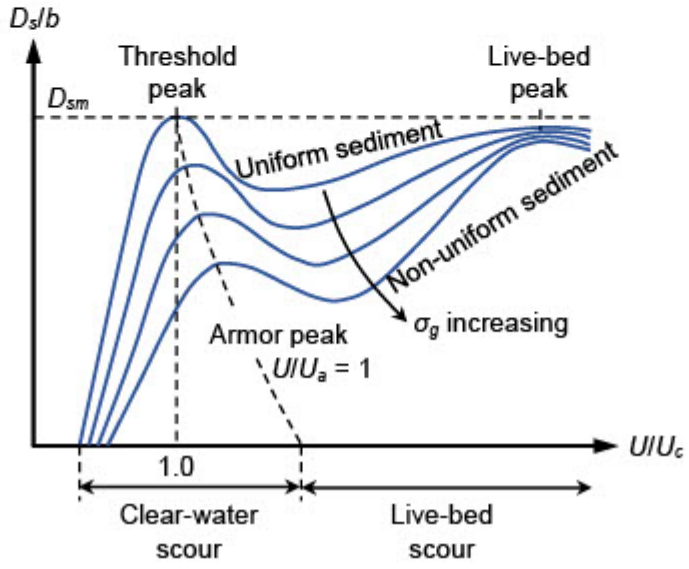


Fig. 3.10 Local scour depth variation with flow intensity.

3.6.9 Flow Shallowness (h_w/b)

Flow shallowness represents the effects of the flow depth (h_w) relative to the pier diameter (b). For deep flows relative to the pier width, which corresponds to narrow piers, the scour depth increases proportionally with the pier width and is unaffected by h_w. For instance, the maximum scour depth at a relatively narrow circular bridge pier is approximately 2.4 times the pier diameter, regardless of the flow depth. In contrast, for shallow flows relative to the pier width, the scour depth increases proportionally with h_w and is independent of b. For intermediate flow depths, scour depth depends on both the h_w and b (Melville, 2008). These trends are illustrated schematically in Fig. 3.11.

The depth of local scour is influenced by flow shallowness because the formation of a surface roller (or bow wave) at the leading edge of a pier impacts the horseshoe vortex, which is the primary cause of scour. These two vortices rotate in opposite directions. Ideally, if these vortices do not interfere with each other, the local scour depth remains unaffected by flow depth, that is the scour occurs at narrow piers. As flow depth decreases, the surface roller becomes more prominent, reducing the ability of the base vortices to entrain sediment. Consequently, local scour depth diminishes in shallower flows. In extremely shallow flows, the local scour depth becomes independent of flow depth, and the scour is considered to occur at wide piers.

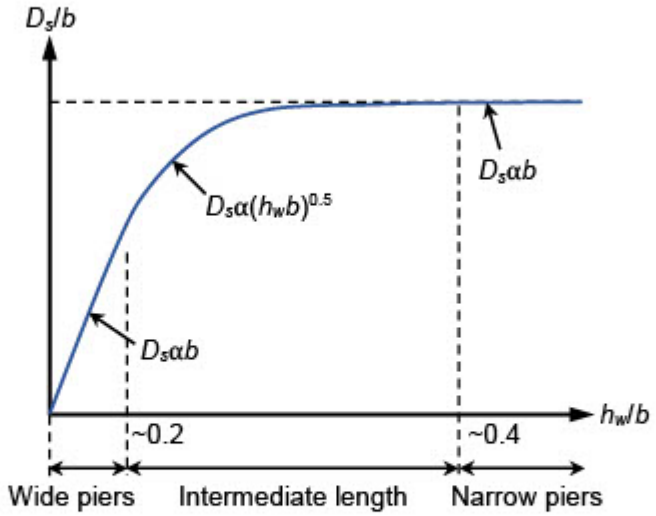


Fig. 3.11 Local scour depth variation with flow shallowness.

3.6.10 Sediment Coarseness (b/d_{50})

The pier diameter (b) relative to the median particle size (d_{50}) is known as the sediment coarseness. For uniform sediments, local scour depths are generally not affected by sediment size unless the sediment is relatively coarse (Melville, 2008). Laboratory studies indicate that sediment size influences local scour depth when the ratio $b/d_{50} < 50$. According to Ettema (1980), for local scour at piers, when the sediment coarseness ratio is large, individual grains are significantly larger compared to the scour hole formed by the downflow. This causes erosion to be impeded, as the porous bed absorbs some of the downflow energy. In such cases, the scour is described as occurring in coarse sediment. When $b/d_{50} < 8$, the individual grains are so large compared to the pier that the erosion phase does not occur and scouring is restricted to the entrainment of particles at the sides of the pier, leading to a further reduction in overall scour depth (Chiew, 1984). The variation of local scour depth with sediment coarseness is shown in Fig. 3.12 (from Melville, 2008).

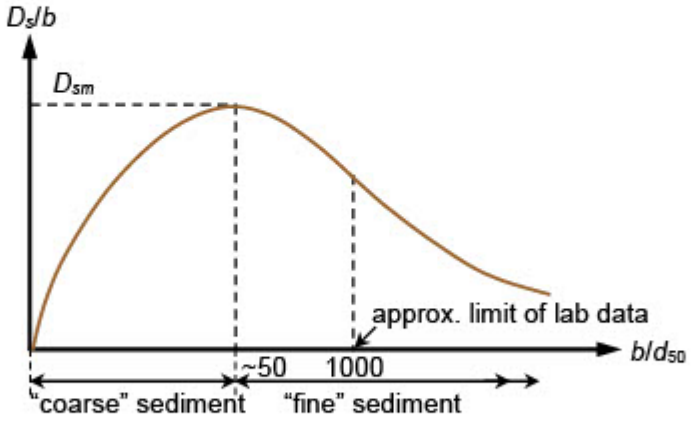


Fig. 3.12 Local scour depth variation with sediment coarseness

3.6.11 Contraction Ratio (B/b)

The ratio of the flume width to the pier diameter is known as the contraction ratio. The equilibrium depth of local scour at a pier is influenced by the contraction ratio. To minimize blockage effects in experimental investigations under clear-water scour conditions, the flume width should be at least eight times the diameter of the pier (Shen et al., 1969). For live-bed scour conditions, the flume width should be at least ten times the pier diameter to prevent a reduction in scour depth due to changes in bed features as they move through the constriction.

3.6.12 Sediment Nonuniformity (σ_g)

Ettema (1976, 1980) conducted systematic laboratory studies to examine how sediment nonuniformity affects local scour depth at piers under clear-water conditions. Similar research under live-bed conditions was carried out by Chiew (1984) (as reported by Melville, 2008). Sediment gradation is typically described by the geometric standard deviation of sand size, $\sigma_g = (d_{84}/d_{16})^{0.5}$. For natural river sand, σ_g is approximately 1.8, whereas for uniform sand, it is around 1.3 (Hoffmans and Verheij, 1997). Raudkivi (1998) proposed that the sediment can be considered uniform when $\sigma_g < 2$. Ettema (1980) conducted the experiments at the threshold of sediment motion for the median size of the sediment used. He found that as the standard deviation of the particle size distribution increases, both the rate of scour hole development and the equilibrium scour depth decrease. For non-uniform sediments (i.e., higher σ_g values), armoring occurs on the approach flow bed and at the base of the scour hole around the threshold condition ($U_*/U_{*c} \approx 1$). This armoring significantly reduces local scour depth. However, at high values of U_*/U_{*c}, where the flow can entrain most grain sizes in the non-uniform sediment, the effect of sediment non-uniformity on scour depth is minimal.

3.6.13 Froude Number (Fr)

The Froude number is a dimensionless number comparing inertia and gravitational forces. It is used to quantify the resistance of an object moving through water and compare objects of different sizes. Named after William Froude, the Froude number is based on the speed-to-length ratio as defined by him.

$$\mathrm{Fr} = \frac{U}{\sqrt{g h_w}} \tag{3.1}$$

where U is a characteristic velocity for rectangular cross-sections with uniform depth h_w, For $\mathrm{Fr} < 1$, the flow is called a subcritical flow. Further for $\mathrm{F_r} > 1$, the flow is characterized as a supercritical flow and when $\mathrm{F_r} \approx 1$, the flow is denoted as critical flow.

Kassem et al. (2023) observed from the experimental results that the maximum scour depth around unprotected and protected piers increases with an increase in Froude number. However, the trend of the increase in the scour depth is different for the two combinations as shown in Fig. 3.13.

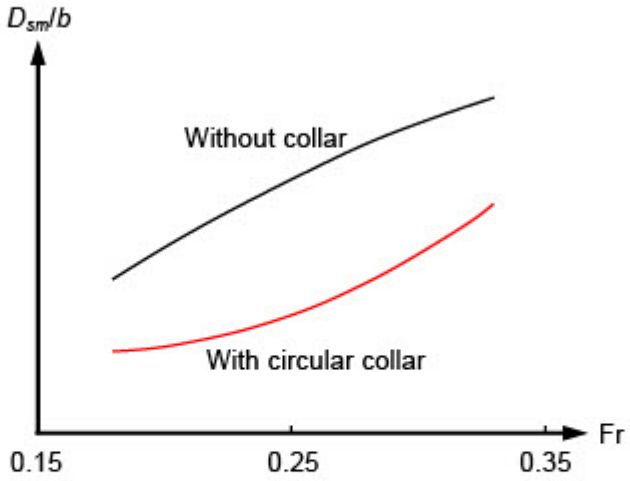


Fig. 3.13 Maximum non-dimensional scour depth at the pier without the collar and with a circular collar at different Froude numbers (Kassem et al., 2023).

3.6.14 Time (t)

The process of scouring is asymptotic. In clear-water conditions, the scour depth asymptotically approaches the equilibrium depth. Conversely, under live-bed conditions, the equilibrium depth is reached more rapidly, but the scour depth then oscillates due to the movement of bed features around the pier or abutment.

The shape of the flood flow hydrograph is crucial, as is the duration of the flood. Generally, the duration of the flood influences whether equilibrium live-bed scour will occur. Once the flood peak has passed, the flow begins to recede. The duration of this recession period is also significant. During the recession, clear-water conditions might prevail, potentially causing further scour, particularly if near-threshold conditions persist for an extended period.

3.7 Dimensional Analysis

Dimensional analysis is a mathematical technique used to understand and analyse the relationships between various physical quantities. Dimensional analysis is conducted to identify the parameters that impact scour around a bridge pier. The scour depth around a smooth circular pier protected with a collar, placed in a rectangular flume with a movable sediment bed under steady and uniform flow conditions, is denoted as D_{sct} for any given elapsed time (t). The scour around the pier in the presence of a circular and airfoil collar is influenced by several factors.

Temporal scour depth (D_{sct}) around the pier with a circular collar can be represented by a functional relationship (Eq. 3.2):

$$f_1\left(D_{sct}, b, b_c, t_c, h_c, h_w, U, U_c, B, d_{50}, \rho_f, \rho_s, \nu, g, \sigma_g, t\right) = 0 \qquad (3.2)$$

To perform the dimensional analysis, we have considered Buckingham's π-theorem method because when a large number of variables are involved, Rayleigh's method becomes lengthy.

Here, we have considered the repeating variables as b, U, and ρ_f, where b is the geometric property, U is the flow property and ρ_f is the fluid property. Here total number of parameters, n =16, and the number of independent parameters, m = 3. Therefore, we get a total (n-m = 16-3 = 13) of 13 numbers of π terms (Eqs. 3.3-3.4) as follows,

$$f_1\left(\pi_1, \pi_2, \pi_3, \cdots\cdots\cdots, \pi_{n-m}\right) = 0 \tag{3.3}$$

$$f_1\left(\pi_1, \pi_2, \pi_3, \cdots\cdots\cdots, \pi_{13}\right) = 0 \tag{3.4}$$

The 13 π-terms can be written as:

$\pi_1 = b^{a1}U^{b1}\rho_f{}^{c1}D_{sct}$, $\pi_2 = b^{a2}U^{b2}\rho_f{}^{c2}v$, $\pi_3 = b^{a3}U^{b3}\rho_f{}^{c3}g$, $\pi_4 = b^{a4}U^{b4}\rho_f{}^{c4}\rho_s$,
$\pi_5 = b^{a5}U^{b5}\rho_f{}^{c5}d_{50}$, $\pi_6 = b^{a6}U^{b6}\rho_f{}^{c6}h_w$, $\pi_7 = b^{a7}U^{b7}\rho_f{}^{c7}U_c$, $\pi_8 = b^{a8}U^{b8}\rho_f{}^{c8}B$,
$\pi_9 = b^{a9}U^{b9}\rho_f{}^{c9}t_c$, $\pi_{10} = b^{a10}U^{b10}\rho_f{}^{c10}b_c$, $\pi_{11} = b^{a11}U^{b11}\rho_f{}^{c11}h_c$, $\pi_{12} = b^{a12}U^{b12}\rho_f{}^{c12}t$,
$\pi_{13} = b^{a13}U^{b13}\rho_f{}^{c13}\sigma_g$.

The process of obtaining each π-term in dimensionless form is detailed after assigning dimensions to individual parameters in each equation (Eqs. 3.5-3.29).

Now for the first π-term, we can write, $\pi_1 = b^{a1}U^{b1}\rho_f{}^{c1}D_{sct}$
The variables can be expressed in terms of their fundamental dimension as,

$$M^0L^0T^0 = L^{a1}\left(LT^{-1}\right)^{b1}\left(ML^{-3}\right)^{c1}L \tag{3.5}$$

Equating the exponents of M, L, and T on both sides of the equations we get,
$a1 = -1$, $b1 = 0$, $c1 = 0$
Therefore the first π-term (Eq. 3.6) we have,

$$\pi_1 = \frac{D_{sct}}{b} \tag{3.6}$$

Similarly, we can write 2nd π-term as, $\pi_2 = b^{a2}U^{b2}\rho_f{}^{c2}v$
The variables can be expressed in terms of their fundamental dimension as,

$$M^0L^0T^0 = L^{a2}\left(LT^{-1}\right)^{b2}\left(ML^{-3}\right)^{c2}\left(L^2T^{-1}\right) \tag{3.7}$$

Equating the exponents of M, L, and T on both sides of the equations we get,
$a2 = -1$, $b2 = -1$, $c2 = 0$
Therefore the second π-term (Eq. 3.8) we have,

$$\pi_2 = \frac{v}{bU} \tag{3.8}$$

Similarly, we can write the third π-term as, $\pi_3 = b^{a3}U^{b3}\rho_f{}^{c3}g$
The variables can be expressed in terms of their fundamental dimension as,

$$M^0L^0T^0 = L^{a3}\left(LT^{-1}\right)^{b3}\left(ML^{-3}\right)^{c3}\left(LT^{-2}\right) \tag{3.9}$$

Equating the exponents of M, L, and T on both sides of the equations we get,
$a3 = 1$, $b3 = -2$, $c3 = 0$
Therefore the third π-term (Eq. 3.10) is,

$$\pi_3 = \frac{bg}{U^2} \tag{3.10}$$

Similarly, we can write the fourth π-term as, $\pi_4 = b^{a4} U^{b4} \rho_f^{c4} \rho_s$

$$M^0L^0T^0 = L^{a4}\left(LT^{-1}\right)^{b4}\left(ML^{-3}\right)^{c4}\left(ML^{-3}\right) \tag{3.11}$$

Equating the exponents of M, L, and T on both sides of the equations we get,
$a4 = 1$, $b4 = 0$, $c4 = -1$
Therefore the fourth π-term (Eq. 3.12) is,

$$\pi_4 = \frac{\rho_s}{\rho_f} \tag{3.12}$$

Similarly, we can write the fifth π-term as, $\pi_5 = b^{a5} U^{b5} \rho_f^{c5} d_{50}$

$$M^0L^0T^0 = L^{a5}\left(LT^{-1}\right)^{b5}\left(ML^{-3}\right)^{c5} L \tag{3.13}$$

Equating the exponents of M, L, and T on both sides of the equations we get,
$a5 = -1$, $b5 = 0$, $c5 = 0$
Therefore the fifth π-term (Eq. 3.14) is,

$$\pi_5 = \frac{d_{50}}{b} \tag{3.14}$$

Similarly, we can write the sixth π-term as, $\pi_6 = b^{a6} U^{b6} \rho_f^{c6} h_w$

$$M^0L^0T^0 = L^{a6}\left(LT^{-1}\right)^{b6}\left(ML^{-3}\right)^{c6} L \tag{3.15}$$

Equating the exponents of M, L, and T on both sides of the equations we get,
$a6 = -1$, $b6 = 0$, $c6 = 0$
Therefore the sixth π-term (Eq. 3.16) is,

$$\pi_6 = \frac{h_w}{b} \tag{3.16}$$

Similarly, we can write the seventh π-term as, $\pi_7 = b^{a7} U^{b7} \rho_f^{c7} U_c$

$$M^0L^0T^0 = L^{a7}\left(LT^{-1}\right)^{b7}\left(ML^{-3}\right)^{c7}\left(LT^{-1}\right) \tag{3.17}$$

Equating the exponents of M, L, and T on both sides of the equations we get,
$a7 = 0$, $b7 = -1$, $c7 = 0$
Therefore the seventh π-term (Eq. 3.18) is,

$$\pi_7 = \frac{U_c}{U} \tag{3.18}$$

Similarly, we can write the eighth π-term as, $\pi_8 = b^{a8} U^{b8} \rho_f^{c8} B$

$$M^0L^0T^0 = L^{a8}\left(LT^{-1}\right)^{b8}\left(ML^{-3}\right)^{c8} L \tag{3.19}$$

Equating the exponents of M, L, and T on both sides of the equations we get,
$a8 = -1$, $b8 = 0$, $c8 = 0$
Therefore the eighth π-term (Eq. 3.20) is,

$$\pi_8 = \frac{B}{b} \tag{3.20}$$

Similarly, we can write the ninth π-term as, $\pi_9 = b^{a9} U^{b9} \rho_f{}^{c9} t_c$

$$M^0L^0T^0 = L^{a9}\left(LT^{-1}\right)^{b9}\left(ML^{-3}\right)^{c9} L \tag{3.21}$$

Equating the exponents of M, L, and T on both sides of the equations we get,
$a9 = -1$, $b9 = 0$, $c9 = 0$
Therefore the ninth π-term (Eq. 3.22) is,

$$\pi_9 = \frac{t_c}{b} \tag{3.22}$$

Similarly, we can write the 10th π-term as, $\pi_{10} = b^{a10} U^{b10} \rho_f{}^{c10} b_c$

$$M^0L^0T^0 = L^{a10}\left(LT^{-1}\right)^{b10}\left(ML^{-3}\right)^{c10} L \tag{3.23}$$

Equating the exponents of M, L, and T on both sides of the equations we get,
$A1 = -1$, $b10 = 0$, $c10 = 0$
Therefore the 10th π-term (Eq. 3.24) is,

$$\pi_{10} = \frac{b_c}{b} \tag{3.24}$$

Similarly, we can write the 11th π-term as, $\pi_{11} = b^{a11} U^{b11} \rho_f{}^{c11} h_c$

$$M^0L^0T^0 = L^{a11}\left(LT^{-1}\right)^{b11}\left(ML^{-3}\right)^{c11} L \tag{3.25}$$

Equating the exponents of M, L, and T on both sides of the equations we get,
$a11 = -1$, $b11 = 0$, $c11 = 0$
Therefore the 11th π-term (Eq. 3.26) is,

$$\pi_{11} = \frac{h_c}{b} \tag{3.26}$$

Similarly, we can write the 12th π-term as, $\pi_{12} = b^{a12} U^{b12} \rho_f{}^{c12} t$

$$M^0L^0T^0 = L^{a12}\left(LT^{-1}\right)^{b12}\left(ML^{-3}\right)^{c12} T \tag{3.27}$$

Equating the exponents of M, L, and T on both sides of the equations we get,
$a12 = -1$, $b12 = 1$, $c12 = 0$
Therefore the 12th π-term (Eq. 3.28) is,

$$\pi_{12} = \frac{Ut}{b} \tag{3.28}$$

Similarly, we can write the 13th π-term as, $\pi_{13} = b^{a13} U^{b13} \rho_f{}^{c13} \sigma_g$

$$M^0L^0T^0 = L^{a13}\left(LT^{-1}\right)^{b13}\left(ML^{-3}\right)^{c13}\left(M^0L^0T^0\right) \tag{3.29}$$

Equating the exponents of M, L, and T on both sides of the equations we get,
$a13 = 0, b13 = 0, c13 = 0$
Therefore the 13th π-term (Eq. 3.30) is,

$$\pi_{13} = \sigma_g \tag{3.30}$$

Hence, the function can be expressed in terms of independent dimensionless parameters as given in Eq. 3.31.

$$f_2\left(\frac{D_{sct}}{b}, \frac{\nu}{bU}, \frac{bg}{U^2}, \frac{\rho_s}{\rho_f}, \frac{d_{50}}{b}, \frac{h_w}{b}, \frac{U_c}{U}, \frac{B}{b}, \frac{t_c}{b}, \frac{b_c}{b}, \frac{h_c}{b}, \frac{Ut}{b}, \sigma_g\right) = 0 \tag{3.31}$$

The above equation can be rewritten as the set of dependent variables as a function of the independent variable given in Eq. 3.32.

$$\frac{D_{sct}}{b} = f_3\left(\frac{bU}{\nu}, \frac{U^2}{bg}, \frac{\rho_s}{\rho_f}, \frac{b}{d_{50}}, \frac{h_w}{b}, \frac{h_c}{b}, \frac{U}{U_c}, \frac{B}{b}, \frac{t_c}{b}, \frac{b_c}{b}, \frac{Ut}{b}, \sigma_g\right) \tag{3.32}$$

In the case of an airfoil collar, we get an extra parameter l_c (collar length), and the temporal scour depth (D_{sct}) around the pier is represented by a functional relationship (Eq. 3.33):

$$f_4\left(D_{sct}, b, b_c, l_c, t_c, h_c, h_w, U, U_c, B, d_{50}, \rho_f, \rho_s, \nu, g, \sigma_g, t\right) = 0 \tag{3.33}$$

Hence, we have 14 numbers of π-terms and 13 of them are similar to what we get for a circular collar. Now we can calculate the 14th π-term (Eq. 3.34) similarly and that is

$$\pi_{14} = \frac{l_c}{b} \tag{3.34}$$

Therefore, the function can be expressed in terms of independent dimensionless parameters as given in Eq. 3.35.

$$f_5\left(\frac{D_{sct}}{b}, \frac{\nu}{bU}, \frac{bg}{U^2}, \frac{\rho_s}{\rho_f}, \frac{d_{50}}{b}, \frac{h_w}{b}, \frac{U_c}{U}, \frac{B}{b}, \frac{t_c}{b}, \frac{b_c}{b}, \frac{l_c}{b}\frac{h_c}{b}, \frac{Ut}{b}, \sigma_g\right) = 0 \tag{3.35}$$

Equation 3.35 can be rewritten as the set of dependent variables as a function of the independent variable given in Eq. 3.36.

$$\frac{D_{sct}}{b} = f_6\left(\frac{bU}{\upsilon}, \frac{U^2}{bg}, \frac{\rho_s}{\rho_f}, \frac{b}{d_{50}}, \frac{h_w}{b}, \frac{h_c}{b}, \frac{U}{U_c}, \frac{B}{b}, \frac{t_c}{b}, \frac{b_c}{b}, \frac{l_c}{b}\frac{Ut}{b}, \sigma_g\right) \tag{3.36}$$

In this study, we focus on the scour mechanism without and with collars positioned within the sediment bed for our analysis. The research objectives and methodology are determined based on a review of the literature and prioritize the most effective pier-collar position given in the following chapter.

CHAPTER – 4

OBJECTIVES AND METHODOLOGY

4.1 Objectives

This study was conducted at the Fluvial Hydraulics Laboratory of the School of Water Resources Engineering at Jadavpur University using a physical hydraulic model. The research focuses on uniform, non-cohesive bed materials and clear-water scour conditions. The main goal is to perform experiments to observe how maximum scour around circular piers changes over time when using two different collar shapes. Specifically, the study aims to reduce scour around circular piers by using either circular or airfoil collars. The primary objectives are:

- To observe the development of scour depth over time around circular piers with collars and compare it to the scour depth around isolated piers without collars. One experiment was conducted without a collar, along with five experiments using circular piers with circular collars, and another five using airfoil collars. These experiments were performed with a fixed pier diameter of 7 cm, a constant inflow depth of 11.5 cm, and a constant discharge of 25.5 l/s while varying the width of the circular collar and both the width and length of the airfoil collar.
- To observe the scour morphology in each experiment and compare it to the scour morphology in the isolated pier experiment without a collar.
- To observe the sediment transport and different scour dimensions for each experiment with collar and compare those with that for an unprotected pier.
- To find a robust machine learning model to well represent the time series data which can easily be used to accurately estimate the temporal variation of scour for such an arrangement.
- To compare the effectiveness and applicability of the present machine learning model over the empirical equation developed in the previous literature.
- To propose an empirical equation to calculate the temporal scour depth around a circular pier fitted with a circular collar using the non-linear regression method and compare it with the equations proposed in the previous literatures.

4.2 Methodology

4.2.1 Methods for Flow Conditions

The critical condition for bed material movement was checked before each experiment using the following steps:

- The flow depth in the flume was adjusted by a tailgate. The approaching flow depth (h_w) was maintained at 0.115 m for all the tests by operating the tailgate. The bed slope (S_o) was kept constant at 1:2400 for all the experiments.
- The water discharge was measured by a flow meter connected to the upstream pipe at the inlet of the flume and that discharge was kept constant at 25.5 l/s.
- The depth-averaged approaching flow velocity (U) was estimated using Manning's equation (Eq. 4.1),

$$U = \frac{1}{n} R^{\frac{2}{3}} S_o^{\frac{1}{2}} \tag{4.1}$$

Here, the coefficient of roughness (n) was determined by using Strickler's formula (Eq. 4.2).

$$n = \frac{1}{24} d_{50}^{\frac{1}{6}} \tag{4.2}$$

- Considering steady uniform flow in a rectangular flume, the bed shear stress (τ_o) can be expressed as $\tau_o = \rho_f g R \sin\alpha$, where ρ_f is the mass density of the fluid, g is the gravitational acceleration, R is the hydraulic radius, and α is the angle between the longitudinal sloping bed and horizontal direction.
- The critical bed shear stress (τ_{oc}) was determined using the expression $\tau_{oc} = \Theta_c \Delta \rho_f g d_{50}$, where $\Delta = S\text{-}1$, Θ_c is the critical Shields parameter and is calculated using the following van Rijn's empirical equations (Eq. 4.3) for the Shields curve (van Rijn, 1984):

$$\Theta_c = \begin{cases} 0.24 / D_* & D_* \le 4 \\ 0.14 / D_*^{0.64} & 4 < D_* \le 10 \\ 0.04 / D_*^{0.10} & 10 < D_* \le 20 \\ 0.013 D_*^{0.29} & 20 < D_* \le 150 \\ 0.055 & 150 < D_* \end{cases} \tag{4.3}$$

where D_* is the dimensionless particle parameter, expressed as $D_* = d_{50}(\Delta g/\nu^2)^{1/3}$. The value of D_* was estimated as 18.24 in this study. The critical bed shear stress (τ_{oc}) was calculated as 0.3457 N/m^2.

- The critical velocity (U_c) was calculated from Eq. 4.3.

$$\frac{U_c}{U_{*c}} = 5.75 \log\left(\frac{h_w}{2d_{50}}\right) + 6 \tag{4.3}$$

where, U_{*c} is the critical shear velocity, expressed as $U_{*c} = (\tau_o/\rho)^{0.5}$. Finally, the critical discharge (Q_c) was determined using the continuity equation. The critical shear flow Reynolds number, R_{*c} (= $U_{*c}R/\nu$) was determined at 20°C temperature of water.

- Figure 4.1 shows the experimental results of Shields which relate critical Shields parameters Θ_c and R_{*c} and is known as the Shields diagram (1936). The threshold of sediment motion occurs when $\Theta > \Theta_c$ or, $\tau_{oc} > \tau_{oc}$ or, $U_* > U_{*c}$. From Fig. 4.1, it is clear that the discharge during each test run was lower than the minimum discharge required for the incipient motion or threshold conditions of the bed particles. Therefore, it can be said that all the experiments were carried out under clear water scour conditions.

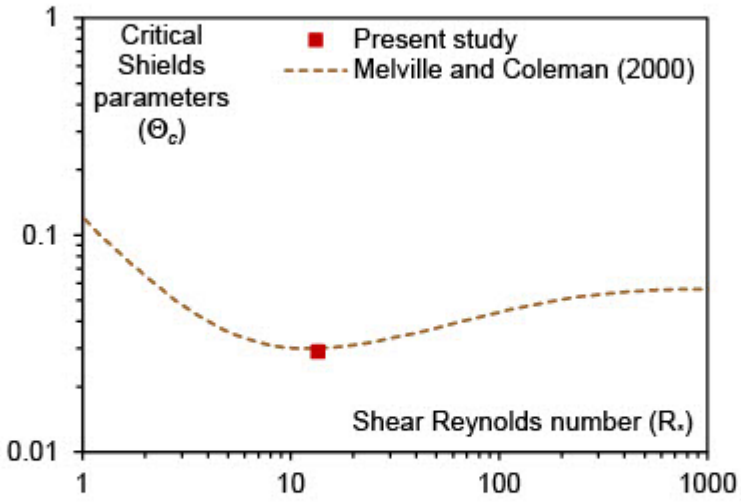


Fig. 4.1 Shields diagram showing the clear water condition for the present study.

- The flow intensity (U/U_c) was maintained at 0.87 to satisfy clear-water scour conditions. It was determined from the measured vertical profile of the approaching flow velocity 2 m upstream of the pier, that the presence of the pier did not affect the approaching flow. To satisfy clear water scour conditions, average bed shear stress (τ_{oc}) must be less than or equal to critical bed shear stress (τ_{oc}).

4.2.2 Methods for selection of pier dimension

The selection criteria for this study were based on a review of previous research. One important consideration was ensuring a negligible side wall effect, which occurs when the constriction ratio (B/b) ≥ 10, according to Chiew and Melville (1987). In this study, we chose a pier diameter (b) of 7 cm because the flume width (B) is 0.81 meters, meeting the required criteria. Table 4.1 provides details on the constriction ratios (B/b) used in previous studies, as well as the conditions applied in our current research.

Table 4.1 Specification of pier and flume dimensions in the literature studies.

Literature	Selected pier diameter (b) (cm)	Flume width (B) (m)	B/b
Tanaka and Yano (1967)	3	–	–
Ettema (1980)	4.5	0.46	10.22
Darghi (1990)	15		
Chiew (1992)	3.2	0.3	9.38
Kumar et al. (1999)	6.1, 11.25	1	16.39, 8.89
Singh et al. (2001)	2.5, 6.2	–	–
Mashahir et al. (2004)	4	0.75	18.75
Garg et al. (2005)	6.2	0.6	9.68

Zarrati et al. (2006)	4	0.75	18.75
Alabi (2006)	11.5, 7.3	1.22	10.61,16.71
Mashahir et al. (2009)	4	0.74	18.5
Moncada-M et al. (2009)	7.3	0.5	6.85
Zarrati et al. (2010)	4	0.41	10.25
Izadinia et al. (2012)	4	0.4	10
Tafarojnoruz et al. (2012)	4	0.485	12.13
Jahangirzadeh et al. (2014)	3	0.3	10
Khodashenas et al. (2018)	2.5	0.3	12
Tabarestani et al. (2019)	7	0.75	10.71
Wang et al. (2019)	10	2	20
Pandey et al. (2020)	6.6, 8.4	1	15.15, 11.9
Pandey et al. (2022)	6.6, 8.4	1	15.15, 11.9
Kassem et al. (2023)	6	0.77	12.83
Gupta et al. (2023*a*)	6	0.8	13.33
Gupta et al. (2023*b*)	5, 6	0.8	16, 13.33
Gupta et al. (2024)	6	0.8	13.33
Present Study	7	**0.81**	**11.57**

4.2.3 Methods for selection of collar dimensions

The criteria for choosing the collar diameter (b_c) in this study were based on a review of previous research. Various research groups have used different collar diameters relative to the pier diameter (b), as shown in Table 4.2 for circular collars and Table 4.3 for airfoil collars. Based on this review, we selected collar diameters (b_c) for both circular and airfoil piers, and the length of the collar (l_c), to align with those used in previous studies. This ensures that our study employs effective and proven ranges, allowing for comparison and consistency with established methods. Additionally, the collar elevation was kept at the bed level, as previous research demonstrated that this positioning achieved around 90% efficiency in reducing scour compared to cases without collars.

Table 4.2 The collar (circular) diameter adopted by different research groups

Literature	**Pier diameter (b) (cm)**	**Collar diameter (b_c)**	**Collar elevation (h_c/h_w)**	**Collar thickness (t_c) (mm)**
Chiew (1992)	3.2	2b, 3b	–	1
Kumar et al. (1999)	11.3	1.5b, 2b, 2.5b, 3b, 4b	0	3
	6.1	2.5b		
Singh et al. (2001)	2.5, 6.2	1.5b, 2b, 2.50b	–	–
Mashahir et al. (2004)	4	3b	0	–

Garg et al. (2005)	6.2	1.5*b*, 2*b*, 3*b*	-0.19 – 0.19	–
Alabi (2006)	11.5	3*b*	0	5
	11.5, 7.3	2*b*, 3*b*		
Zarrati et al. (2006)	4	3*b*	0	2
Mashahir et al. (2009)	4	3*b*	0	2
Moncada-M et al. (2009)	7.3	2*b*, 3*b*	[a] -6, -3, 0, 3, 6, 9	2
Zarrati et al. (2010)	4	2*b*, 3*b*	0	–
Izadinia et al. (2012)	4	3*b*	0	–
Tafarojnoruz et al. (2012)	4	3*b*	0	5
Jahangirzadeh et al. (2014)	3	2*b*, 2.5*b*, 3*b*, 3.5*b*	-0.125, 0, 0.125	0.8
Tabarestani et al. (2019)	7	3*b*	0	2
Khodashenas et al. (2018)	7	1.5*b*, 2*b*, 2.5*b*	-0.1, 0, 0.1	1
Wang et al. (2019)	10	1.5*b*, 2*b*, 2.5*b*, 3*b*	-0.04, 0, 0.04, 0.1	5
Pandey et al. (2020)	6.6, 8.4	1.5*b*, 2*b*, 2.3*b*	0, 0.25, 0.5, 0.75	3
Pandey et al. (2022)	6.6, 8.4	1.5*b*, 2*b*, 2.3*b*	0, 0.25, 0.5, 0.75	–
Kassem et al. (2023)	6	3*b*	0	–
Gupta et al. (2024)	6	1.5*b*, 2*b*, 2.5*b*, 3*b*	0, 0.25, 0.5, 0.75	–
Present Study	**7**	**1.5*b*, 2*b*, 2.5*b*, 3*b*, 3.5*b***	**0**	**7**

[a] h_c given in cm since corresponding flow depths (h_w) were not provided in the literature

Table 4.3 The collar (airfoil) diameter and the length adopted by different research groups

Literature	**Pier diameter (*b*) (cm)**	**Collar diameter (b_c)**	**Collar length (l_c)**	**Collar elevation (h_c/h_w)**	**Collar thickness (t_c) (mm)**
Gupta et al. (2023*a*)	6	1.5*b*, 2*b*, 2.5*b*, 3*b*	$2b_c$	0, 0.25, 0.5, 0.75	4
Gupta et al. (2023*b*)	5, 6	1.5*b*, 2*b*, 2.5*b*, 3*b*	$2b_c$	0, 0.25, 0.5, 0.75	4
Present Study	**7**	**1.5*b*, 2*b*, 2.5*b*, 3*b*, 3.5*b***	**$2b_c$**	**0**	**7**

4.2.4 Instruments Used for Measurements

Different instruments have been used to measure experimental data. To control the discharge into the flume, measuring the temporal scour depth around the pier, measuring the scour bed profile after the experimental run, to taking pictures of experiments, specific instruments were used and these measuring methods are discussed in the following sections.

Acoustic Doppler Velocimeter

The Vectrino, a high-resolution acoustic Velocimeter, is utilized for assessing turbulence and 3D water velocity across various settings, spanning from laboratory experiments to river and oceanic studies. Its fundamental measurement principle relies on coherent Doppler processing, ensuring accurate data output without significant zero offsets. In our investigation, we utilize an Acoustic Doppler Velocimeter to monitor the temporal evolution of scour depth, depicted in Fig. 4.2. The specific model employed is the VECTRINO PROFILER FIXED PROBE 10 MHz (Model Number: 4198-1-131), with the probe identified as VON 9619 and the hardware designated as VNO 1617 Uw housing.

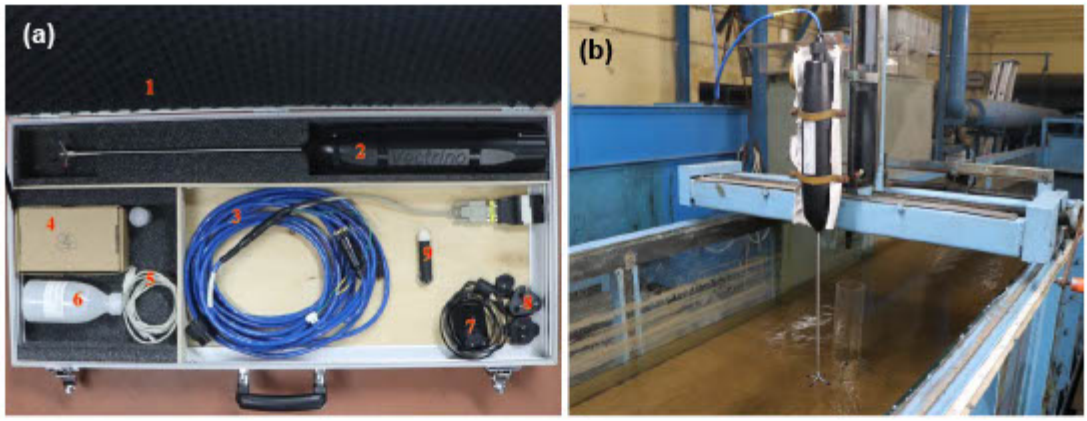


Fig. 4.2 (a) The components of the acoustic Doppler velocimeter. (1) Transportation and storage case; (2) Vectrino velocimeter; (3) External power/signal cable; (4) Tool kit, Nortek; (5) USB to serial converter; (6) Seeding material (bottle of 250 ml); (7) AC/DC voltage transformer, 24 V DC; (8) International kit with AC plugs; (9) USB memory stick with Vectrino software, and **(b)** measurement using ADV during experimentation.

Laser Distance Meter

Laser distance meters are utilized to accurately measure the distance between objects without physical contact, employing laser technology for this purpose. The grid points were measured using a Laser Distance Meter, specifically the DISTOTM D110 model, as shown in Fig. 4.3. It is important to note that these measurements were taken after the sand bed had been thoroughly dried. This ensured the accuracy and reliability of the grid point data.



Fig. 4.3 Laser Distance Meter.

Flow Meter

A Flow Meter is an essential device for monitoring and measuring the fluid flow, pressure, or discharge in both liquid and gas systems. It plays a critical role in numerous industries, facilitating accurate management and control of fluid dynamics. In the present study, we used a flow meter to measure the flow discharge (Q), as shown in Fig. 4.4. Specifically, we used the DASMESH analog flow meter, ensuring the acquisition of precise and reliable data for our analysis.



Fig. 4.4 Flow Meter.

4.2.5 Method for Predictive Modelling of Scour Depth: CART

Classification and Regression Trees (CART) is a variation of the decision tree algorithm that can handle both classification and regression tasks. MINITAB employs the Classification and Regression Tree (CART) algorithm for training models, which can be accessed via *Stat* > *Predictive Analytics* > *CART® Regression*. Initially introduced by Breiman et al. (1984), CART is a supervised learning algorithm that uses labeled data to make predictions on new, unseen data.

For regression tasks, CART constructs a tree-like model to predict continuous target variables. This model consists of nodes representing decision points and branches depicting the possible outcomes of these decisions. Each leaf node in the tree holds the predicted value for the target variable.

The regression CART algorithm operates by recursively splitting the training data into smaller subsets based on specific criteria, aiming to minimize the residual sum of squares within each subset. This recursive partitioning continues until the data is appropriately segmented to accurately predict the target variable.

Residual Reduction: Residual reduction measures how much the average squared difference between predicted and actual target values decreases after a split. A lower residual reduction indicates a better fit of the model to the data.

Splitting Criteria: CART evaluates all possible splits at each node and chooses the one that most reduces the residual error. This process repeats until a stopping criterion is met, such as a maximum tree depth or a minimum number of instances in a leaf node.

CART has several *advantages:* it produces simple and easy-to-understand results, and as a nonparametric and nonlinear method, it handles diverse data types effectively. It implicitly performs feature selection and is robust to outliers. Additionally, CART requires minimal supervision. However, CART also has *limitations:* it is prone to overfitting, has high variance and low bias, and the resulting tree structure can be unstable.

CART is often preferred over traditional regression models because of its ability to handle complex, nonlinear relationships and interactions without requiring explicit specification. It is robust to outliers and can automatically select important variables. It offers a more intuitive, interpretable model through its decision tree structure. Unlike traditional regression, which may require complete datasets and transformation of categorical variables, CART can manage missing data effectively and handle both continuous and categorical variables easily. Such features make CART a flexible and powerful option, particularly for datasets with complexities that traditional regression models find challenging to handle effectively (Breiman et al., 1984; Loh, 2011).

4.2.6 Statistical Indices for Model Evaluation

Coefficient of Determination (R^2)

It is a statistical measure indicating how well independent variables explain the variation in the dependent variable in a machine learning/regression model. The range of R^2 lies from 0 to 1, where 1 signifies a perfect fit (ideal value) given in Eq. 4.1.

It quantifies how much of the variance in one variable is explained by another. As an example, $R^2 = 0.50$ means 50% of the variation in the dependent variable is explained by the model's inputs. Higher R^2, suggests a better fit, important for evaluating predictive models in finance, economics, and social sciences. High R^2 does not imply causation; other statistical measures should be used to assess model performance and reliability.

$$R^2 = \left[\frac{N\sum_{i=1}^{N}\left(\frac{D_{sct}}{b}\right)_{oi}\left(\frac{D_{sct}}{b}\right)_{ci} - \sum_{i=1}^{N}\left(\frac{D_{sct}}{b}\right)_{oi}\sum_{i=1}^{N}\left(\frac{D_{sct}}{b}\right)_{ci}}{\sqrt{N\sum_{i=1}^{N}\left(\frac{D_{sct}}{b}\right)_{oi}^{2} - \left\{\sum_{i=1}^{N}\left(\frac{D_{sct}}{b}\right)_{oi}\right\}^{2}}\sqrt{N\sum_{i=1}^{N}\left(\frac{D_{sct}}{b}\right)_{ci}^{2} - \left\{\sum_{i=1}^{N}\left(\frac{D_{sct}}{b}\right)_{ci}\right\}^{2}}} \right]^2 \quad (4.1)$$

where, $(D_{sct}/b)_o$ and $(D_{sct}/b)_c$ are observed and computed temporal scour depths.

Root Mean Squared Error (RMSE)

The RMSE is a widely used metric for measuring the accuracy of a regression model. It represents the square root of the average squared differences between the predicted values and the observed values, as shown in Eq. 4.2.

RMSE is always non-negative, with lower values indicating a better fit of the model to the data. An RMSE value of 0 signifies a perfect fit (ideal value), meaning the model's predictions exactly match the actual observations and the worst value is ∞. RMSE is particularly useful for understanding the magnitude of prediction errors and is commonly used in fields such as finance, economics, and environmental modeling to evaluate model performance. While RMSE provides insight into the overall accuracy of a model, it is important to consider other metrics to fully assess the model's reliability and predictive power.

$$\text{RMSE} = \sqrt{\frac{1}{N}\sum_{i=1}^{N}\left\{\left(\frac{D_{sct}}{b}\right)_{oi} - \left(\frac{D_{sct}}{b}\right)_{ci}\right\}^2} \quad (4.2)$$

Mean Absolute Deviation (MAD)

Mean absolute deviation (MAD) is a measure of the average absolute distance between each data point and the mean of a data set, as given in Eq. 4.3. Similar to standard deviation, MAD is a parameter or statistic that measures the spread, or variation, in the data. Larger MAD values indicate that data points are more spread out from the average, while smaller values mean that the data points are closer together. Lower MAD values indicate that the data points are close to the average and have low variability, which could suggest reliability, stability, or homogeneity. Conversely, high MAD values mean that the data points are more spread out from the mean and have high variability, which could suggest noise, instability, or heterogeneity. MAD is always non-negative, with lower values indicating a better fit of the model to the data.

The definition of the Mean Absolute Deviation (MAD) seems similar to that of the standard deviation (SD), as both measure variability. However, they are calculated differently. Recently, some advocates have argued that MAD should replace SD as the primary measure of variability because it is simpler to understand and may better reflect real-world scenarios.

$$\mathrm{MAD} = \frac{1}{N}\sum_{1}^{N}\left|\left(\frac{D_{sct}}{b}\right)_{ci} - \overline{\left(\frac{D_{sct}}{b}\right)_{c}}\right| \tag{4.3}$$

Mean Absolute Error (MAE)

Mean Absolute Error (MAE) quantifies the average magnitude of errors in a set of predictions without considering their direction. It is the average absolute difference between predicted and actual values as given in Eq. 4.4. Unlike RMSE, MAE does not square the errors, so it does not penalize larger errors as severely. In a range of [0, ∞), the smaller the value of MAE the better. A MAE value of 0 represents the perfect fit of a model.

$$\mathrm{MAE} = \frac{1}{N}\sum_{1}^{N}\left|\left(\frac{D_{sct}}{b}\right)_{oi} - \left(\frac{D_{sct}}{b}\right)_{ci}\right| \tag{4.4}$$

MAE is less sensitive to outliers compared to RMSE. While RMSE squares the errors before averaging, giving more weight to large deviations, MAE treats all errors equally by using their absolute values. This makes MAE a more reliable metric in datasets with outliers or high variability. However, if the test set contains many outliers, the model performance will be mediocre. MAE is also easier to interpret since it is expressed in the same units as the data. For instance, if the MAE for predicting a product's price is 5, it means that, on average, predictions are off by 5 units of currency. This straightforward interpretation helps in understanding the performance of the model more intuitively.

CHAPTER – 5

EXPERIMENTAL PROCEDURE

5.1 Experimental Setup

The experimental arrangement, data acquisition system, and variables measured in the model study are described. Typical investigation of scour depth development around a bridge pier model has been carried out through various experiments. The experimental setup of the present study and conditions of the work given in Table 5.1 are described in detail in this chapter. All the experiments were conducted in the Fluvial Hydraulics laboratory of the School Water Resources Engineering department at Jadavpur University in Kolkata, West Bengal, India. Table 5.2 provides a detailed summary of the experimental setups and conditions adopted in previous literature. This table highlights the parameters used in prior research, offering a comprehensive overview of how experiments were conducted across different investigations.

Table 5.1 Details of the experiments conducted with a pier of diameter, $b = 7$ cm keeping the collar on the bed ($h_c = 0$)

Exp. No.	Pier/ Collar Shape	b_c (cm)	l_c (cm)	B (m)	h_w (cm)	d_{50} (mm)	Q (l/s)	U (cm/s)	U/U_c	σ_g	S	Fr
1	Circular / –	–	–	0.81	11.5	0.724	25.5	27.38	0.87	1.94	2.63	0.258
2		10.5	–	0.81	11.5	0.724	25.5	27.38	0.87	1.94	2.63	0.258
3	Circular	14.0	–	0.81	11.5	0.724	25.5	27.38	0.87	1.94	2.63	0.258
4	/	17.5	–	0.81	11.5	0.724	25.5	27.38	0.87	1.94	2.63	0.258
5	Circular	21.0	–	0.81	11.5	0.724	25.5	27.38	0.87	1.94	2.63	0.258
6		24.5	–	0.81	11.5	0.724	25.5	27.38	0.87	1.94	2.63	0.258
7		10.5	21	0.81	11.5	0.724	25.5	27.38	0.87	1.94	2.63	0.258
8	Circular	14.0	28	0.81	11.5	0.724	25.5	27.38	0.87	1.94	2.63	0.258
9	/	17.5	35	0.81	11.5	0.724	25.5	27.38	0.87	1.94	2.63	0.258
10	Airfoil	21.0	42	0.81	11.5	0.724	25.5	27.38	0.87	1.94	2.63	0.258
11		24.5	49	0.81	11.5	0.724	25.5	27.38	0.87	1.94	2.63	0.258

Table 5.2 Experimental setup adopted by different research groups

Literature	($L\times W\times D$) (m^3)	($L_w\times W_w\times D_w$) (m^3)	# (m)	d_{50} (mm)	h_w (cm)	Q (m^3/s)	U/U_c or U_*/U_{*c}	σ_g	S	t_m (hrs)
Chiew (1992)	8×0.3×0.45	–	–	0.33	18	–	0.9	–	2.65	72
Kumar et al. (1999)	30×1×0.60	2×1×0.90	11	0.78, 1.18, 1.54	–	–	0.75-0.98	–	–	–
Singh et al. (2001)	–	–	–	0.285	–	–	–	2.51	–	5
Mashahir et al. (2004)	10×0.75×0.55	–	–	0.95	13-14	0.03-0.04	0.92	<1.2	–	44, 90
Garg et al. (2005)	12×0.6×0.75	–×0.6×0.3	–	0.28	15.63-16.8	0.019	–	2.51	–	5
Zarrati et al. (2006)	12×0.75×0.8	2×0.75×0.25	6.5	0.95	19.5	0.05	0.9	–	–	90
Alabi (2006)	20×1.22×0.61	12.43×1.22×0.16	5.64	0.53	14.6-23	0.044-0.07	0.7-0.89	1.23	2.65	49-955
Moncada-M et al. (2009)	8.5×0.5×0.5	–	–	1.4	11.84-19.74	0.0145-0.0384	–	–	–	6
Mashahir et al. (2009)	10×0.74×–	–×0.75×–	6	0.95	12	0.028	0.92	<1.2	–	44, 90
Zarrati et al. (2010)	6.5×0.41×–	1.2×0.41×0.2	3	0.72	24	0.024	–	1.13	2.65	56, 70
Izadinia et al. (2012)	8×0.4×0.6	1.6×0.4×0.15	4	0.72	16	0.0192	0.9	1.12	–	12, 50
Tafarojnoruz et al. (2012)	9.66×0.485×–	1.5×0.485×0.205	6.05	0.76	10	0.0127	0.92	1.46	2.67	72-120
Jahangirzadeh et al. (2014)	12×0.3×0.45	–×0.3×0.15	–	0.8	12	0.012	0.95	1.37	2.65	72
Khodashenas et al. (2018)	10×0.3×0.5	1.5×0.3×0.16	5	0.8	10.5	0.01	0.9	–	–	15
Tabarestani et al. (2019)	14×0.75×0.6	–	8	0.67	–	–	0.99	1.2	2.65	–
Wang et al. (2019)	60×2×1.8	7.5×2×0.35	–	0.324	50	0.35	1.15	–	2.65	2
Pandey et al. (2020)	24×1×0.3	4×1×0.25	12	0.27	12	0.018-0.0264	0.64-0.9	1.22	–	20
Pandey et al. (2022)	20×1×–	8×1×0.38	7	0.27, 0.4	12	0.0264	0.62-0.88	1.23, 1.2	–	24
Kassem et al. (2023)	12×0.77×0.6	4×0.77×0.2	6	0.8	8.5	0.02	0.93	1.44	2.65	4
Gupta et al. (2023*a*)	15.3×0.8×0.4	2.3×0.8×0.4	7	0.32	10	0.02	0.95	1.31	–	9
Gupta et al. (2023*b*)	10.3×0.8×0.5	2.3×0.8×0.5	4	0.32	10	0.016, 0.020	0.98	1.31	2.65	8-10
Gupta et al. (2024)	10.3×0.8×0.5	2.3×0.8×0.5	4	0.32	12	0.024	0.95	1.31	2.65	10
Present Study	**11×0.81×0.6**	**3×0.81×0.2**	**2.9**	**0.724**	**11.5**	**0.026**	**0.87**	**1.94**	**2.63**	**3-9.7**

Note: (–) indicates the missing value or not given in the manuscript; # - indicates the distance of the working section from the flume inlet gate. ($L\times W\times D$) indicates length, width, and depth of flume, ($L_w\times W_w\times D_w$) indicates length, width, and depth of working section, d_{50} is median size of sediment, h_w is approaching flow depth, Q is the discharge of flow, U/U_c is flow intensity, σ_g is geometric standard deviation, S is the relative density of sand, t_m is experimental run time.

5.1.1 Tilting Flume

All the experiments were carried out in a recirculating tilting flume (Fig. 5.1) with a length of 11 m, a width of 0.81 m, and a depth of 0.60 m. The working section of the flume was filled with sand of a uniform thickness of 0.20 m. The length of the sand bed was 7 m and the width was 0.81 m. The sand bed was located 2.9 m upstream from the flume inlet to make the fully developed flow. The working section of the flume was made up of a steel bottom and Plexiglas side walls along two sides for most of its length to facilitate visual observations. A movable trolley equipped with a vernier point gauge was positioned on the flume. A vertical scale was fixed to the point gauge to measure the water level, initial bed level, and scour depth. The recirculating flow system was served by a centrifugal pump located at the upstream end of the tilting flume. The experimental setup is described with the help of the schematic diagram as shown in Fig. 5.2.



Fig. 5.1 Tilting flume used during the experimentation.

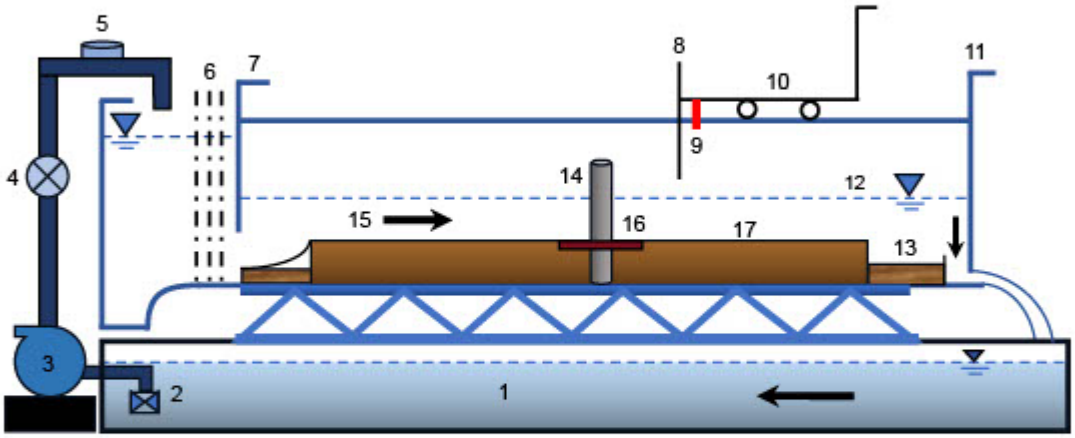


Fig. 5.2 Schematic diagram of tilting flume with pier-collar arrangement: 1. Reservoir, 2. Check valve or foot valve, 3. Pump, 4. Control valve, 5. Flow meter, 6. Baffle plate, 7. Inlet gate, 8. Point gauge, 9. Laser distance sensor, 10. Movable trolley, 11. Outlet gate, 12. Water level, 13. Collector, 14. Pier, 15. Flow direction, 16. Collar fixed on bed level, 17. Sand bed.

5.1.2 Pump

The hydraulic machines which convert mechanical energy into hydraulic energy are called pumps. The hydraulic energy is in the form of pressure energy. In the present study, the recirculating flow system was served with a 10hp variable-speed centrifugal pump (Fig. 5.3) located at the upstream end of the tilting flume. The pump operated at a rotational speed of 1,430 RPM, had a power capacity of 7.5 kW, and a maximum discharge rate of 25.5 L/s. Water discharge was measured using a flow meter connected to the upstream pipe at the flume's inlet. Water flowed directly into the flume through a 0.2-meter diameter pipeline. There were two pumps for alternative use.



Fig. 5.3 Pump used to recirculate the flow.

5.1.3 Circular pier

In the present study, we have used a circular pier constructed using Perspex sheets. One circular pier of diameter of 7 cm (Fig. 5.4) has been used for all the experiments.



Fig. 5.4 Circular Pier of 7 cm diameter.

The height of the pier was 45.6 cm. We have chosen this dimension based on previous studies. According to Chiew and Melville (1987), the pier diameter should not exceed 10% of the internal width of the channel. This guideline was kept in mind during the experiments to avoid the wall friction factor and prevent the flume sidewalls from influencing the scour pattern around the piers.

5.1.4 Circular and Airfoil Collars

In this study, circular and airfoil collars of different sizes made from Perspex sheets (Fig. 5.5b and Fig. 5.6b) were used for the experiments. Circular and airfoil collars of 10.5, 14, 17.5, 21, and 24.5 cm diameters were used, and the lengths of the airfoil collars were 21, 28, 35, 42, and 49 cm, respectively.

The dimensions and specifications of the collars are provided in Tables 4.3 and 4.4 in the previous section. The schematic diagram of the pier and collar showing each component is given in Fig. 5.5(a) and Fig. 5.6(a).

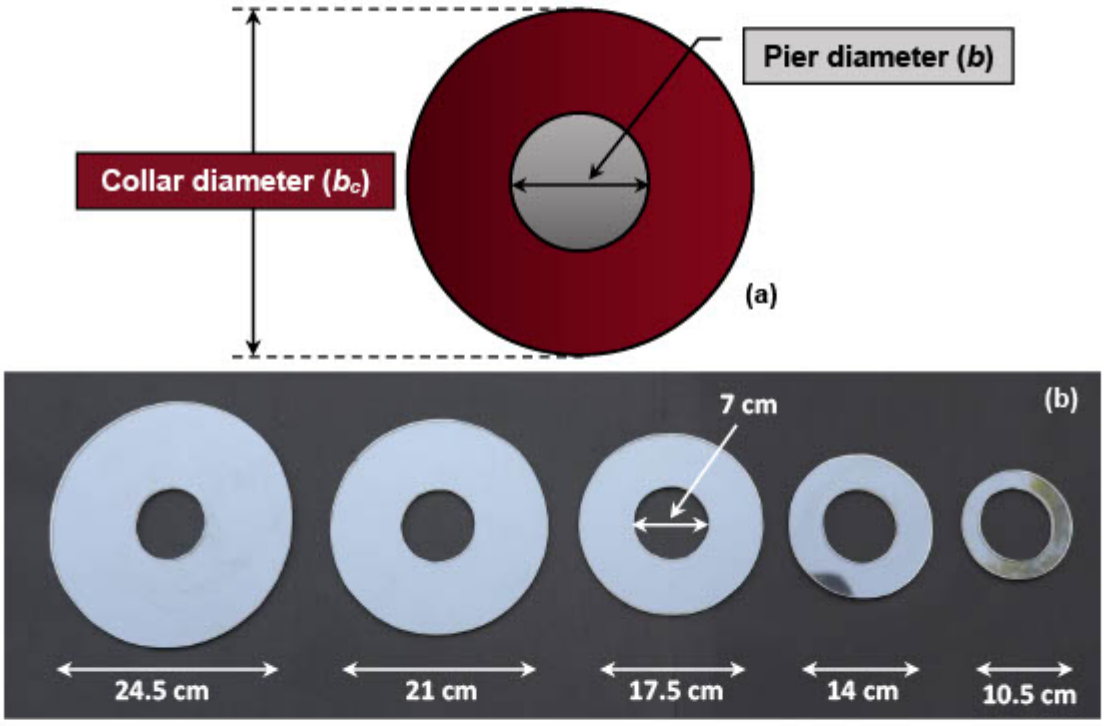


Fig. 5.5 (a) Plan view showing the schematic diagram of a circular pier with a circular collar and **(b)** Physical models of circular collars of different sizes made by the perspex sheet.

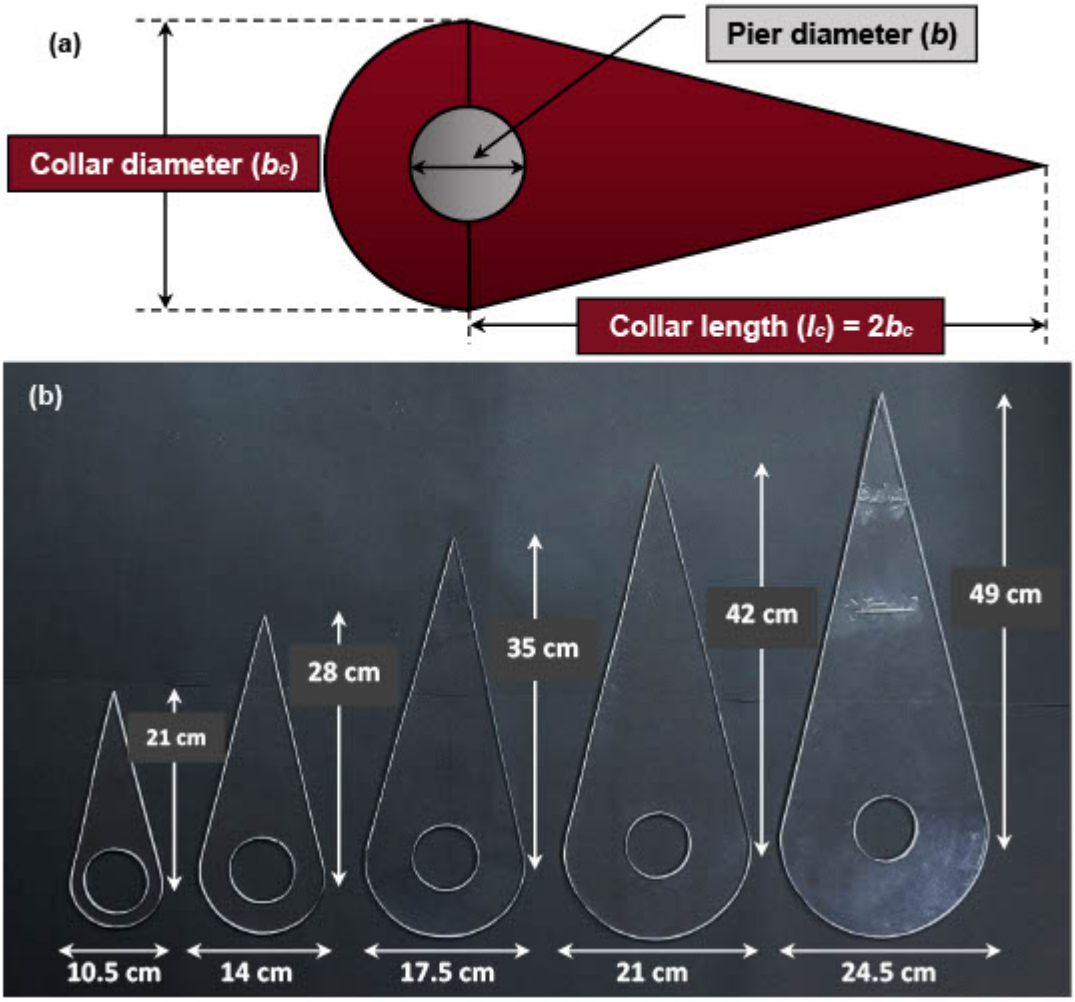


Fig. 5.6 (a) Plan view showing the schematic diagram of a circular pier with an airfoil collar and **(b)** Physical models of airfoil collars of different sizes made by the perspex sheet.

5.1.5 Pier-collar arrangement

In this study, circular piers were fitted with both circular and airfoil collars to test how well they reduce clear-water scour in coarse sand. The collars were made from perspex sheets. The dimensions and details of the collars are listed in Tables 4.2 and 4.3 and also shown in Fig. 5.5b and Fig. 5.6b. The diagram showing the pier and collar arrangement is represented in Fig. 5.7. The experiments were conducted in uniform, clear-water scour conditions over a coarse sand bed to see how effectively each collar shape reduces scour around the piers. Different widths and shapes of collars were used to compare their performance and find the best design for minimizing scour.

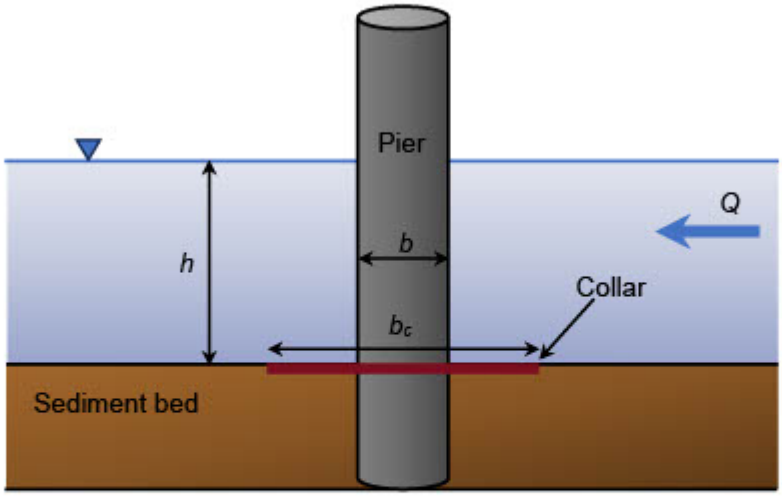


Fig. 5.7 Schematic diagram showing the elevation view of Pier-Collar arrangement.

5.1.6 Sand Bed

A series of tests were conducted to characterize the sand bed material present in the flume used for the present study in the laboratory. The soil tests carried out included a vibrating sieve analysis and specific gravity measurement. The results of the tests showed that the bed material consists of cohesionless sand with a relative density (S) of 2.63. From the sieve analysis test, the median diameter of sand (d_{50}) was determined as 0.724 mm, d_{16} as 0.5 mm, d_{84} as 1.62 mm, and d_{90} as 1.78 mm. Based on the gathered data from the sieve analysis, a plot was generated to visualize the particle size distribution as given in Fig. 5.8. The geometric standard deviation of sediment size (σ_g) was calculated to be 1.94. According to Raudkivi (1998), the sand can be considered uniform when $\sigma_g < 2$, which implies that the sand used in the present study is of uniform size distribution.

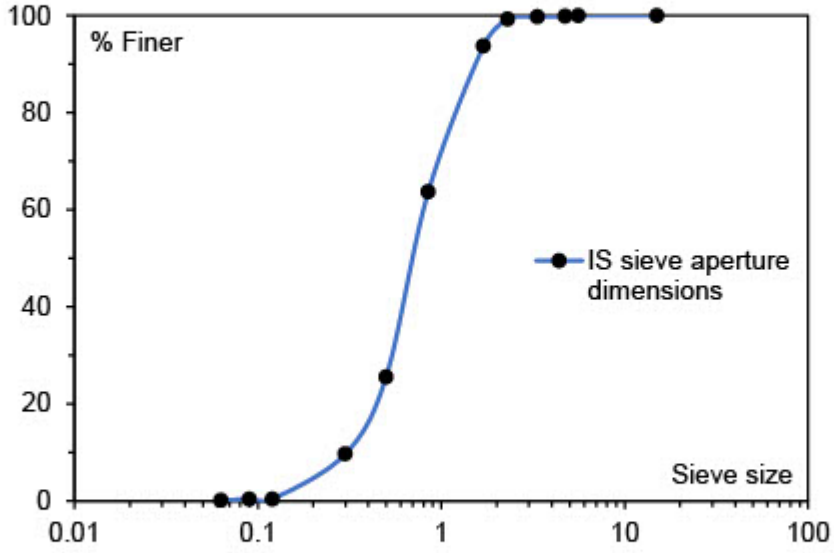


Fig. 5.8 Grading curve for the present study to determine the d_{50}.

The pier diameter was also carefully chosen so that sediment size had a negligible effect on the scour depth. When $b/d_{50} > 50$, the impact of sediment size on the depth of the scour hole becomes negligible (Chiew and Melville, 1987). For the present study, $b/d_{50} = 96.69$, which more than satisfies the criterion of Chiew and Melville (1987).

After placing the piers in the proper position with proper alignment a flat sand bed was prepared (Fig. 5.9). A very good experiment requires a properly prepared flat sand bed, which is essential for attaining more accurate experimental results. A 3 m long and 0.81 m wide flat sand bed was prepared and the level of the sand bed was checked with spirit level. The sand bed preparation was done for every new setup of piers arrangement.

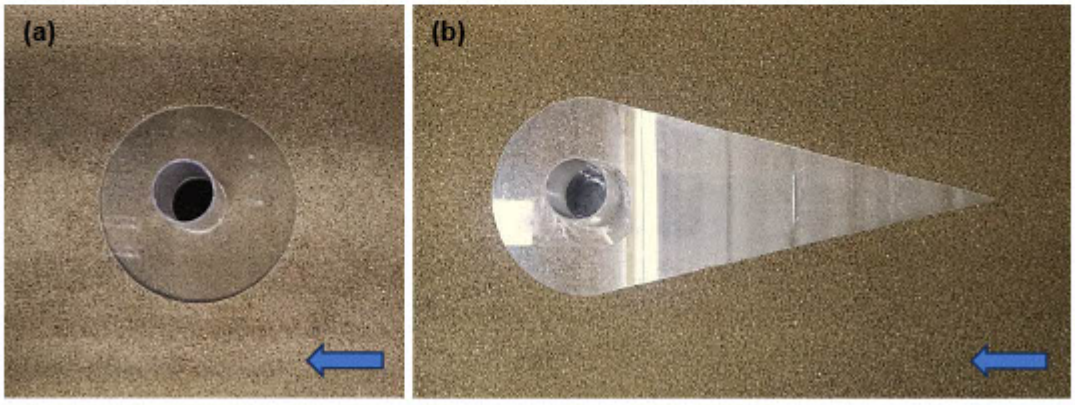


Fig. 5.9 Leveled sand bed **(a)** circular collar and pier arrangement, and **(b)** airfoil collar and pier arrangement.

5.2 Experimental Procedure

In the present study, an investigation of scour depth around a circular pier with and without collar has been carried out. The experimental setup and conditions for the study are described in detail previously in Table 5.1. Now, the experimental procedure for each test is narrated below.

- The experiments were carried out in a recirculating flume. The flume bed was filled with sand to a uniform thickness of 0.20 m, a length of the sand bed of 3 m, and a width of 0.81 m. The sand bed was located 2.9 m upstream from the flume inlet. The recirculating flow system was served by a centrifugal pump which was located at the upstream end of the tilting flume. The water discharge was measured by a flow meter connected to the upstream pipe at the inlet of the flume and it was kept constant at 25.5 l/s. Water flowed through a 0.2 m diameter pipe line which runs directly into the flume.
- The average bed shear stress was 0.26 Pa and the angle of repose of bed sand and critical bed shear stress were estimated at 360 and 0.35 Pa respectively. The flow depth in the flume was adjusted by operating a tailgate and was kept constant at 11.5 cm. The depth-averaged approaching flow velocity was found from the measured vertical profile of the approaching flow velocity at 2 m upstream of the pier where the presence of the pier did not affect the approaching flow. Froude number (Fr) flow Reynolds number (Re) and pier

Reynolds number ($Re_p = Ub/v$) for all the experiments were calculated as 0.258, 2.4×10^4, and 1.9×10^4 respectively.

- The pier was first installed in the flume at the desired location. Before each test, care is taken to level the sand bed throughout the entire length of the flume. First of all, we have to produce a sand bed having a smooth, uniform surface. For this purpose, we used a spirit level to check the uniformity of the bed surface. The uneven bed surface is leveled using a hand trowel. After that, we measured the bed level by point gauge randomly to check the leveling of the flume. The sand bed preparation is the very key as far as the experiment is concerned. Unevenness or defect in the channel bed can compromise the accuracy of the experimental results.
- During each experiment, it was kept in mind that the width of the experimental flume is more than seven times the pier width (b) to avoid the effect due to the wall friction. The minimum value of the ratio between flume width and pier width is 6.25, proposed by Raudkivi and Ettema (1983) that could be used without a measurable effect from the side walls on the local scour at the pier.
- To start the test, the flume was slowly filled with water to the required depth from downstream. It should be noted that extra care is required when filling the flume with water, especially for tests of this nature where no sediment movement was allowed. Any deformity in the bed surface may develop ripples or dunes and general movement of the sand if the shear stress on the smooth bed is close to the critical shear stress. The pump was then turned on and the desired flow rate was achieved by controlling the control valve and a bypass valve.
- Concurrent with getting the pump up to speed, the tailgate was adjusted to maintain the correct depth of flow (=11.5 cm) in the flume. The experiments were continued until the maximum scour depth was achieved. After that, the pump was stopped to allow the flume to slowly drain without disturbing the scour topography. The flume bed was then allowed to dry, during which time photos of the scour topography around the pier were taken. After the bed was dried, the scour morphology was measured using the laser distance meter.

CHAPTER – 6

RESULTS AND DISCUSSION

6.1 Results

In this chapter, the results obtained from all of the experiments conducted are presented, along with analyses and discussions of those results. This study consists of a total of 11 experiments with and without collars around the pier. For each test, the general observations have been summarized. This section examined the impact of two collar shapes, namely a circular collar and an airfoil collar on the temporal development of scour, the reduction of scour depths and the geometry of the scour hole under various clear water scour conditions.

In these experiments, a circular pier of 7 cm was used. The tests were conducted under a flow intensity (U/U_c) of 0.87 (<1). It represents that a clear-water scour condition was maintained throughout all the experiments. In this study, the value of h_w/b was set at 1.64 to get controlled flow in the flume. The sand having a median grain size (d_{50}) of 0.724 mm and a relative density (S) of 2.63 was used in this study. All the experiments were conducted with constant discharge (Q) of 25.5 l/s and constant flow depth (h_w) of 11.5 cm, where the mean approach velocity (U) of water was kept at 0.2738 m/s.

In the present study, five different circular collars of diameters (b_c) 10.5, 14, 17.5, 21, and 24.5 cm and five different airfoil collars of diameters 10.5, 14, 17.5, 21, and 24.5 cm having their lengths of 21, 28, 35, 42, and 49 cm, respectively were used. For the experiments, all collars were placed at sediment bed level around the pier. From previous studies, we see that the most important location is the upstream face of the pier as the maximum scour depth occurs at that location for an unprotected pier and causes a collapse. But in the present study, temporal scour depth was measured at four different measuring points (0°, 90°, 135° and 180°). The locations other than the upstream face were taken into account because applying collars may alter the flow pattern and scouring can occur at different locations. The experimental findings are discussed in detail in the following sections.

6.2 Experiments Conducted

6.2.1 Experiment Number 1 (Unprotected Circular Pier: 7 cm Diameter)

The first experiment was conducted to study the scour pattern around a single pier without any collar. This experiment was continued for 540 minutes to achieve the equilibrium scour depth. The quasi-equilibrium scour condition is accepted to be attained when the increase in the scour depth is below a limiting value. We measured the temporal scour depth at four different points i.e., 0°, 90°, 135° and 180°. The time variation of scour depth is shown in the next section. After 540 minutes the maximum scour depth (D_{sm}) measured at the four different locations were 3.67, 2.58, 1.49, and 0.399 cm at 0°, 90°, 135° and 180° respectively. From

this experimental data, we find that the maximum scour depth for an unprotected single pier occurred at the upstream face of the pier. The sediment bed profile before and after the experiment is presented in Fig. 6.1.

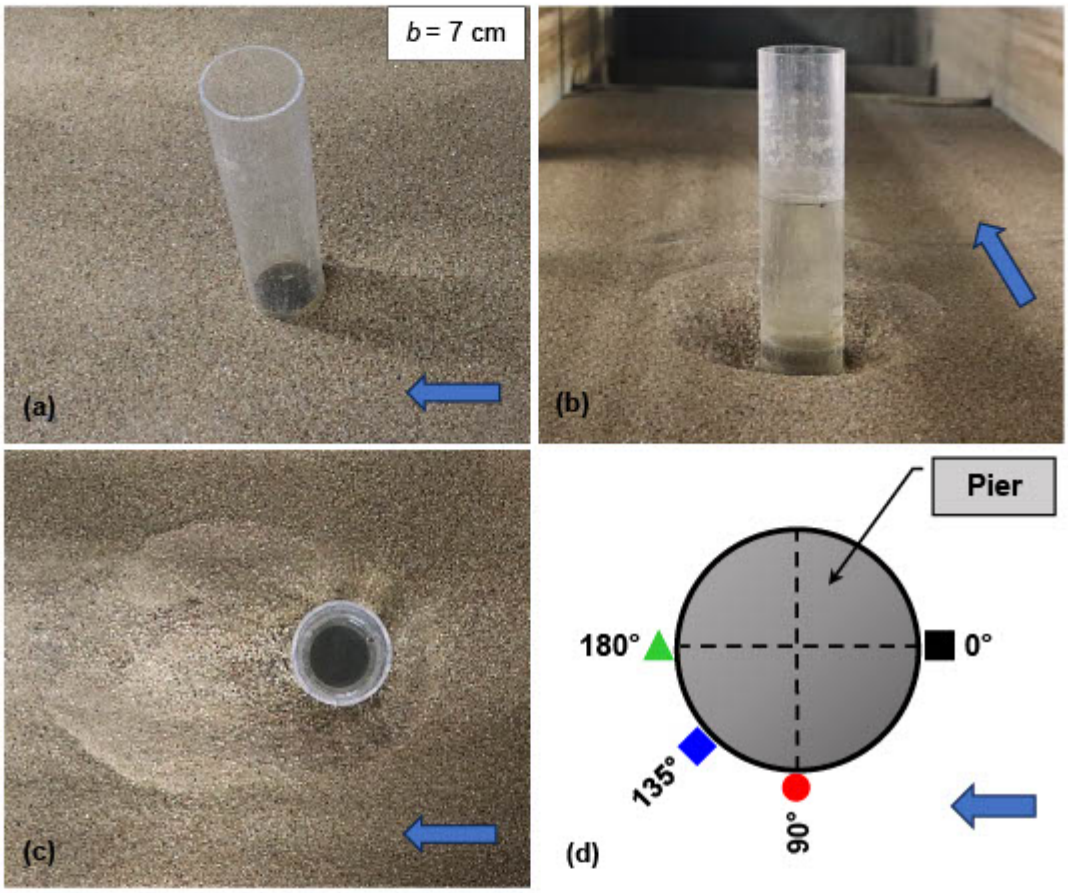


Fig. 6.1 Photographs showing the sand bed **(a)** before the experimental run (without collar), **(b)** after the experimental run (front view), and **(c)** after the experimental run (top view); **(d)** Location of measuring points of temporal scour depth around the unprotected pier.

6.2.2 Experiment Number 2 (Circular Pier with 1.5*b* Circular Collar)

In the second experiment, we fixed a circular collar of diameter (b_c) 10.5 cm around the pier. The collar was inserted into the bed and the upper surface of the collar was kept at the sediment bed level. This experiment was carried out for 180 minutes. Here also we measured the temporal scour depth at four different points i.e., at the upstream of the pier (0°), side of the pier (90°), at an angle downstream of the pier (135°), and immediately downstream face of the per (180°). The schematic diagram of the location of the measuring points is given in Fig. 6.2f. The time variation of scour depth is shown in the next section. The maximum scour depth (D_{scm}) measured at the four different locations were 1.8, 2.76, 1.6, and -0.33 cm at 0°, 90°, 135° and 180° respectively. The minus sign indicates a deposition at that point. The sediment bed profile before and after the experiment is presented in Fig. 6.2.

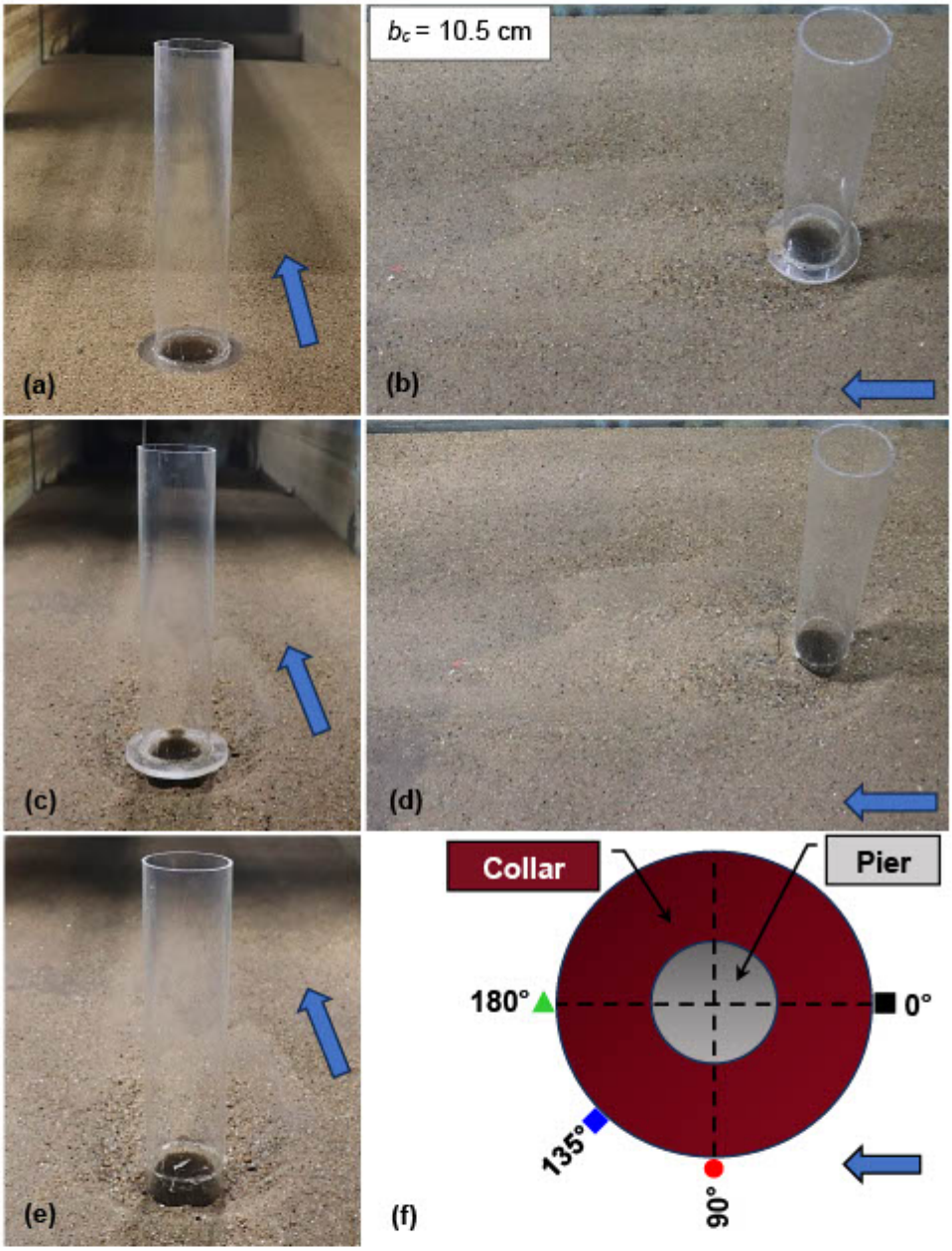


Fig. 6.2 Sand bed (for 1.5*b* circular collar) **(a)** before the experimental run; **(b)** after the experimental run; **(c)** after the experimental run (front view); **(d)** after removing collar; **(e)** after removing collar (front view); **(f)** Location of measuring points for temporal scour depths with a circular collar.

6.2.3 Experiment Number 3 (Circular Pier with 2*b* Circular Collar)

In the third experiment, we fitted a circular collar of diameter (b_c) 14 cm around the pier. The collar was inserted into the bed and the upper surface of the collar was kept at the sediment

bed level. This experiment was carried out for 400 minutes. Here also we measured the temporal scour depth at four different points i.e., 0°, 90°, 135° and 180°. The time variation of scour depth is shown in the next section. The schematic diagram of the location of the measuring points is given in Fig. 6.2. The maximum scour depth (D_{scm}) measured at the four different locations were 1.43, 2.73, 2.25, and 1.75 cm at 0°, 90°, 135° and 180° respectively. The sediment bed profile before and after the experiment is presented in Fig. 6.3.

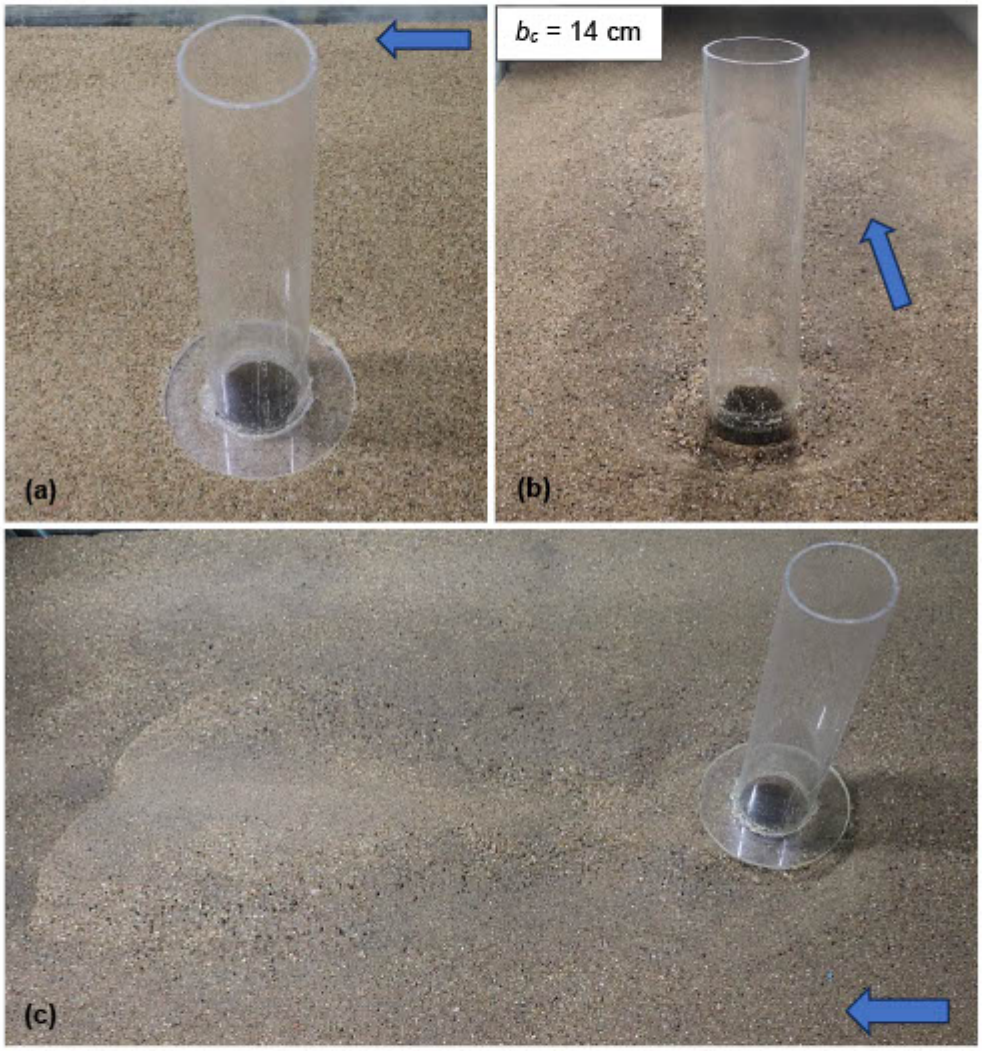


Fig. 6.3 Sand bed (for 2*b* circular collar) **(a)** before experimental run; **(b)** after experimental run after removing collar (front view); **(c)** after experimental run before removing collar.

6.2.4 Experiment Number 4 (Circular Pier with 2.5*b* Circular Collar)

In the fourth experiment, we fitted a circular collar of diameter (b_c) 17.5 cm around the pier. The collar was inserted into the bed and the upper surface of the collar was kept at the sediment bed level. This experiment was carried out for 580 minutes. Here also we measured

the temporal scour depth at four different points i.e., 0°, 90°, 135° and 180°. The time variation of scour depth is shown in the next section. The schematic diagram of the location of the measuring points is given in Fig. 6.2. The maximum scour depth (D_{scm}) measured at the four different locations were 1.725, 1.85, 2.28, and 0.9 cm at 0°, 90°, 135° and 180° respectively. The sediment bed profiles before the experiment and scoured bed after the experiment are presented in Fig. 6.4.

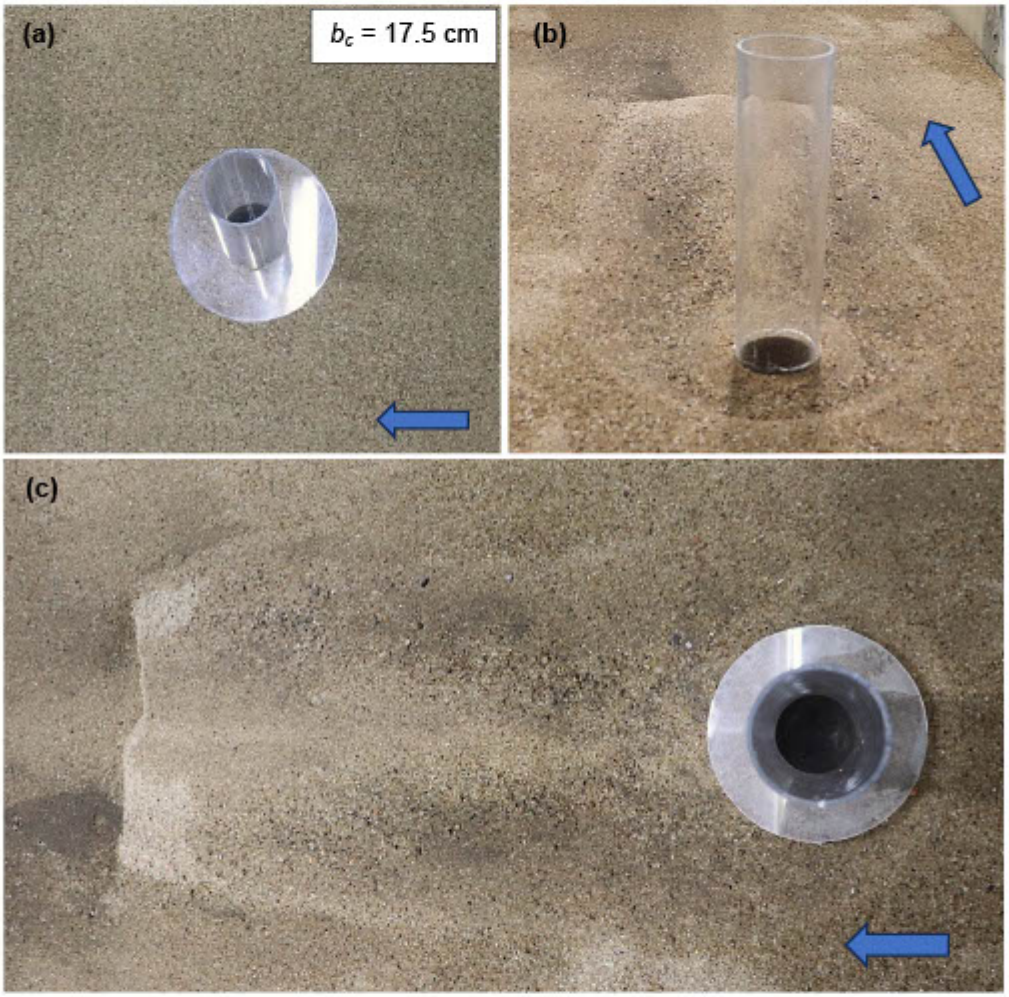


Fig. 6.4 Sand bed (for 2.5*b* circular collar) **(a)** before experimental run; **(b)** after experimental run after removing collar (front view); **(c)** after experimental run (top view)

6.2.5 Experiment Number 5 (Circular Pier with 3*b* Circular Collar)

In the fifth experiment, we fitted a circular collar of diameter (b_c) 21 cm around the pier. The collar was inserted into the bed and the upper surface of the collar was kept at the sediment bed level. This experiment was carried out for 360 minutes. Here also we measured the temporal scour depth at four different points i.e., 0°, 90°, 135° and 180°. The time variation of scour depth is shown in the next section. The schematic diagram of the location of the

measuring points is given in Fig. 6.2. The maximum scour depth (D_{scm}) measured at the four different locations were 0.49, 1.58, 2.89, and 1.2 cm at 0°, 90°, 135° and 180° respectively. The leveled sediment bed profiles before the experiment and scoured bed after the experiment are presented in Fig. 6.5.

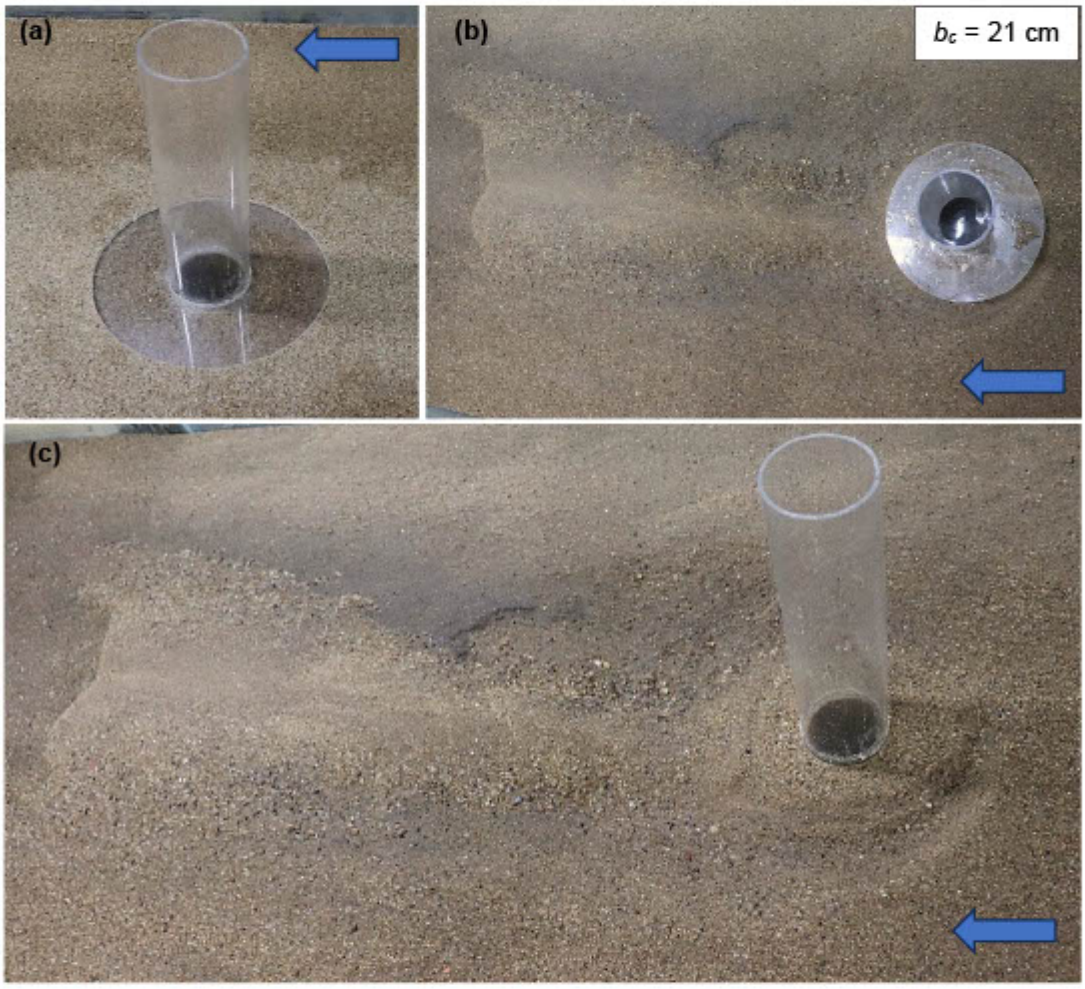


Fig. 6.5 Sand bed (for 3*b* circular collar) **(a)** before the experimental run; **(b)** after the experimental run (top view); **(c)** after the experimental run after removing the collar

6.2.6 Experiment Number 6 (Circular Pier with 3.5*b* Circular Collar)

In the sixth experiment, we fitted a circular collar of diameter (b_c) 24.5 cm around the pier. The collar was inserted into the bed and the upper surface of the collar was kept at the sediment bed level. This experiment was carried out for 360 minutes. Here also we measured the temporal scour depth at four different points i.e., 0°, 90°, 135° and 180°. The time variation of scour depth is shown in the next section. The schematic diagram of the location of the measuring points is given in Fig. 6.2. The maximum scour depth (D_{scm}) measured at the four different locations were 0, 2.14, 2.77, and 0.98 cm at 0°, 90°, 135° and 180° respectively. The

levelled sediment bed profile before the experiment and scoured bed after the experiment are presented in Fig. 6.6.

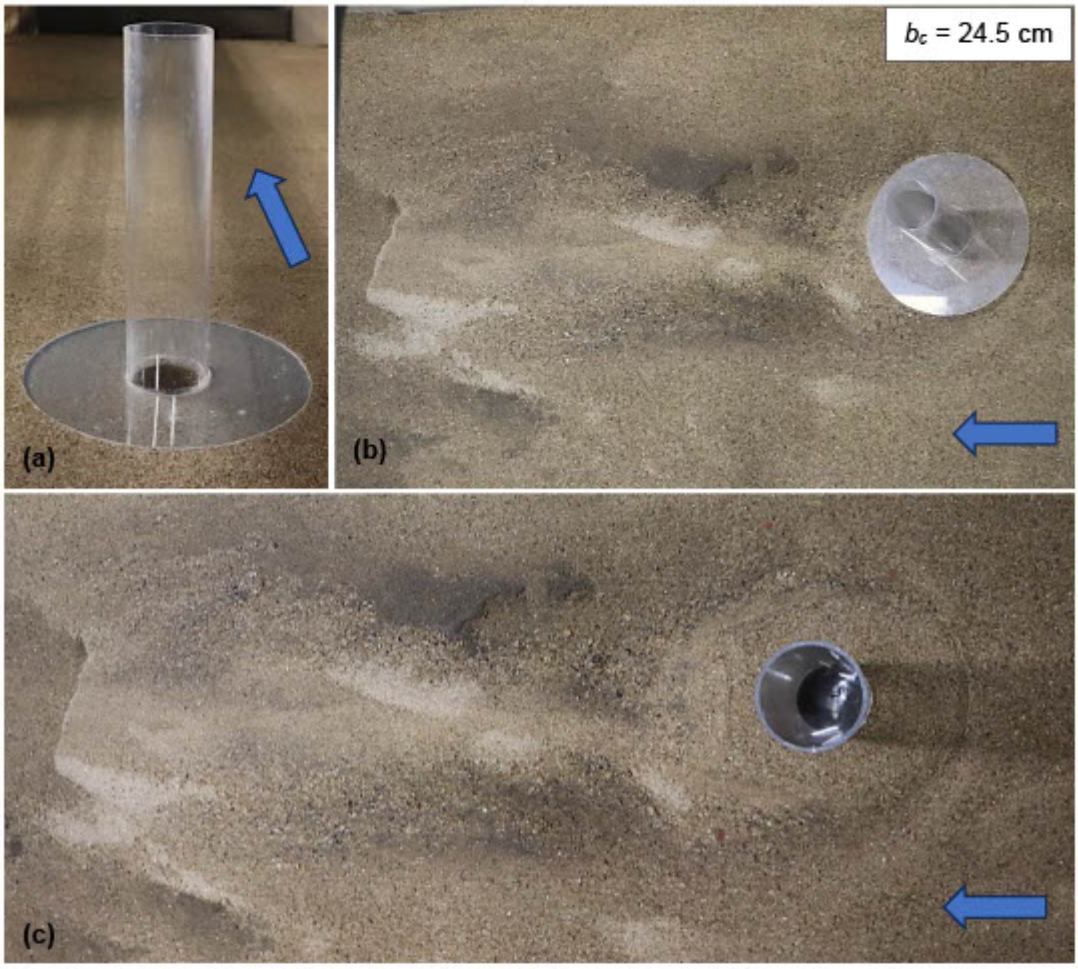


Fig. 6.6 Sand bed (for 3.5*b* circular collar) **(a)** before the experimental run; **(b)** after the experimental run (top view); **(c)** after the experimental run after removing the collar.

6.2.7 Experiment Number 7 (Circular Pier with 1.5*b* Airfoil Collar)

In the seventh experiment, we fitted an airfoil collar of diameter (b_c) of 10.5 cm and length (l_c) of 21 cm around the pier. The collar was inserted into the bed and the upper surface of the collar was kept at the sediment bed level. The triangular side of the collar was kept at the upstream of the pier. This experiment was carried out for 300 minutes. Here also we measured the temporal scour depth at four different points i.e., 0°, 90°, 135° and 180°. The time variation of scour depth is shown in the next section. The schematic diagram of the location of the measuring points is given in Fig. 6.7. The maximum scour depth (D_{scm}) measured at the four different locations were 0.012, 2.139, 1.29, and -0.29 cm at 0°, 90°, 135°, and 180° respectively. The minus sign indicates a deposition at that location. The leveled sediment bed profile before the experiment and scoured bed after the experiment is presented in Fig. 6.7.

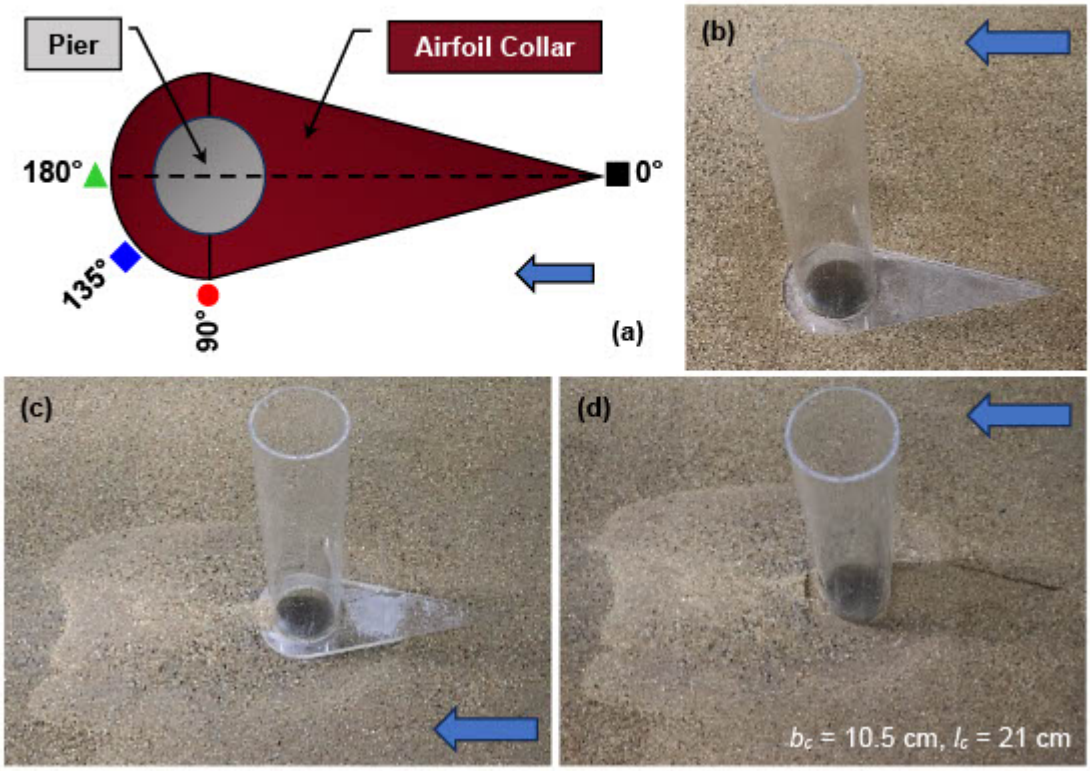


Fig. 6.7 Sand bed (for 1.5*b* airfoil collar) **(a)** Location of measuring points for temporal scour depths with airfoil collar, **(b)** before the experimental run; **(c)** after the experimental run; **(d)** after the experimental run after removing the collar.

6.2.8 Experiment Number 8 (Circular Pier with 2*b* Airfoil Collar)

In the eighth experiment, we fitted an airfoil collar of diameter (b_c) of 14 cm and length (l_c) of 28 cm around the pier. The collar was inserted into the bed and the upper surface of the collar was kept at the sediment bed level. The triangular side of the collar was kept at the upstream of the pier. This experiment was carried out for 360 minutes. Here also we measured the temporal scour depth at four different points i.e., 0°, 90°, 135° and 180°. The time variation of scour depth is shown in the next section. The schematic diagram of the location of the measuring points is given in Fig. 6.7. The maximum scour depth (D_{scm}) measured at the four different locations were 0, 1.98, 1.69, and -0.04 cm at 0°, 90°, 135°, and 180° respectively. The minus sign indicates a deposition at that location. The leveled sediment bed profile before the experiment and scoured bed after the experiment is presented in Fig. 6.8.

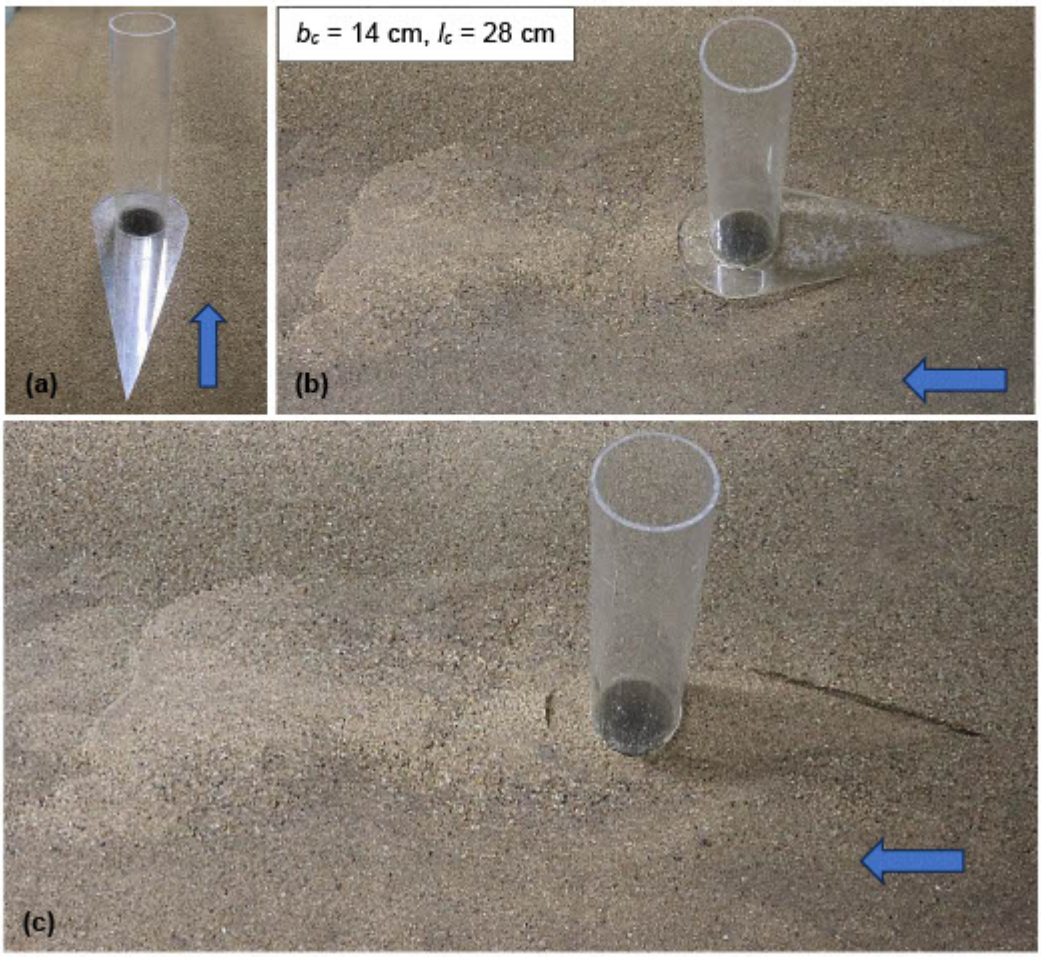


Fig. 6.8 Sand bed (for 2*b* airfoil collar) **(a)** before the experimental run; **(b)** after the experimental run; **(c)** after the experimental run after removing the collar.

6.2.9 Experiment Number 9 (Circular Pier with 2.5*b* Airfoil Collar)

In the ninth experiment, we fitted an airfoil collar of diameter (b_c) of 17.5 cm and length (l_c) of 35 cm around the pier. The collar was inserted into the bed and the upper surface of the collar was kept at the sediment bed level. The triangular side of the collar was kept at the upstream of the pier. This experiment was carried out for 180 minutes. Here also we measured the temporal scour depth at four different points i.e., 0°, 90°, 135° and 180°. The time variation of scour depth is shown in the next section. The schematic diagram of the location of the measuring points is given in Fig. 6.7. The maximum scour depth (D_{scm}) measured at the four different locations were 0, 2, 2.15, and 1.13 cm at 0°, 90°, 135°, and 180° respectively. The minus sign indicates a deposition at that location. The leveled sediment bed profile before the experiment and scoured bed after the experiment are presented in Fig. 6.9.

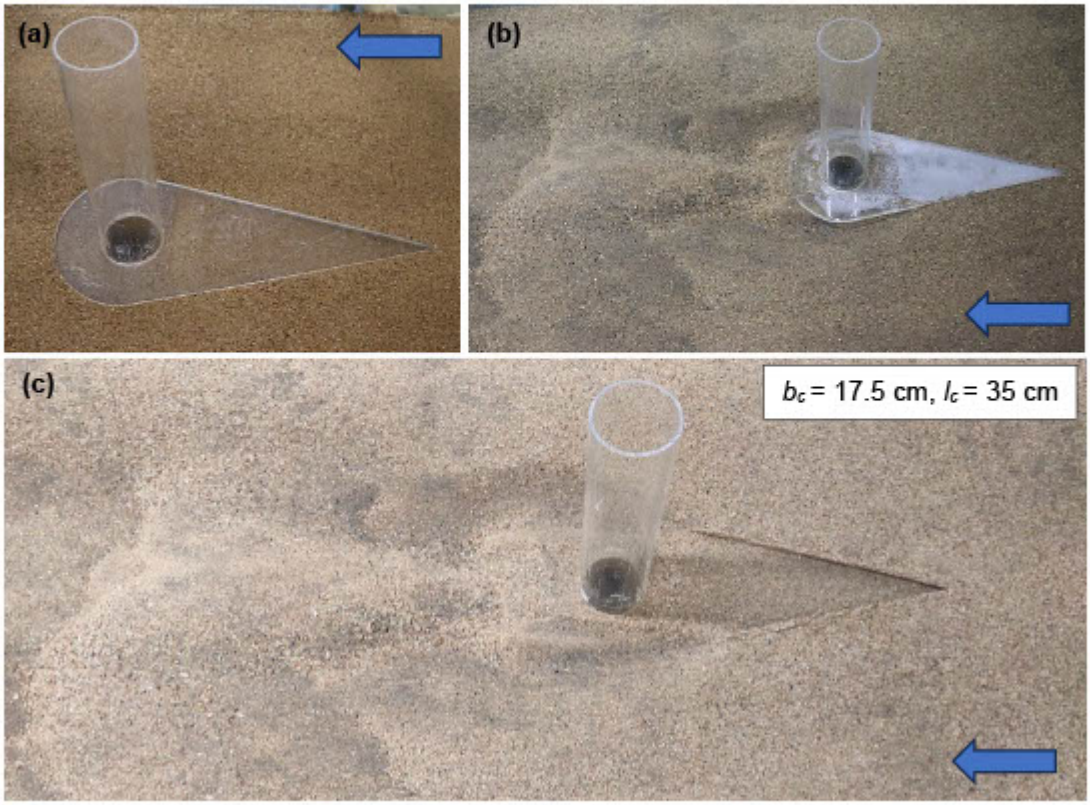


Fig. 6.9 Sand bed (for 2.5*b* airfoil collar) **(a)** before the experimental run; **(b)** after the experimental run; **(c)** after the experimental run after removing the collar.

6.2.10 Experiment Number 10 (Circular Pier with 3*b* Airfoil Collar)

In the tenth experiment, we fitted an airfoil collar of diameter (b_c) of 21 cm and length (l_c) of 42 cm around the pier. The collar was inserted into the bed and the upper surface of the collar was kept at the sediment bed level. The triangular side of the collar was kept at the upstream of the pier. This experiment was carried out for 540 minutes. Here also we measured the temporal scour depth at four different points i.e., 0°, 90°, 135° and 180°. The time variation of scour depth is shown in the next section. The schematic diagram of the location of the measuring points is given in Fig. 6.7. The maximum scour depth (D_{scm}) measured at the four different locations were 0, 2.23, 3.58, and 2.03 cm at 0°, 90°, 135°, and 180° respectively. The minus sign indicates a deposition at that location. The leveled sediment bed profiles before the experiment and scoured bed after the experiment are presented in Fig. 6.10.

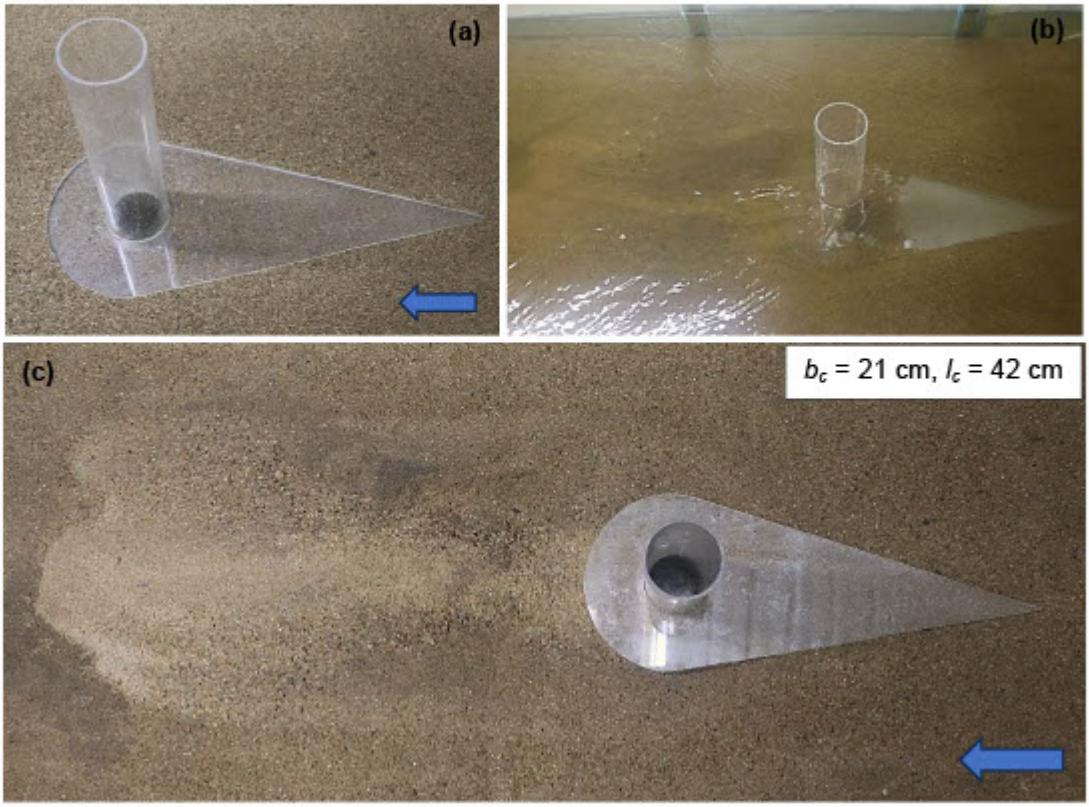


Fig. 6.10 Sand bed (for 3*b* airfoil collar) **(a)** before the experimental run; **(b)** during the experimental run (top view); **(c)** scoured bed profile after the experimental run.

6.2.11 Experiment Number 11 (Circular Pier with 3.5*b* Airfoil Collar)

In the eleventh experiment, we fitted an airfoil collar of diameter (b_c) of 24.5 cm and length (l_c) of 49 cm around the pier. The collar was inserted into the bed and the upper surface of the collar was kept at the sediment bed level. The triangular side of the collar was kept at the upstream of the pier. This experiment was carried out for 480 minutes. Here also we measured the temporal scour depth at four different points i.e., 0°, 90°, 135° and 180°. The time variation of scour depth is shown in the next section. The schematic diagram of the location of the measuring points is given in Fig. 6.7. The maximum scour depth (D_{scm}) measured at the four different locations were 0, 2.5, 3.61, and 1.62 cm at 0°, 90°, 135°, and 180° respectively. The minus sign indicates a deposition at that location. The leveled sediment bed profiles before the experiment and scoured bed after the experiment are presented in Fig. 6.11.

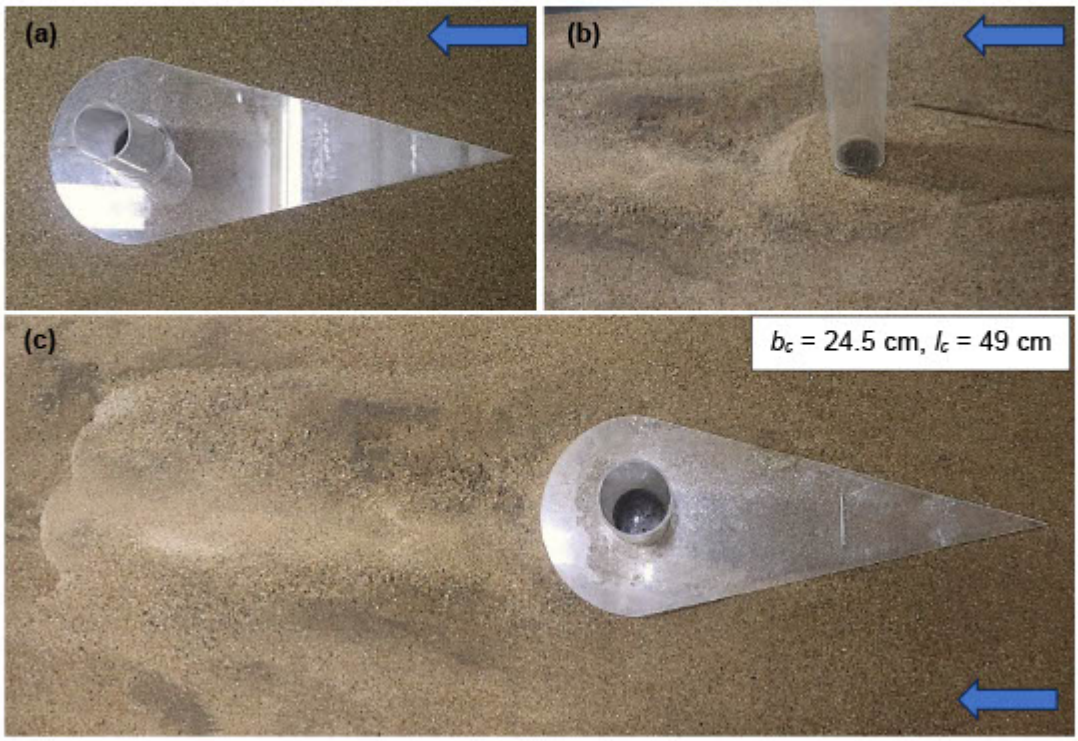


Fig. 6.11 Sand bed (for 3.5*b* airfoil collar) **(a)** before the experimental run; **(b)** after the experimental run after removing collar; **(c)** after the experimental run before removing collar (top view)

6.3 Temporal Variation of Scour Depth

In the present study temporal variation of scour depth has been observed for each experiment. A non-dimensional scour depth vs non-dimensional time plot for the pier with and without a collar is given for all the experiments.

6.3.1 Circular Pier without Collar

For this test, the effect of the scouring process was noticed immediately upon starting the test. The scour initially began at the sides of the pier. It then quickly spread around the pier's perimeter from both sides towards the centreline of the pier at the upstream face. As the scour process continued, the scoured sand material was deposited in the wake region. The maximum scour depth was found at the upstream face of the pier. Fig. 6.12 shows the temporal development of scour depth at four different locations around the unprotected pier ($b = 7$ cm).

From the plot, it is seen that scour depth increases rapidly with time at the beginning of the experiment. Fig. 6.12 shows that around 81% of the maximum scour depth occurred during the first 90 minutes (17% of the maximum time). However, the rate of scour is decreased with time. Scour rate is defined as the change in scour depth per unit time. Even though equilibrium was not attained, the rate of scour was very low by the end of the test. For

an unprotected circular pier, the most important location is the upstream face of the pier because the maximum scour depth (D_{scm}) is observed at that point.

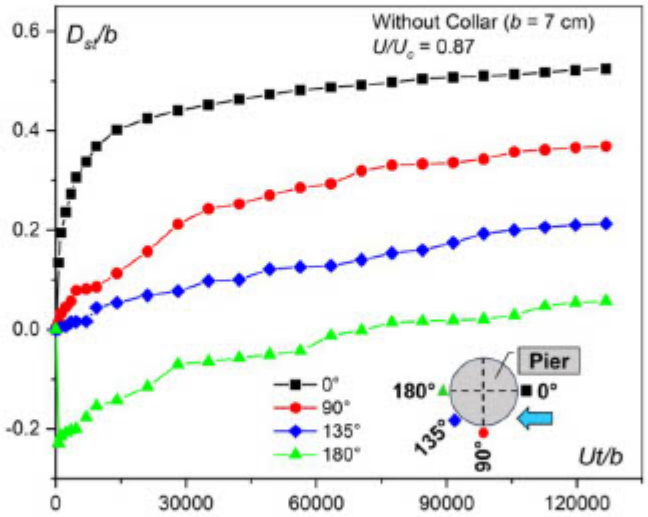


Fig. 6.12 Temporal variation between measured dimensionless scour depth (D_{st}/b) versus dimensionless time (Ut/b) for Experiment Number 1 (without collar).

6.3.2 Circular Pier with Circular Collars

In the case of a circular pier fitted with a circular collar on the bed, scour initially started at the edge of the collar on either side toward the downstream portion as illustrated in Fig. 6.13. Within the first few minutes, scour holes were formed on either side of the collar at the interface with the sand bed. As the test progressed, these scour holes extended towards the sides of the collar (90°) and later towards the upstream along the collar, eventually converging at the centreline (0°). The scour pattern then progressed beneath the collar and eventually to the upstream face of the pier (0°P in Fig. 6.13).

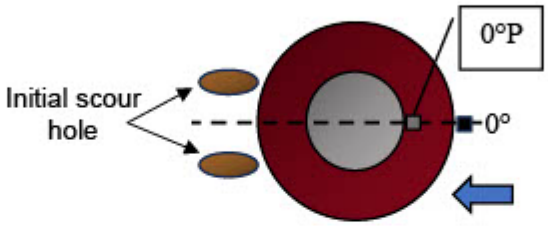


Fig. 6.13 Schematic illustration of initial scour hole development with a circular collar.

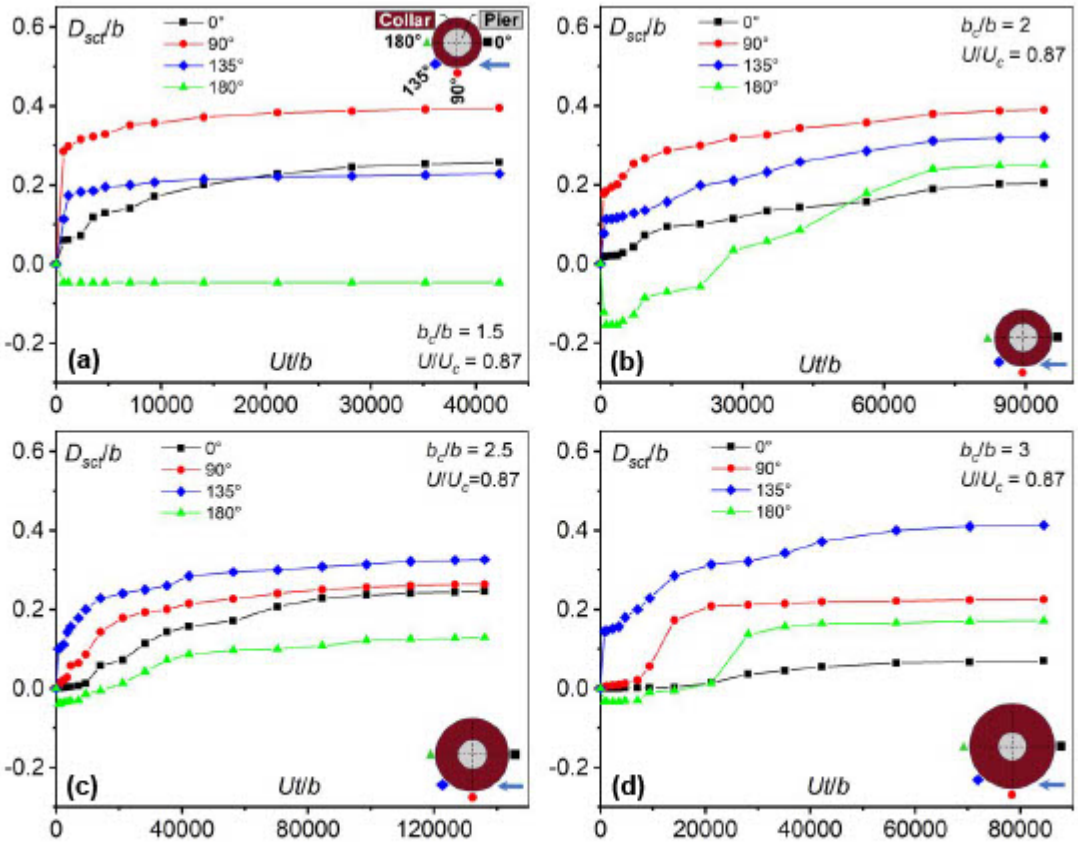
As sediment was removed from beneath the collar upstream of the pier, it was deposited in the scour holes around the collar periphery and in the wake region. Consequently, the maximum scour depth which was initially located within the scour holes, decreased as sediment removal continued below the collar. Overall, the progression of scour showed initial scour hole formation at the collar edges, extending upstream and eventually shifting the

maximum scour depth at the upstream face of the pier, accompanied by sediment deposition downstream.

In Fig. 6.14(a-e) temporal variation of scour depths around a circular pier with circular collars of five different sizes (collar diameter, b_c = 1.5b, 2b, 2.5b, 3b, and 3.5b) at four different measuring points (0°, 90°, 135° and 180°) are shown. In the case of 1.5b and 2b collars, the scouring rate is very high initially at 90° and then it propagates towards the upstream face of the pier. That is why the scouring at the upstream is delayed by a few minutes. But 1.5b and 2b collars are not effective in reducing scour. After some time, these collars were undermined totally and were unable to protect the pier.

However, the collars of diameter 2.5b, 3b, and 3.5b protected the pier and 3.5b was found to be the most effective among them. In the case of these three collars, the maximum scour depth was observed downstream of the pier at 135° which is far from the rear nose of the pier. For 2.5b and 3b collars, around 81% of maximum scour depth was reached under 50% of the maximum time (t_m), while it was only 17% of t_m for the pier without the collar. Though the collar of diameter 1.5b is not effective, it took around 36% of the maximum time to reach 81% of the maximum depth. Hence, it can be seen that the rate of scour is much less for piers protected with collars than the unprotected piers.

From Fig. 6.14(d, e) we can see that in the case of the collar of diameter 3b scouring process was delayed at the upstream face of the pier and no scour was seen for the first 15 minutes at 0° and the collar of diameter 3.5b was observed to be protecting the scour around the pier completely.



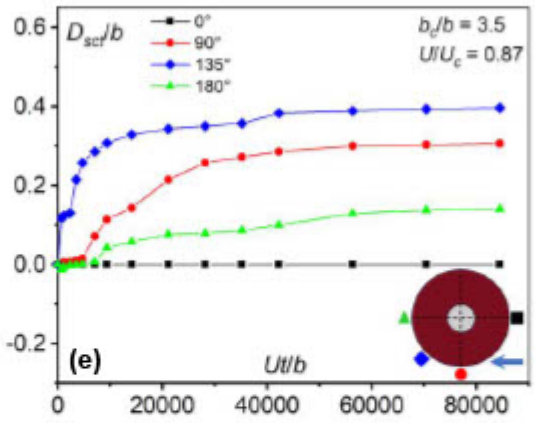


Fig. 6.14 Variation of dimensionless scour depth at the pier with circular collars of diameters **(a)** 1.5*b*; **(b)** 2*b*; **(c)** 2.5*b*; **(d)** 3*b*; **(e)** 3.5*b* with increasing dimensionless time.

6.3.3 Circular Pier with Airfoil Collar

In Fig. 6.16a temporal variation of scour depth around the pier in the presence of the airfoil collar of diameter (b_c) 1.5*b* has been shown at four different points towards 0°, 90°, 135° and 180°. In the case of airfoil collars, scour was first observed at the edge of the collar on either side at the downstream portion of the collar as shown in Fig. 6.15. Within the first few minutes of the experiment, scour holes were observed to form on the sides (90°) of the collar at the interface with the sand bed. The groves then extended towards both the downstream and upstream sides of the collar.

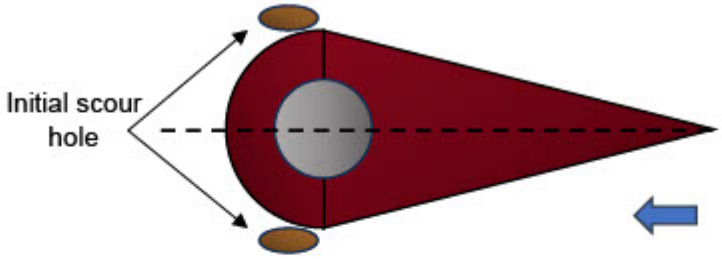


Fig. 6.15 Schematic illustration of initial scour hole development with an airfoil collar.

From Fig. 6.16a it is seen that the maximum scour depth occurred at the sides of the collar and the collar (1.5*b*) protected the upstream face of the pier (0°). At the immediate downstream of the pier along the centreline, a deposition of sediment was observed initially. At 135° also scour depth was increasing with time but it was less than that of the 90°. At both points rate of scour was high at first and it reduced with time but the rate of scouring was much less than that for pier without collar.

In Fig. 6.16b temporal variation of scour depth around the pier in the presence of an airfoil collar of diameter (b_c) equalling 2*b* has been shown at four different points (0°, 90°, 135° and 180°). In this case, at 90°, the initial scour hole developed and within 30 minutes almost 80% of the maximum scour depth was reached. Then the rate of scouring decreased.

Initially, at 135° scour was developed at a slower rate and after about 90 minutes the scour rate increased. It is seen that airfoil collars delay the scouring process at 135° and the upstream face of the pier is protected.

From Fig. 6.16c it is seen that in the case of a pier with an airfoil collar of diameter (b_c) equaling 2.5b, initially at 90° the scour depth developed and then extended towards 135°.

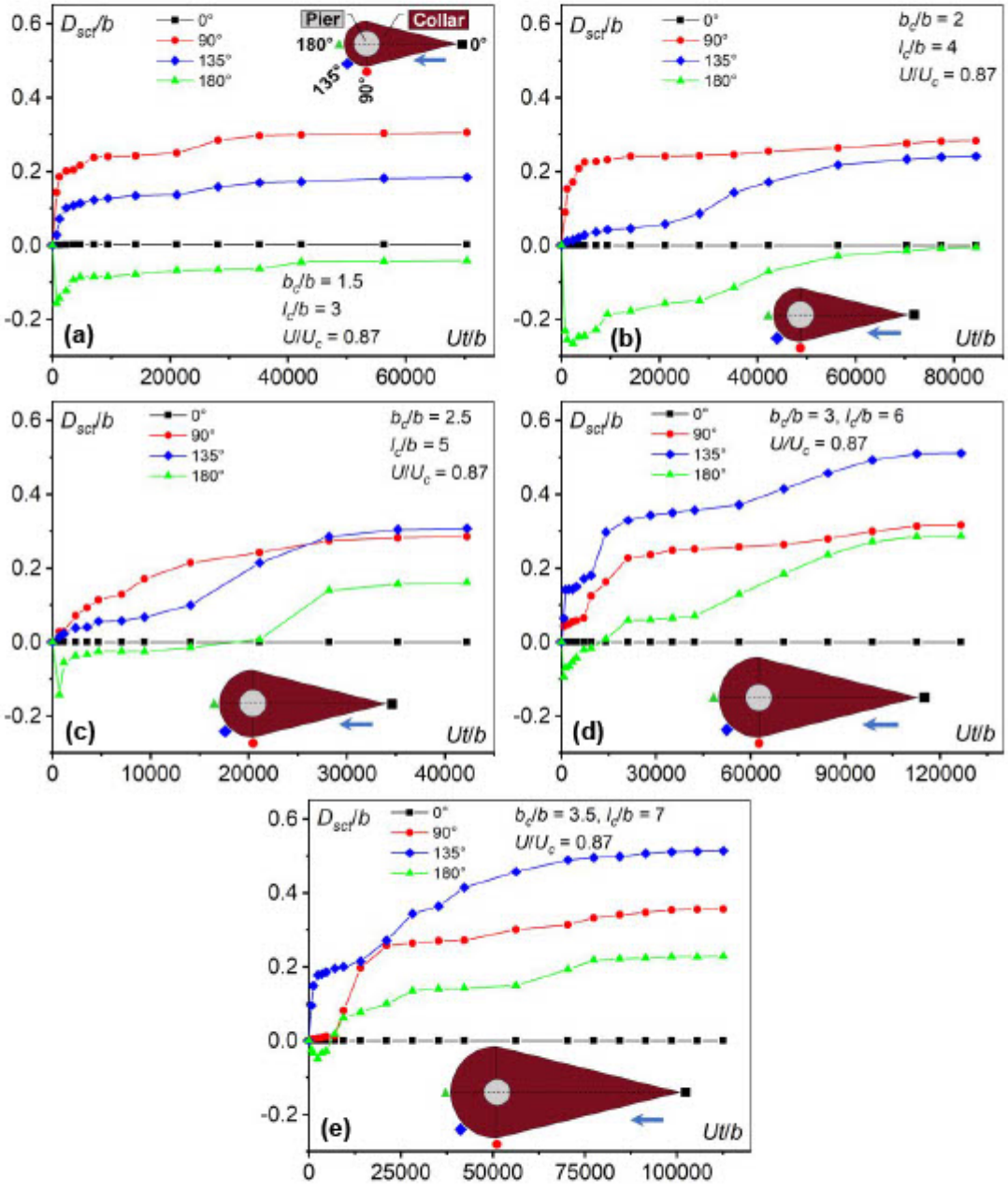


Fig. 6.16 Dimensionless scour depth (D_{scr}/b) varying with dimensionless time at the pier with airfoil collars of diameters **(a)** 1.5b; **(b)** 2b; **(c)** 2.5b; **(d)** 3b; **(e)** 3.5b.

But in the case of collars of diameters 3b and 3.5b, scouring was observed much higher at the downstream and then it was propagated towards the sides of the collars. However, all airfoil collars protected the upstream face of the pier and none of them was undermined totally.

6.4 Influence of Collar Diameter on Temporal Development of Scour Depth

In Fig. 6.17(a-d) the temporal scour depth development at a pier for different collar (circular) diameters has been compared with that of an unprotected pier at 0°, 90°, 135°, and 180° respectively. At 0°, the maximum scour depth (D_{scm}) for the circular collar of diameter 3.5b was measured as 0 cm and that for an unprotected pier (D_{sm}) was measured as 3.67 cm. The least effective collar diameter is identified as 1.5b. At 0° and 90° points, the maximum scour depth was obtained for the pier with the collar diameter of 1.5b and the subsequent scour depths were gauged as 1.8 and 2.76 cm. Hence, the collar diameter of 1.5b can be declared the least effective collar.

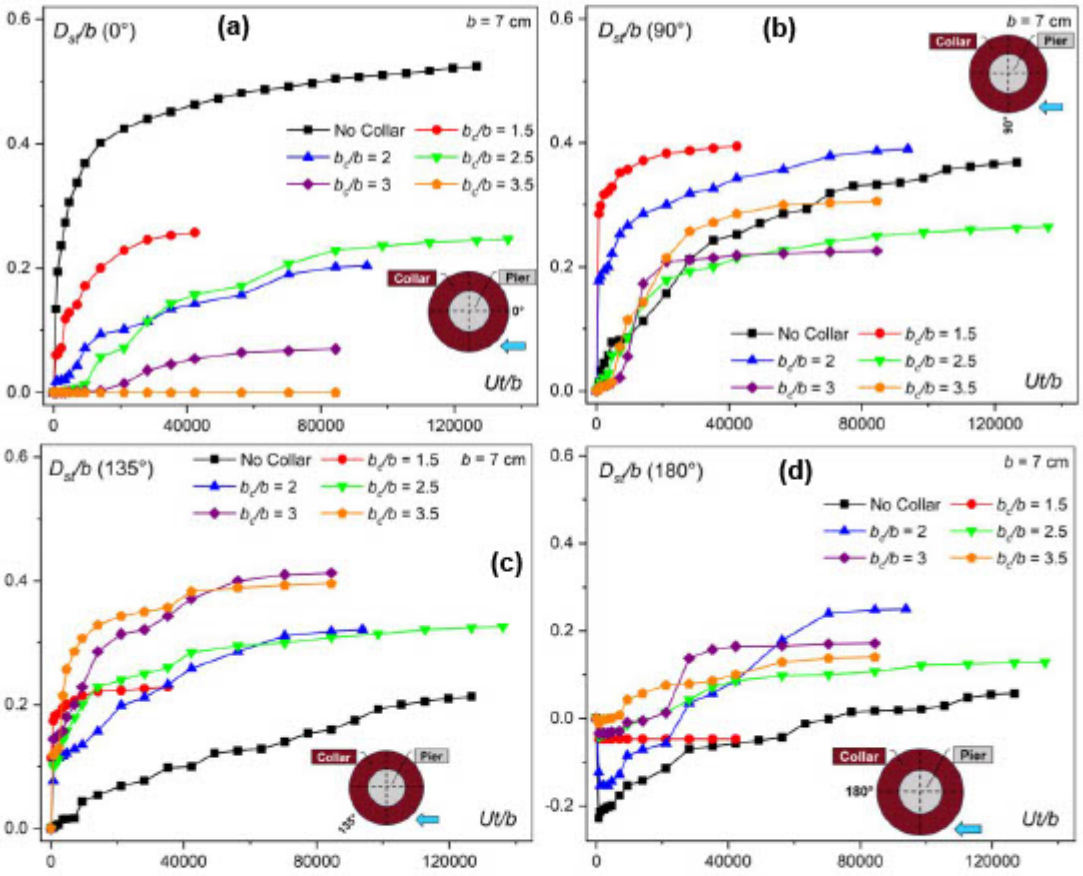


Fig. 6.17 The effect of circular collars of different diameters on temporal scour depth at a point towards **(a)** 0°, **(b)** 90°, **(c)** 135° and **(d)** 180°.

The 0° i.e., the upstream face of the pier is identified as the most important location as the maximum scour was found to be occurred at that point for an unprotected pier. At 0°, D_{scm} for the pier with circular collar diameters $2b$, $2.5b$, and $3b$ were gauged equal to 1.43, 1.72, and 0.49 cm, respectively. At 90°, D_{scm} for the pier with circular collar diameters $2b$, $2.5b$, $3b$, and $3.5b$ were measured 2.73, 1.85, 1.58, and 2.14 cm, respectively. At 135°, D_{sm} for an unprotected pier was measured 1.49 cm and D_{scm} with circular collar diameters $1.5b$, $2b$, $2.5b$, $3b$, and $3.5b$ were measured 1.6, 2.25, 2.28, 2.89, and 2.77 cm, respectively. At 180°, D_{sm} for an unprotected pier was gauged 0.399 cm, and D_{scm} with circular collar diameters $1.5b$, $2b$, $2.5b$, $3b$, and $3.5b$ were gauged -0.33, 1.75, 0.9, 1.2, and 0.98 cm, respectively.

In Fig. 6.18(a-d) the temporal scour depth development at a pier for different collar (airfoil) diameters has been compared with that of an unprotected pier at 0°, 90°, 135°, and 180° respectively. At 0°, no scour depth was observed for the airfoil collars. At 90°, for $1.5b$ and $2b$ collars, the scouring rate was initially found to be the highest. The rate of the scour for $2.5b$ collar was found more than $1.5b$ and $2b$ collars. However, it was found less than $3b$ and $3.5b$ collars. Also, the scouring process was delayed for $3b$ and $3.5b$ collars.

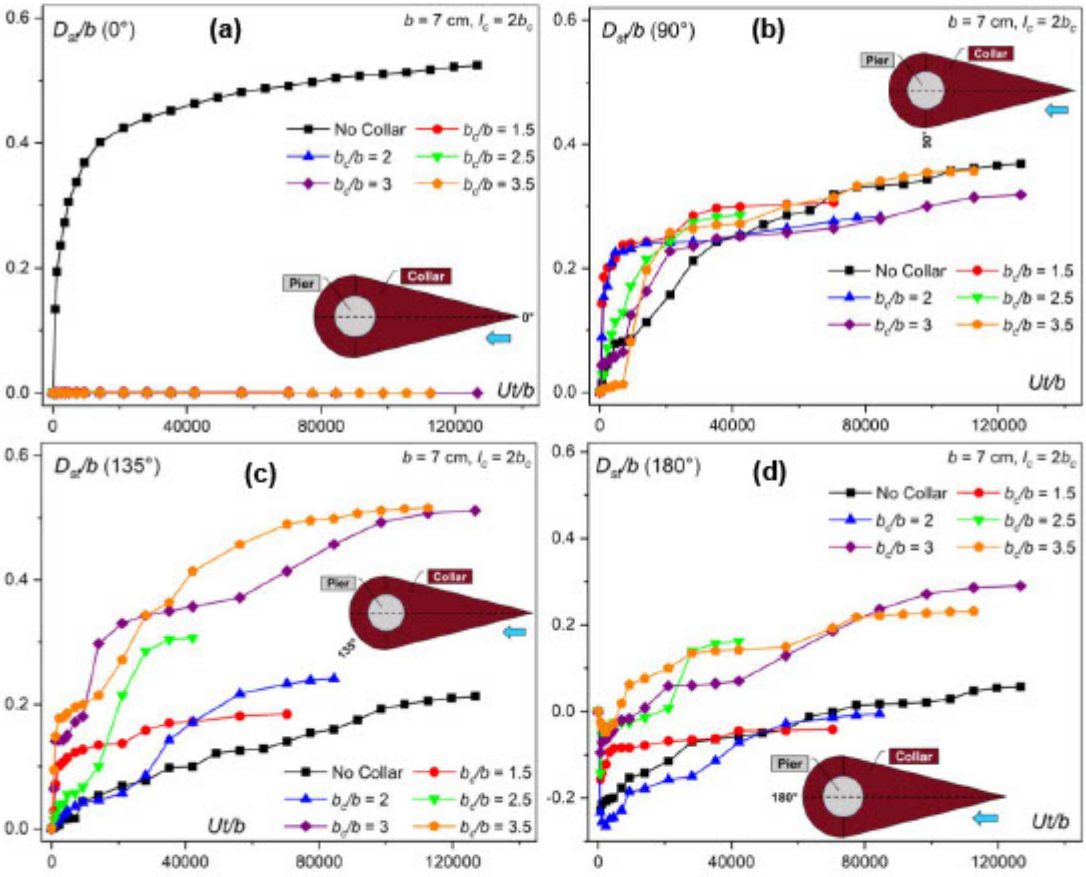


Fig. 6.18 The effect of airfoil collar of different diameters on temporal scour depth at **(a)** 0°, **(b)** 90°, **(c)** 135° and **(d)** 180°.

6.5 Reduction of Temporal Scour Depth with Circular and Airfoil Collars

The percentage reduction (%R) of scour depth around a pier protected with a collar compared to an unprotected pier can be defined as the protection efficiency of the collar.

$$\%R = \left(\frac{D_{sm} - D_{scm}}{D_{sm}} \right) \times 100 \tag{6.1}$$

The percentage reductions (%R) of scour depths for the circular collars of diameters 1.5b, 2b, 2.5b, 3b, and 3.5b at 0° (upstream face of unprotected pier and upstream face of collar for protected pier) are calculated 50.95, 61.04, 53, 86.65, and 100%, respectively. Whereas, the percentage reductions (%R) of scour depths for the circular collars of diameters 1.5b, 2b, 2.5b, 3b, and 3.5b at 90° (sides of unprotected pier and sides of collar for protected pier) are computed only -6.98, -5.81, 28.29, 38.76, and 17.05%, respectively.

Table 6.1 shows the maximum scour depths measured during the experiments and the protection efficiencies of each collar at four different points around the pier.

Table 6.1 Percentage reductions of maximum scour depths in the presence of a collar

Shape of Collar	b_c/b	l_c/b	t_m **(min)**	**Max Scour Depth (D_{scm}) (cm)**				**% Reduction (%R)**			
				0°	**90°**	**135°**	**180°**	**0°**	**90°**	**135°**	**180°**
Without Collar	1	–	540	3.67	2.58	1.49	0.40	–	–	–	–
Circular	1.5	–	180	1.80	2.76	1.60	-0.33	51.0	-7.0	-7.4	182.7
Circular	2	–	400	1.43	2.73	2.25	1.75	61.0	-5.8	-51.0	-338.6
Circular	2.5	–	580	1.73	1.85	2.28	0.90	53.0	28.3	-53.0	-125.6
Circular	3	–	360	0.49	1.58	2.89	1.20	86.7	38.8	-94.0	-200.8
Circular	3.5	–	360	0.00	2.14	2.77	0.98	100	17.1	-85.9	-145.6
Airfoil	1.5	3	300	0.01	2.14	1.29	-0.29	99.7	17.1	13.4	172.7
Airfoil	2	4	360	0.00	1.98	1.69	-0.04	100	23.3	-13.4	110
Airfoil	2.5	5	180	0.00	2.00	2.15	1.13	100	22.5	-44.3	-183.2
Airfoil	3	6	540	0.00	2.23	3.58	2.03	100	13.6	-140.3	-408.8
Airfoil	3.5	7	480	0.00	2.50	3.61	1.62	100	3.1	-142.3	-306

The percentage reduction (%R) of scour depth for the airfoil collar of diameter 1.5b at 0° is 99.67% and 2b, 2.5b, 3b, and 3.5b are 100%. %R for the airfoil collars of diameters 1.5b, 2b, 2.5b, 3b, and 3.5b at 90° are 17.09, 23.26, 22.48, 13.57, and 3.10% respectively. According to Table 6.1, the percentage reduction for the airfoil collars at 135° and 180° shows that in the case of larger size collars the maximum scour occurs at the downstream side of the pier and the upstream face is protected. The negative sign of the percentage reduction indicates that the collar is not effective in protecting the pier but that does not mean that larger collars are ineffective. They protect the upstream face which is our main concern.

6.6 Morphological Geometry of Scour for Pier with and without Collar

The contour lines of the scour holes at the circular pier with and without collars, plotted with Surfer - Golden Software, for experiment numbers 1 to 11 are shown in Figs. 6.19 to 6.21.

Figure 6.19 shows the contours of the scoured bed profile for the pier without any collar. The maximum scour depth is 3.67 cm and the maximum height of the mound is 1.73 cm. The location of the maximum scour depth is obtained at x = -4 cm and y = 0 cm i.e., the upstream face of the pier. The (0,0) reference point is the center of the circular pier.

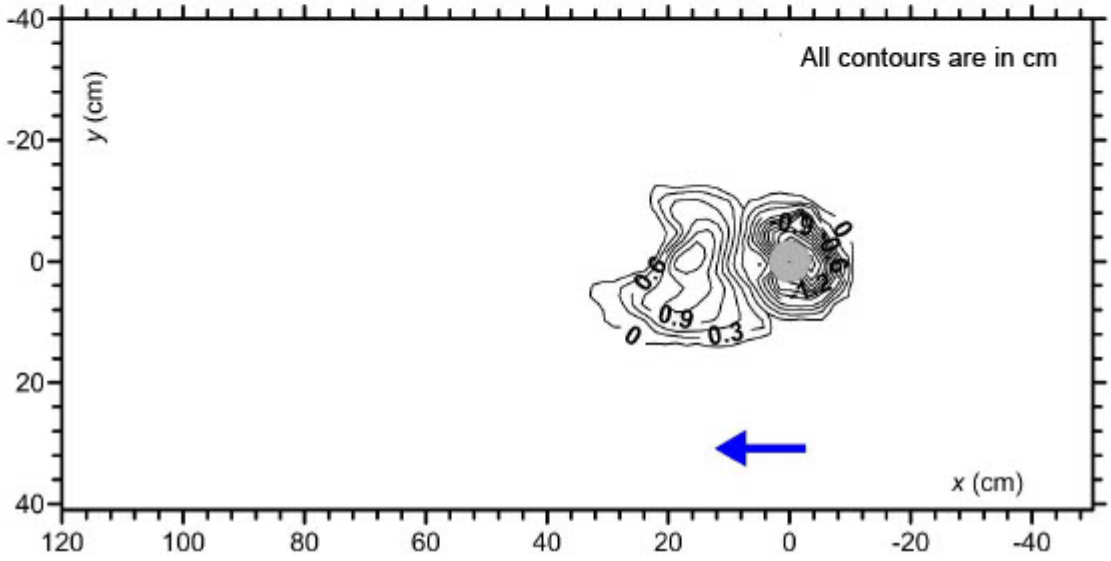


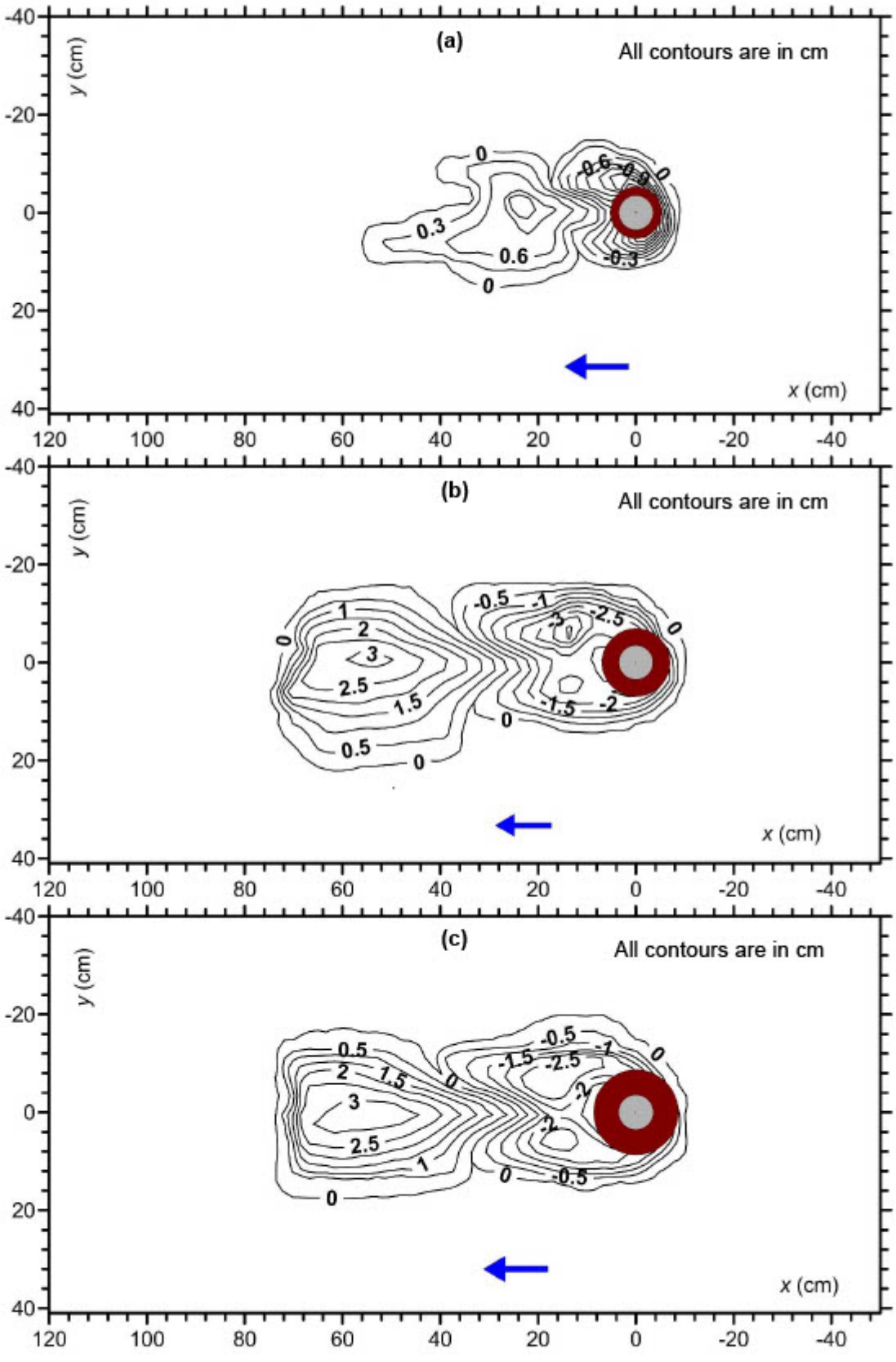
Fig. 6.19 Contours of scour hole for an unprotected pier (b = 7 cm).

Figure 6.20a shows the contours of the scoured bed after the experimental run for the pier with a circular collar of diameter 1.5b (pier dia, b = 7 cm). The maximum scour depth is 3.13 cm and the maximum height of deposition is 1.16 cm. The location of the maximum scour depth obtained is at x = -1 cm and y = -3.7 cm i.e., at the side (90°) of the pier (right side of the axis of symmetry).

Figure 6.20b shows the contours of the scoured bed for the pier with a circular collar of diameter 2b. The maximum scour depth is 4.4 cm and the maximum height of the mound is 3.08 cm. The location of the maximum scour depth obtained is at x = 14 cm and y = -5.5 cm i.e., at the downstream of the pier (right side of the axis of symmetry).

Figure 6.20c shows the contours of the scoured bed for the pier with a circular collar of diameter 2.5b. The maximum scour depth is 3.02 cm and the maximum height of the mound is 3.3 cm. The location of the maximum scour depth obtained is at x = 17 cm and y = -5.5 cm i.e., at the downstream of the pier (right side of the axis of symmetry).

Figure 6.20d shows the contours of the scoured bed for the pier with a circular collar of diameter 3b. The maximum scour depth is 4.14 cm and the maximum height of the sediment deposition is 3.47 cm. The location of the maximum scour depth obtained is at x = 16.5 cm and y = -9 cm i.e., at the downstream of the pier (right side of the axis of symmetry). Figure 6.20e shows the scour contours for the pier with a circular collar of diameter 3.5b.


(a)
All contours are in cm
y (cm)
x (cm)
0
-0.6
-0.9
0
0.3
0.6
-0.3
0
(b)
All contours are in cm
y (cm)
x (cm)
-0.5
-1
-2.5
0
1
2
3
2.5
1.5
-1.5
-2
0
0.5
0
(c)
All contours are in cm
y (cm)
x (cm)
0.5
-0.5
-1
0
2
1.5
-1.5
-2.5
3
2.5
1
0
-0.5
0
-40
-20
0
20
40
120
100
80
60
40
20
0
-20
-40

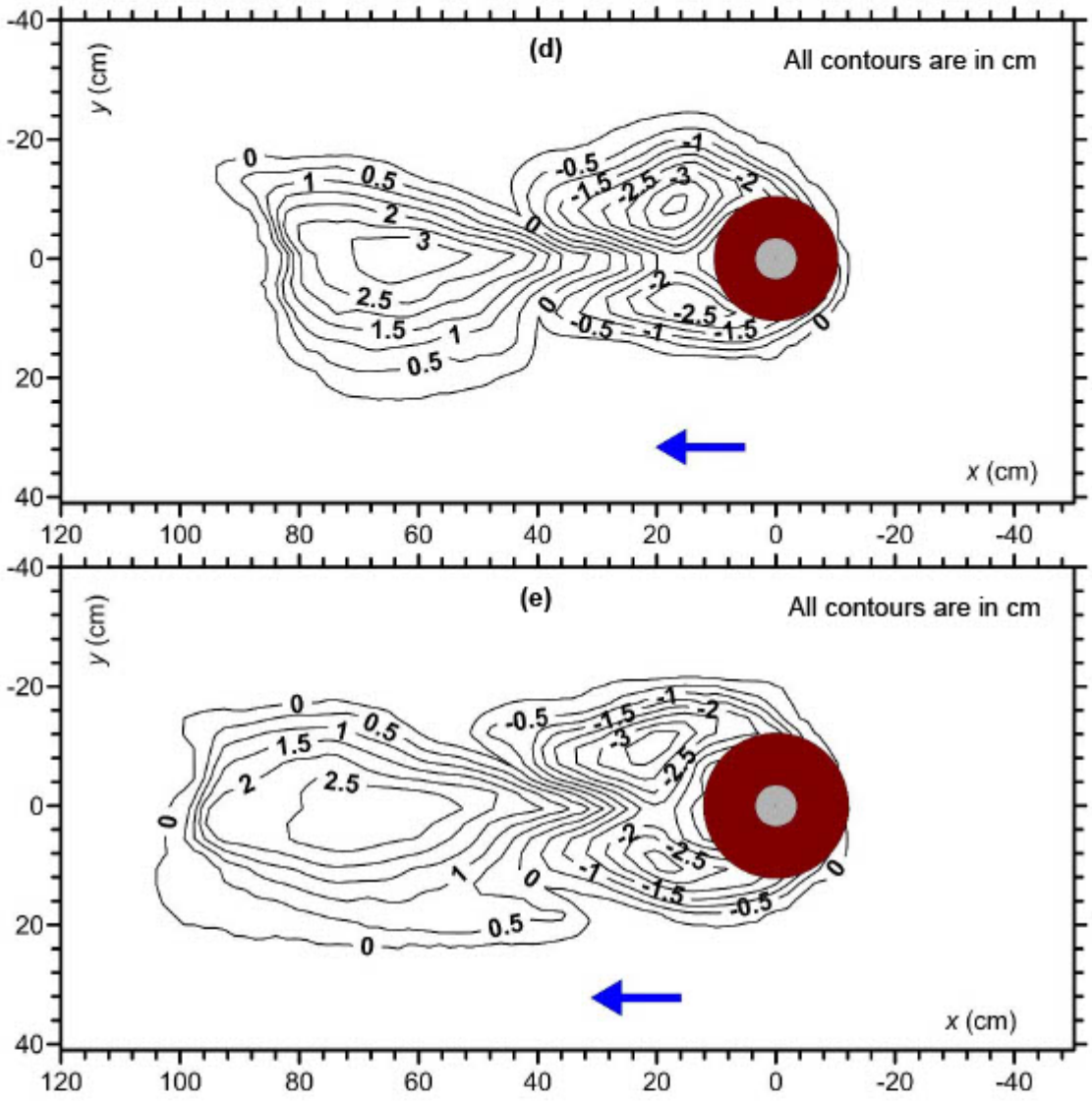


Fig. 6.20 Contours of scour holes and depositions for the pier protected with collars of diameters **(a)** 1.5*b*; **(b)** 2*b*; **(c)** 2.5*b*; **(d)** 3*b*; **(e)** 3.5*b* [Note: in all figures, (-) sign indicates scour and (+) sign indicates deposition].

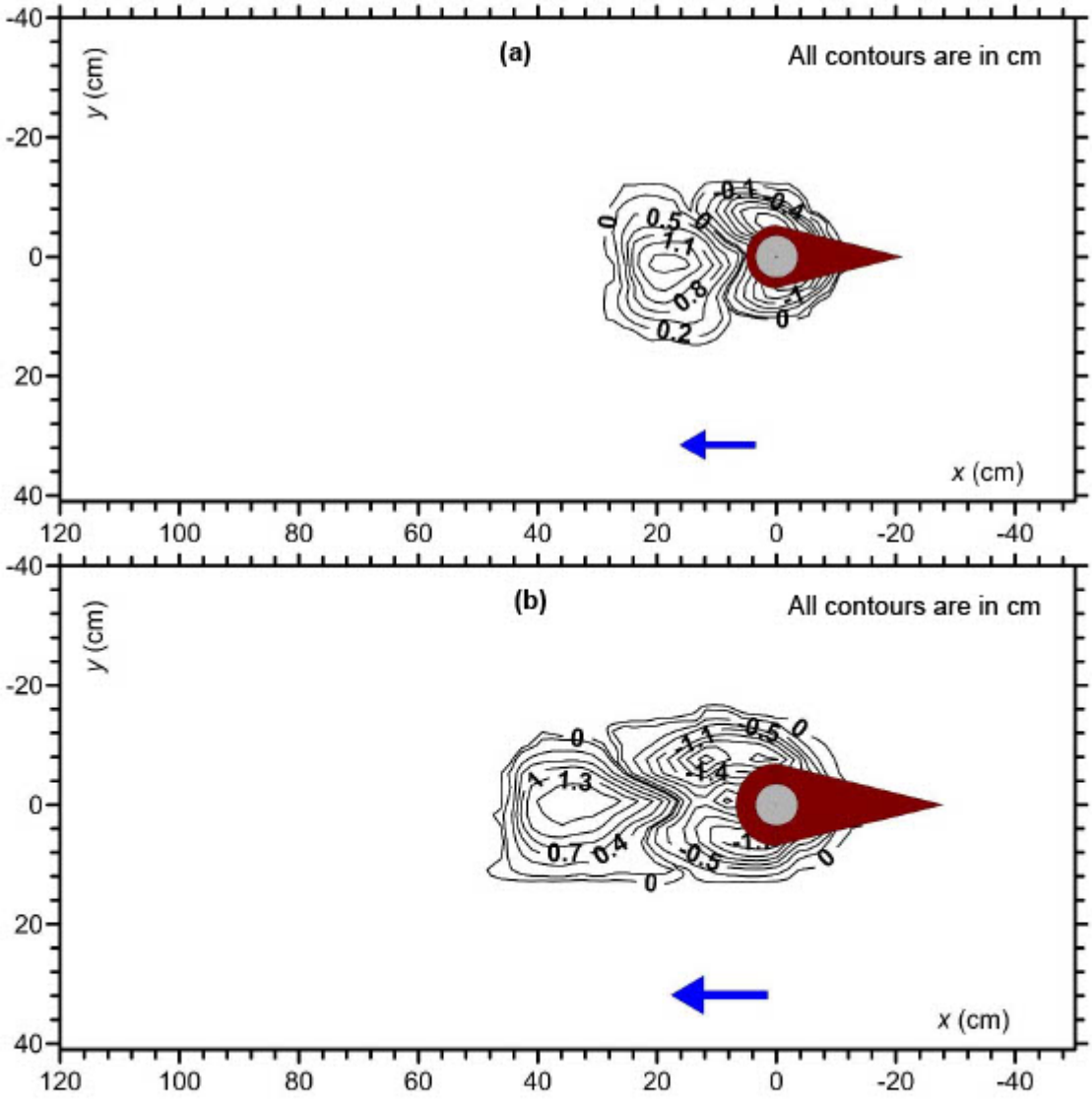
The maximum scour depth is 3.82 cm and the maximum height of the sediment deposition is 3 cm. The location of the maximum scour depth obtained is at $x = 20.5$ cm and $y = -11.5$ cm i.e., at the downstream of the pier (right side of the axis of symmetry). The (0,0) reference point is the center of the circular pier.

Figure 6.21a shows the contours of the scoured bed for the pier with an airfoil collar of diameter 1.5*b* (pier dia, $b = 7$ cm) and length $2b_c$ (collar dia, $b_c = 10.5$ cm). The maximum scour depth is 2.22 cm and the maximum height of deposition is 1.89 cm. The location of the maximum scour depth obtained is at $x = 0.5$ cm and $y = -4$ cm i.e., at the side (90°) of the pier (right side of the axis of symmetry).

Figure 6.21b shows the contours of the scoured bed for the pier with an airfoil collar of diameter $2b$ and length $2b_c$ (b_c = 14 cm). The maximum scour depth is 2.53 cm and the maximum height of deposition is 1.85 cm. The location of the maximum scour depth obtained is at x = 12 cm and y = -8 cm i.e., downstream of the pier (right side of the axis of symmetry).

Figure 6.21c shows the contours of the scoured bed for the pier with an airfoil collar of diameter $2.5b$ and length $2b_c$ (b_c = 17.5 cm). The maximum scour depth is 2.89 cm and the maximum height of deposition is 3.2 cm. The location of the maximum scour depth obtained is at x = 18 cm and y = -6.2 cm i.e., downstream of the pier (right side of the axis of symmetry).

Figure 6.21d shows the contours of the scoured bed for the pier with an airfoil collar of diameter $3b$ and length $2b_c$ (b_c = 21 cm). The maximum scour depth is 4.54 cm and the maximum height of deposition is 3.17 cm. The location of the maximum scour depth obtained is at x = 18.5 cm and y = -8 cm i.e., at the downstream of the pier (right side of the axis of symmetry). Figure 6.21e shows the contours of the scoured bed for the pier with an airfoil collar of diameter $3.5b$ and length $2b_c$ (b_c = 24.5 cm).



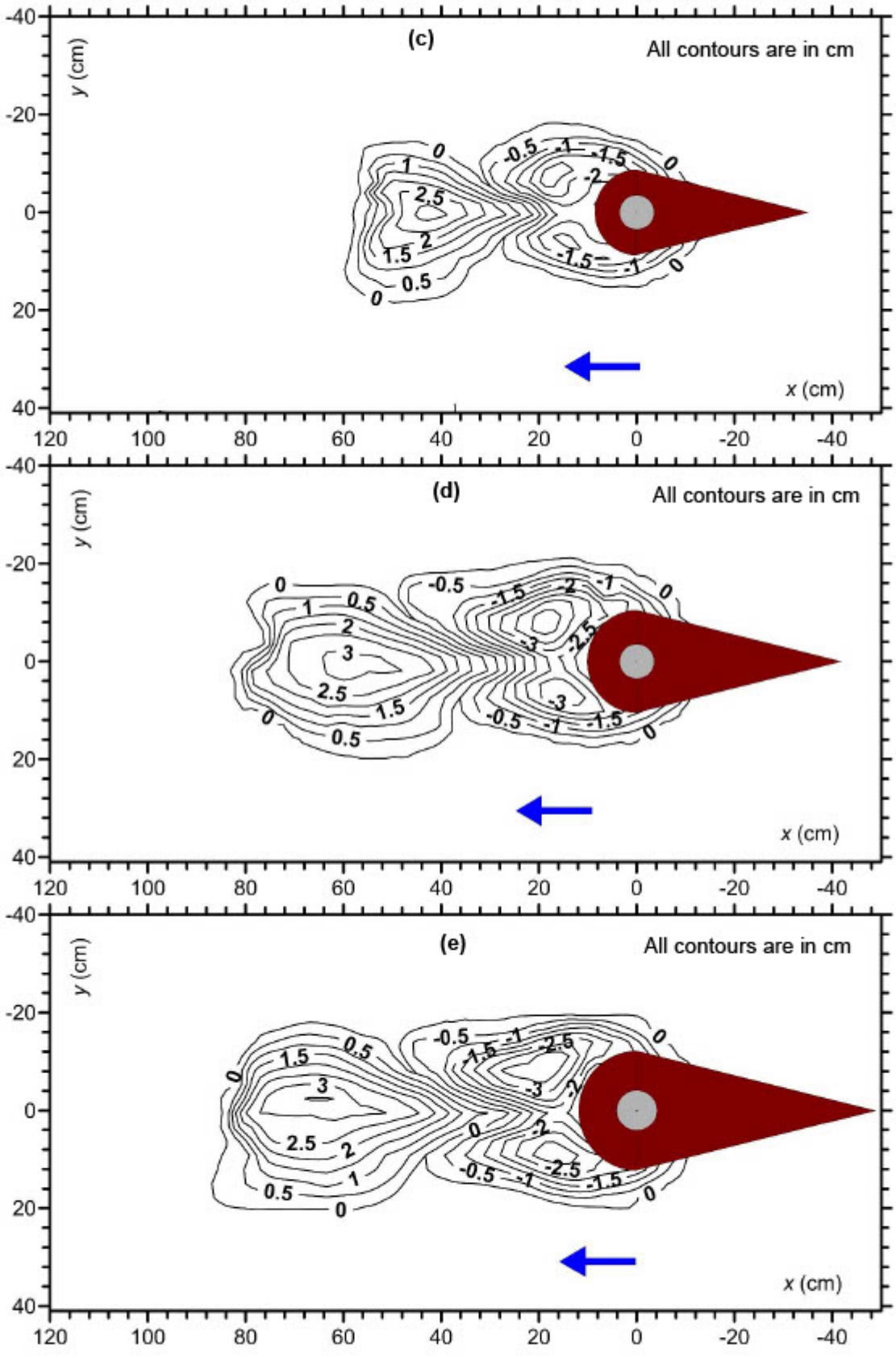

(c)
All contours are in cm
y (cm)
x (cm)
(d)
All contours are in cm
y (cm)
x (cm)
(e)
All contours are in cm
y (cm)
x (cm)

Fig. 6.21 Contours of scour holes for the pier protected with collars of diameters (b_c) equal to **(a)** 1.5b; **(b)** 2b; **(c)** 2.5b; **(d)** 3b; **(e)** 3.5b and collar length (l_c) of 2b_c [Note: in all figures, (-) sign indicates scour and (+) sign indicates deposition].

The maximum scour depth is 3.97 cm and the maximum height of deposition is 3.57 cm. The location of the maximum scour depth obtained is at x = 18.5 cm and y = -10 cm i.e., at the downstream of the pier (right side of the axis of symmetry). The (0,0) reference point is the center of the circular pier.

The location of the maximum scour depth we got at the end of each experiment, for no collar (D_{sm}) and in the presence of different collars (D_{scm}) is given in Table 6.2. The (0,0) point is a reference point located at the center of the circular pier. The locations are plotted in Fig. 6.22.

Table 6.2 Location of maximum scour depth observed during each experiment

Exp. No.	Shape of Collar	B (cm)	b_c/b (-)	(x, y) (cm, cm)
1	–	7	–	(-4.5,0)
2	Circular	7	1.5	(-1,3.7)
3	Circular	7	2	(14,5.5)
4	Circular	7	2.5	(17,5.5)
5	Circular	7	3	(16.5,9)
6	Circular	7	3.5	(20.5,11.5)
7	Airfoil	7	1.5	(0.5,5)
8	Airfoil	7	2	(12,8)
9	Airfoil	7	2.5	(18,6.2)
10	Airfoil	7	3	(18.5,8)
11	Airfoil	7	3.5	(18.5,10)

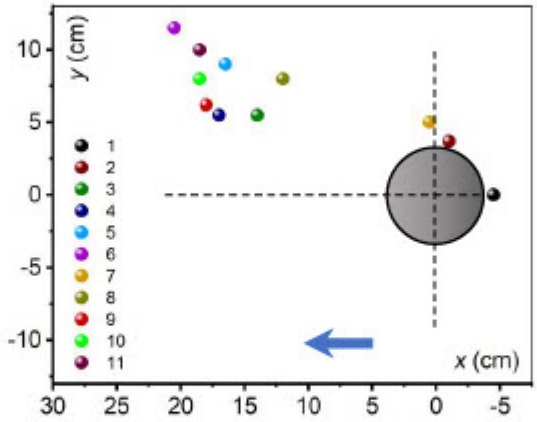


Fig. 6.22 Locations of maximum scour depths identified during 11 experiments.

6.7 Longitudinal Scour Hole Profile

A comparison of the longitudinal scour hole profiles for the cases of the unprotected pier and pier with circular or airfoil collars for different collar sizes is shown in Fig. 6.23. The overall scour hole length at the unprotected pier was observed smaller than that at the protected pier for the experimented flow conditions.

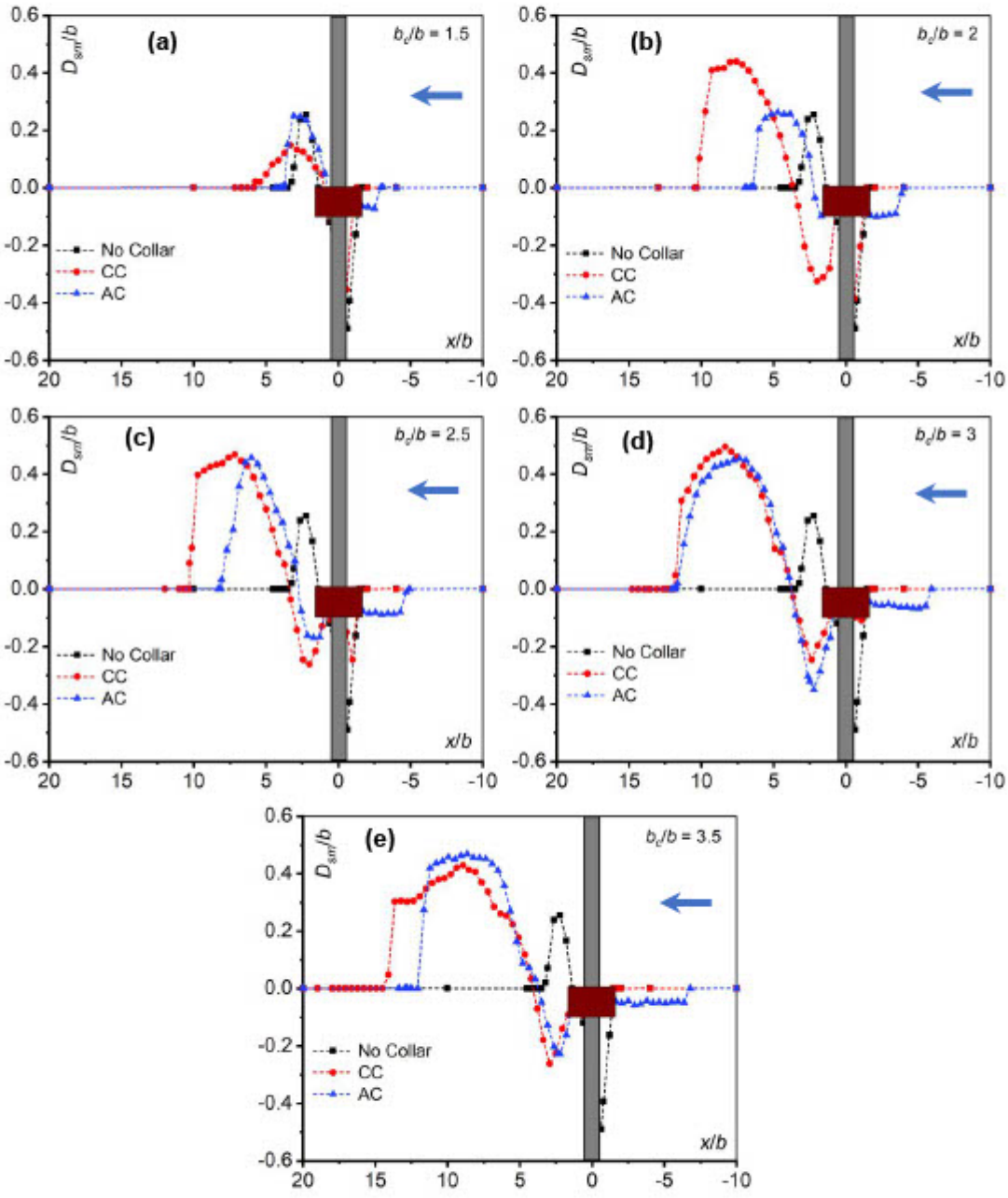


Fig. 6.23 Comparison of the longitudinal scour hole profiles for the pier with and without circular (CC) and airfoil collars (AC) of diameters **(a)** 1.5*b*, **(b)** 2*b*, **(c)** 2.5*b*, **(d)** 3*b*, **(e)** 3.5*b* at the maximum time (Note – Collar diameters and lengths are not in scale in the graphs)

However, the maximum scour depth (D_{scm}) was found the deepest among all for the unprotected pier and it occurred at the immediate upstream face of the pier. In the case of smaller circular collars (1.5b and 2b), the deepest scour was observed at the upstream face of the pier. The graph shows that even in the presence of 3b and 3.5b collars, scour still occurred, resulting in significant scour depth downstream in the wake which agrees with the findings of Kumar et al. (1999). However, this was far from the perimeter of the pier and hence not a major concern. The (0,0) reference point is located at the original bed level at the center of the pier and x is the length of the channel along the flow.

6.8 Scour Dimensions

The lengths, widths, planar areas, surface areas, and volumes of scour holes and depositions obtained from the experiments are given in Table 6.3. The schematic diagram of sediment transportation is shown in Fig 6.24. It can be seen that for an unprotected pier, the length of the scour (l_s) is 8.45% less than the width of the scour (w_s). For circular collars of 1.5b diameter, l_s and w_s are measured almost the same. For circular collars of diameters 2b, 2.5b, 3b, and 3.5b, the scour lengths are measured 54.69, 40.88, 36.54, and 49.76% more than the scour width, respectively. Whereas, for airfoil collars of diameters 1.5b, 2b, 2.5b, 3b, and 3.5b, the scour lengths are gauged 10.34, 42.62, 33.23, 53.47, and 49.37% more than the scour width, respectively.

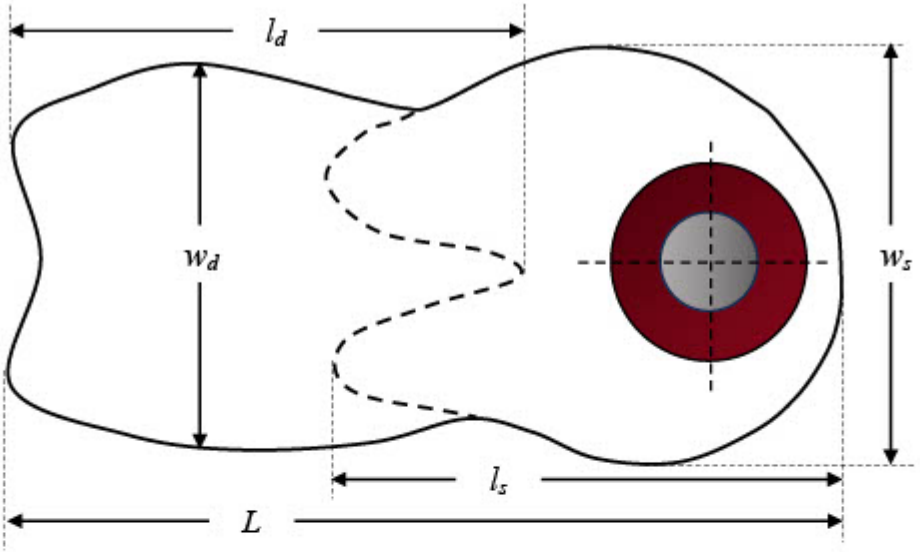


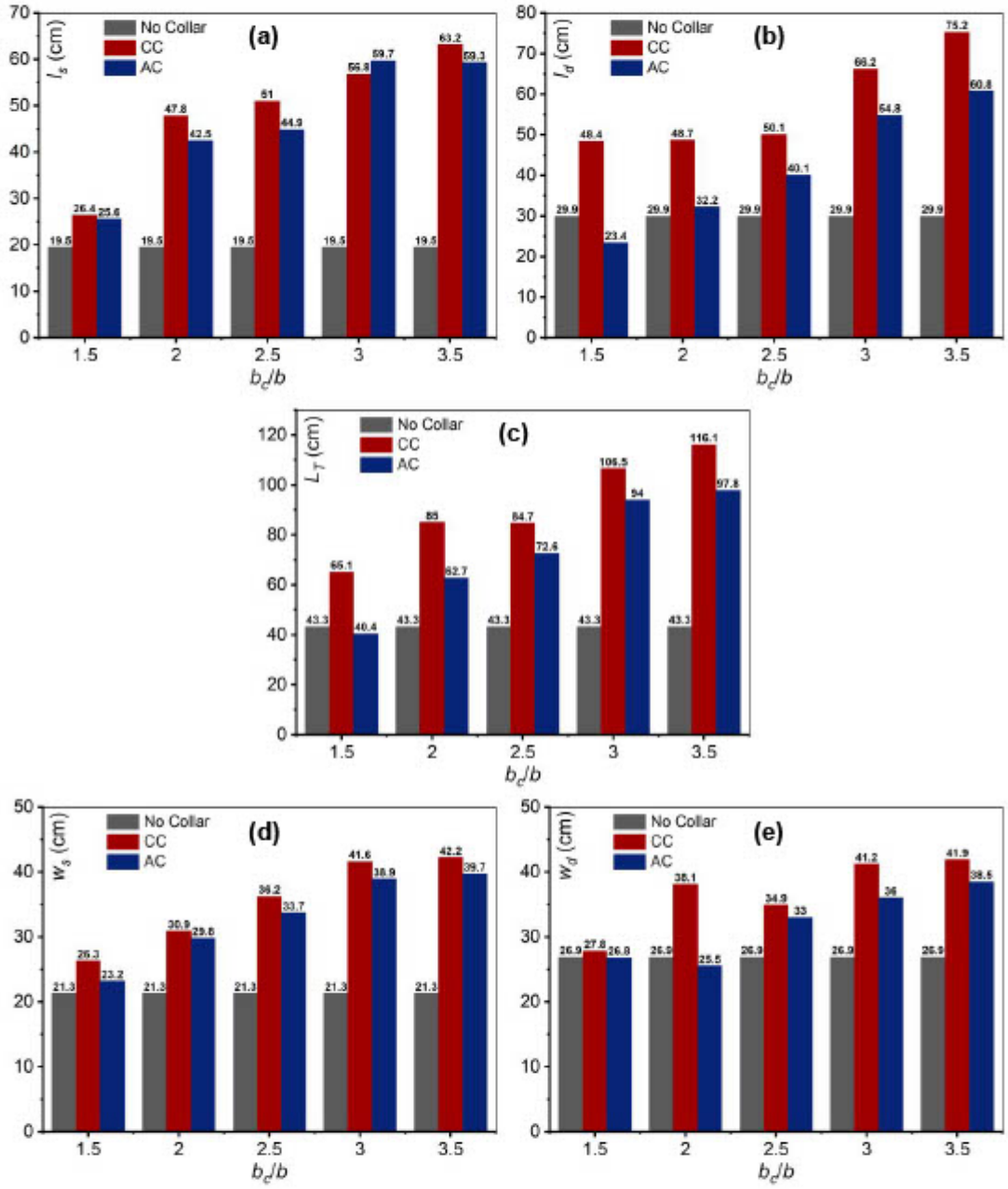
Fig. 6.24 Schematic diagram of sediment transportation after the experimental run for a pier with a circular collar ($b_c = 2.5b$).

Table 6.3 Scour and deposition details highlighting the length, width, area and volume.

Exp. No.	Collar	b (cm)	b_c/b	l_c/b	l_s (cm)	l_d (cm)	L_T (cm)	w_s (cm)	w_d (cm)	a_{ps} (cm^2)	a_{ss} (cm^2)	a_{pd} (cm^2)	a_{sd} (cm^2)	V_s (cm^3)	V_d (cm^3)
1	No Collar	7	–	–	19.5	29.9	43.3	21.3	26.9	517.5	558.0	643.5	656.0	439.9	320.7
2	Circular	7	1.5	–	26.4	48.4	65.1	26.3	27.8	611.8	642.6	698.0	704.0	470.5	320.4
3	Circular	7	2	–	47.8	48.7	85	30.9	38.1	1260.7	1339.8	1345.5	1385.6	1745.7	1669.0
4	Circular	7	2.5	–	51	50.1	84.7	36.2	34.9	1580. 8	1650.4	1584.0	1635.2	1599.3	1829.2
5	Circular	7	3	–	56.8	66.2	106.5	41.6	41.2	2659.2	2734.6	1806.8	1857.9	2387.7	2362.4
6	Circular	7	3.5	–	63.2	75.2	116.1	42.2	41.9	2493.9	2580.6	3591.9	3640.9	2490.7	2859.3
7	Airfoil	7	1.5	3	25.6	23.4	40.4	23.2	26.8	608.4	631.0	629.2	639.2	346.3	317.4
8	Airfoil	7	2	4	42.5	32.2	62.7	29.8	25.5	1165.4	1202.8	921.3	937.3	756.6	442.1
9	Airfoil	7	2.5	5	44.9	40.1	72.6	33.7	33	1348.4	1395.5	1781.5	1816.7	1183.2	1084.3
10	Airfoil	7	3	6	59.7	54.8	94	38.9	36	2840.4	2928.0	1884.7	1931.7	2421.5	1952.8
11	Airfoil	7	3.5	7	59.3	60.8	97.8	39.7	38.5	2953.8	3045.8	2587.6	2638.1	2467.7	2221.4

Note: b is pier diameter, b_c is collar diameter, l_c is the length of airfoil collar, l_s is the length of scour, l_d is the length of deposition, L_T is the total length of sediment transportation, w_s is the width of scour, w_d is the width of deposition, a_{ps} is the planar area of scour, a_{pd} is the planar area of deposition, ass is the surface area of scour, a_{sd} is the surface area of deposition, V_s is the volume of scour, V_d is deposition volume.

A comparison of different scour dimensions for circular and airfoil collars relative to an unprotected pier is shown in the bar charts below (Fig. 6.25). These charts illustrate the scour dimensions for different collar configurations [No Collar, Circular Collar (CC), and Airfoil Collar (AC)] at various ratios of b_c/b.



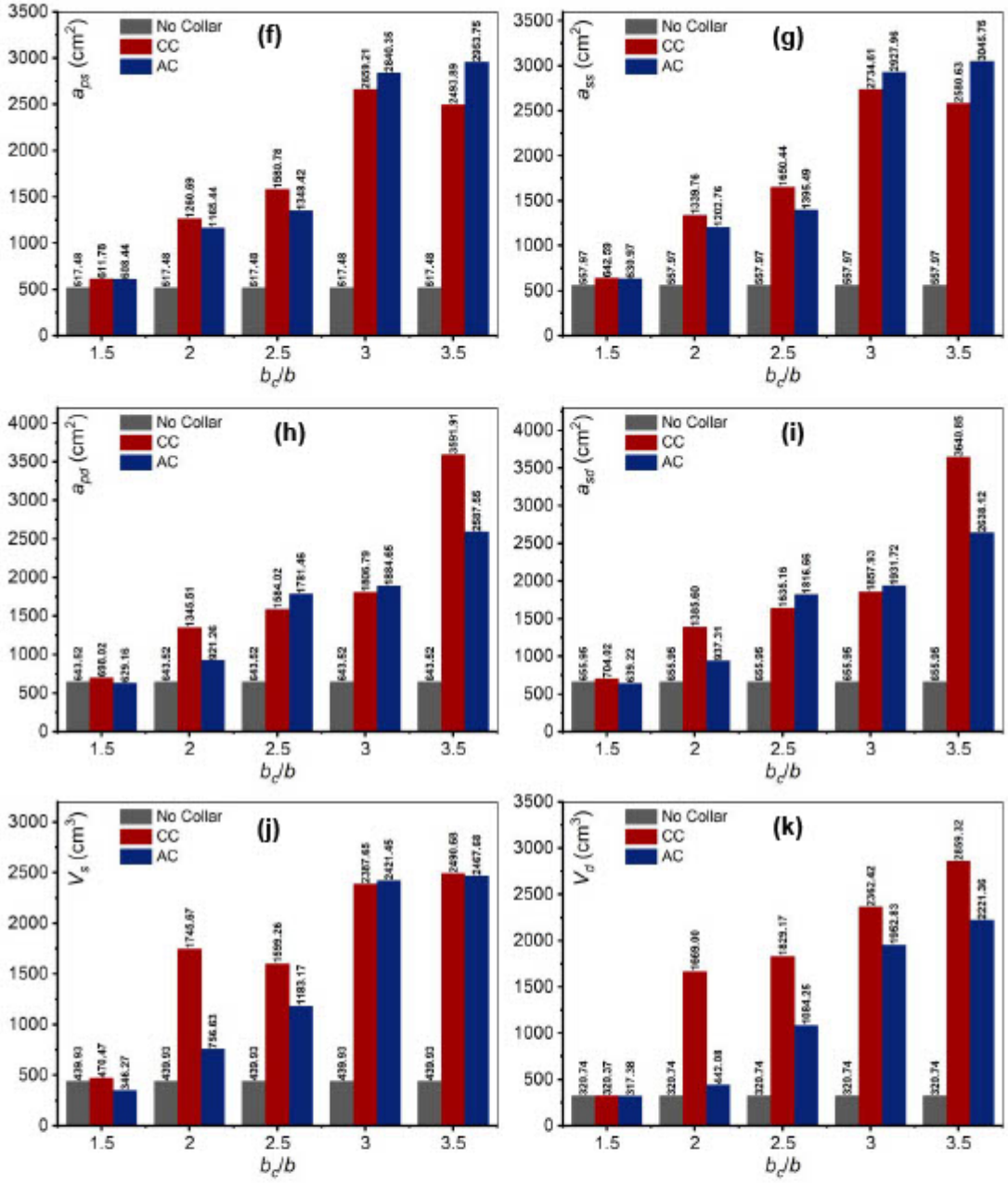


Fig. 6.25 Comparison of different scour dimensions: **(a)** scour length, **(b)** deposition length, **(c)** length of sediment transportation, **(d)** scour width, **(e)** deposition width, **(f)** planar area of scour, **(g)** surface area of scour, **(h)** planar area of deposition, **(i)** surface area of deposition, **(j)** volume of scour, and **(k)** volume of deposition

6.9 Influence of Collar Shape on Scour Protection Efficiency

In the previous sections, we saw the temporal development of scour depths at different locations (upstream face of the pier, edges of collars upstream and downstream, etc). However, from the experiments conducted, we observed that the two most important locations

for scouring around a pier protected with a collar are the upstream face of the pier and the sides of the pier. Also, different shapes of collars have different effects on maximum scour depths. In this section, a comparative study on the protection efficiencies of collars has been carried out between circular and airfoil collars. In this section, we have considered only two locations – (a) the upstream face of the pier and (b) sides of the pier (as shown in Fig. 6.26) for both the unprotected pier and pier protected with the collar. The aim of using a collar is to protect scour in the vicinity of the pier perimeter and that is why we have considered these two locations around the pier perimeter in this section for analysis.

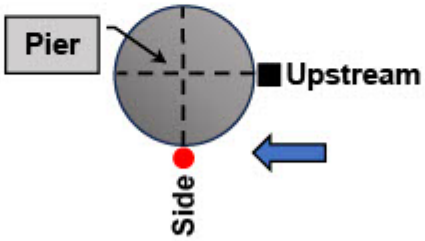


Fig. 6.26 Measuring points of maximum scour depth.

Variation of maximum scour depth with respect to different sizes of different shapes of collars (circular and airfoil) is shown in Fig 6.27. For an unprotected pier, maximum scour depth is observed at the upstream and for a pier protected with collars, it is observed at the sides of the pier. It is because in the presence of a collar the initial scouring pattern and location changes. The larger collars protected the pier completely for both airfoil and circular collars.

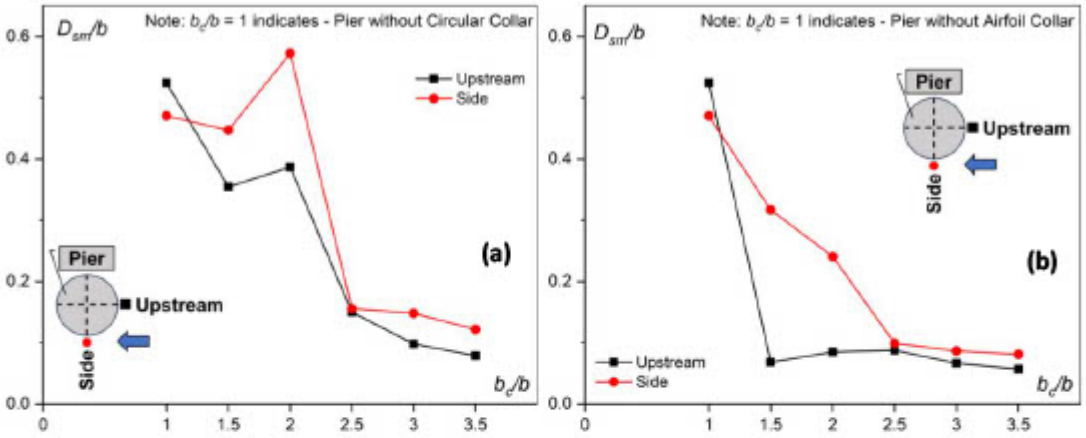


Fig. 6.27 Maximum scour depth variation at the upstream and side of the pier without and with different sizes of **(a)** Circular collar; **(b)** Airfoil collar

In Fig. 6.28, a comparison has been made for maximum scour depth observed at the vicinity of the pier perimeter for an unprotected pier, a pier with circular collars, and a pier with airfoil collars. It is seen that for an airfoil collar, the maximum scour depth is less than

that of a circular collar at both measuring points. It may be due to the length of the airfoil collar which protects the pier scour.

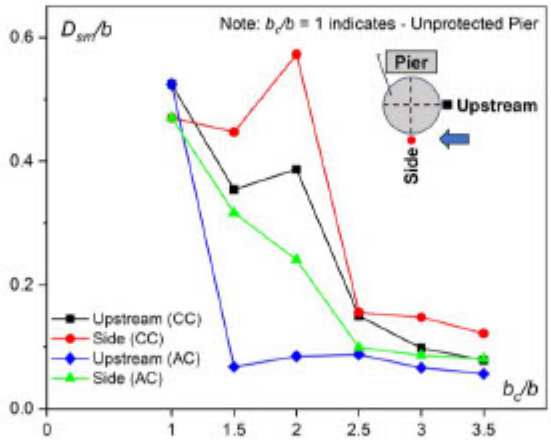


Fig. 6.28 Comparison between maximum scour depths at circular and airfoil collars.

In Table 6.4, the details of maximum scour depth and the percentage reduction of scour depth in the presence of collars are given. Protection efficiency of the collar,

$$\%R = \left(\frac{D_{sm} - D_{scm}}{D_{sm}} \right) \times 100 \tag{6.2}$$

Table 6.4 Protection efficiency of circular and airfoil collar

Shape of Collar	b_c/b	l_c/b	t_m (min)	Max Scour Depth (D_{sm}) (cm)		Protection Efficiency (%)	
				Upstream	Side	Upstream	Side
No Collar	1	–	540	3.670	3.293	–	–
Circular	1.5	–	180	2.480	3.130	32.43	4.94
Circular	2	–	400	2.707	4.007	26.23	-21.70
Circular	2.5	–	580	1.050	1.090	71.39	66.90
Circular	3	–	360	0.686	1.036	81.32	68.55
Circular	3.5	–	360	0.552	0.852	84.96	74.13
Airfoil	1.5	3	300	0.477	2.217	87.00	32.67
Airfoil	2	4	360	0.594	1.684	83.81	48.86
Airfoil	2.5	5	180	0.613	0.693	83.29	78.95
Airfoil	3	6	540	0.465	0.605	87.32	81.62
Airfoil	3.5	7	480	0.396	0.566	89.20	82.80

It can be seen that the protection efficiencies of circular collars compared to an unprotected pier were 32.43, 26.23, 71.39, 81.32, and 84.96% for 1.5*b*, 2*b*, 2.5*b*, 3*b*, and 3.5*b* respectively at upstream and 4.94, 66.9, 68.55, and 74.13% for 1.5*b*, 2.5*b*, 3*b*, and 3.5*b* at the side of the pier. On the other hand for airfoil collar, those were 87, 83.81, 83.29, 87.32, and

89.20% for 1.5*b*, 2*b*, 2.5*b*, 3*b*, and 3.5*b* respectively at upstream and 32.67, 48.86, 78.95, 81.62, and 82.80% for 1.5*b*, 2*b*, 2.5*b*, 3*b*, and 3.5*b* at the side of the pier.

A comparison of the protection efficiencies of circular and airfoil collars at the upstream face of the collar is shown in Fig. 6.29. It is seen from the plot that the airfoil collar is more effective in reducing scour at the upstream face of the pier.

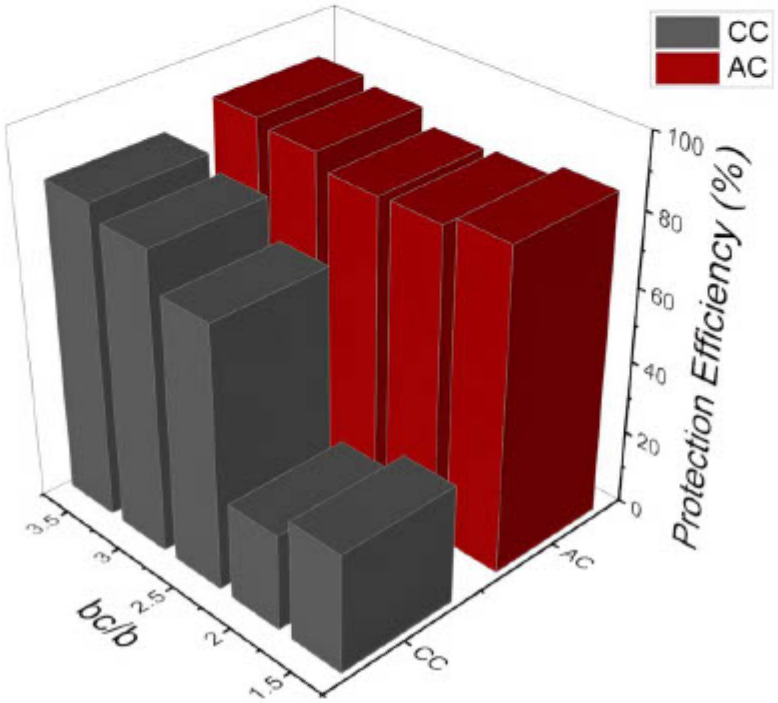


Fig. 6.29 Comparison of protection efficiencies of circular and airfoil collars at the upstream face of the pier.

6.10 Overall Discussion

Scouring around a circular pier built on erodible bed material is a complex and three-dimensional issue. Despite extensive research, the mechanisms behind clear-water scour around bridge piers are still not fully understood. This leads to various methods for estimating scour depth. Several countermeasures have been proposed to mitigate local scour, with the use of collars being one such technique, primarily based on model studies. In real-world scenarios, peak flood flows might last only for a few hours or days, which may not be enough time for the scour depth to reach equilibrium. As a result, the actual scour depth during these short-duration floods may be only a fraction of the equilibrium depth, which could take weeks or even months to fully develop. Installing a collar on a pier prevents downflow from directly hitting the riverbed, which lowers the depth of scour. It not only reduces the maximum scour depth but also reduces the rate of scour significantly. Thus, collars can effectively reduce the development of scour and mitigate its impact on bridge piers during short-duration floods.

From the experiments conducted in the present study and previous literatures, we observed that collars of larger diameters (3*b*-3.5*b*) can be an effective scour countermeasure.

Airfoil collars were found to be more effective than circular collars. The possible reason could be the area coverage by the collar for sediment protection. The area covered by the airfoil collar at the upstream side of the pier was more than that by the circular collar and due to this reason, the airfoil collar protected a larger area of sediment bed from the impingement of downflow and subsequently horseshoe vortex. Maybe because of this, the airfoil collar showed greater protection efficiency.

Also, the maximum scour depth was found to occur downstream of the pier in the case of the collars that protected the upstream side of the pier like the larger-sized collars ($b_c = 3b$-$3.5b$). However, for $1.5b$ and $2b$ circular collars, which were not at all effective in protecting scour, the location of the maximum scour depth was the same as the unprotected pier i.e., the upstream face of the pier. Although the scour depth for the larger-sized collars found downstream of the pier was of significant amount it was not of much concern as the scour was far away from the pier perimeter.

An accurate estimation of scour depth in the presence of a collar is needed, to decide whether the collar will be an effective countermeasure for a given situation or not. That's why in the present study an attempt has been made to develop a predictive model using machine learning techniques and a new equation using nonlinear regression analysis for predicting temporal scour depth around the pier in the presence of a collar and these are discussed in the following chapter.

CHAPTER – 7

PREDICTIVE MODEL AND NEW EMPIRICAL EQUATION

7.1 Predictive Model of Temporal Scour Depth using CART Regression

The maximum depth of scour around a pier with a collar is influenced by several factors, including the collar's diameter and position, as well as parameters that affect scour depth without a collar, such as flow velocity and sediment characteristics, as discussed in Chapter 3. Various researchers have developed equations for maximum and temporal variations in scour depth without a collar (Melville and Chiew, 1999; Oliveto and Hager, 2002; Kothyari et al., 2007). However, a few studies have proposed equations for scour depth around piers protected by circular and airfoil collars (Kumar et al., 1999; Pandey et al., 2020; Pandey et al., 2022; Gupta et al., 2023*b*; Gupta et al., 2024).

In the present study, a predictive model of temporal scour depth around the pier with a collar has been developed using the CART regression method. Classification and Regression Tree (CART) analysis is a very common modeling method used to make a prediction on a variable (Y), based upon several explanatory variables, X_1, X_2, ... , Xp.

7.1.1 Modeling of Scour Depth for Pier with Circular Collars

By rearranging the most important parameters and using dimensional analysis, temporal scour depth around the pier in the presence of a circular collar can be written as Eq. 7.1.

$$\frac{D_{sct}}{b} = f\left(\frac{b_c}{b}, \frac{h}{h_w}, \frac{U}{U_c}, \frac{Ut}{b}, \frac{d_{50}}{b}, \mathrm{Re}, \mathrm{Fr}\right) \tag{7.1}$$

A correlogram is a graphical representation used to display the correlation coefficients between multiple variables in a dataset. Correlation is a statistical term that describes the extent to which two variables are related. A positive correlation between two variables means that an increase in one variable is associated with an increase in the other. Conversely, if an increase in one variable causes a decrease in the other, then they have a negative correlation. It is expressed numerically by the correlation coefficient. The range of correlation coefficient ranges between -1 and 1.

From the correlogram (Fig. 7.1) we can see that Fr (Froude number) and d_{50}/b have a strong relationship hence Fr can be eliminated. Again, Fr and Re_p (Reynolds number) are related and hence Re_p can also be eliminated.

The relative importance of the remaining variables is given in Fig. 7.2. Here, it is found that the most significant influential parameter is Ut/b. The minimum importance is identified for the U/U_c among the five influential parameters.

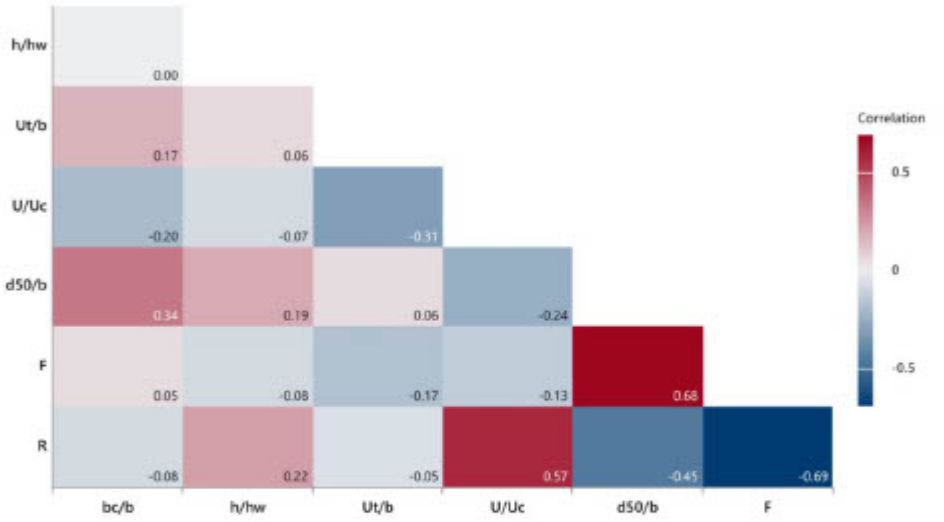


Fig. 7.1 Correlogram showing the correlation between b_c/b, h/h_w, Ut/b, U/U_c, d_{50}/b, Fr, Re_p.

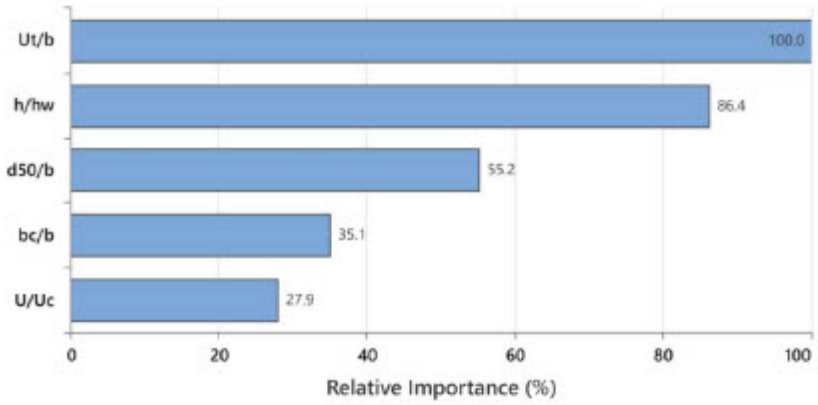


Fig. 7.2 Relative Variable Importance.

The method used for the modeling is given in Table 7.1. In CART regression, the 80-20% training-testing refers to the method of splitting the dataset into a training set (80% of the data for building a predictive model) and a testing set (20% of the data for evaluating the model). A total of 504 data points have been used for building the CART model. The node splitting method used is the least squared error and the criterion for selecting the optimal tree is maximum R^2.

Table 7.1 Methods for building the model (Circular Collar)

Criteria	Method
Node splitting	Least squared error
Optimal tree	Maximum R-squared
Model validation	80/20% training/testing data points
Data points used	504

R-squared (R^2 or the coefficient of determination) is a statistical measure in a regression model that indicates the proportion of variance in the dependent variable explained by the independent variable. In other words, R^2 determines how well the regression model fits the data. The most common interpretation of R-squared is how effectively the regression model explains the observed data. Generally, the higher the R^2 value, the better the model fits the data. R^2 is always between 0% and 100%.

For training 406 data points and for the test 98 data points are used. The descriptive statistics about the response variable are given in Table 7.2. The mean, standard deviation, minimum, median, and maximum are measured in the same units as the original data. Here, the input data, non-dimensional temporal scour depth (D_{sct}/b) is unitless and that is why the mean, standard deviation, etc. values are also unitless.

Table 7.2 Response Information of training and testing data points

Data points	N	% of N	Mean	SD	Minimum	Median	Maximum
Training	406	80.6	0.474	0.442	0	0.358	1.77
Testing	98	19.4	0.541	0.478	0	0.374	1.71

Note: SD is the standard deviation of non-dimensional temporal scour depth (D_{sct}/b), and N is the number of data points.

By default, the starting point for the regression tree is the smallest tree with an R^2 value within 1 standard error of the maximum R^2 value. In analyses involving cross-validation or a separate test data points, the R^2 value is derived from the validation sample.

The plot given in Fig. 7.3 illustrates the R^2 value corresponding to each tree. The regression tree with 51 terminal nodes has an R^2 value of approximately 0.935. It is labeled "Optimal" because it represents the smallest tree with an R^2 value within 1 standard deviation of the maximum R^2 value. Since the R^2 values remain relatively stable for trees with around 40 to 65 nodes (can be seen from Fig. 7.3), we evaluate the performance of a smaller tree that is similar to the one in the results. Generally, an alternative tree is chosen for one of two reasons:

- The tree selected by Minitab is part of a pattern where the criterion improves, and there are one or more trees with slightly more nodes that follow the same pattern. In this case, typically the aim is to use a tree with the highest prediction accuracy possible.
- The tree selected by Minitab is part of a pattern where the criterion remains relatively flat, and there are one or more trees with similar model summary statistics but significantly fewer nodes than the optimal tree. In such cases, a tree with fewer terminal nodes often provides a clearer understanding of how each predictor variable influences the response values. A smaller tree also makes it easier to identify specific target groups for further study. If the decrease in prediction accuracy for a smaller tree is negligible, the smaller tree can be used to analyze the relationships between the response and predictor variables.

The regression tree with 47 terminal nodes has an R^2 value of 0.9319 (Fig. 7.3). The detailed alternative decision tree is given in Appendix I. The tree diagram shows all 406 cases (training dataset) from the full dataset. The root node is the top node in the tree and is the only one without any parent nodes. At each node, data is divided into two child nodes based on

specific characteristics. This process of splitting continues at each node until there is no further data to divide, resulting in terminal nodes that cannot be split any further. When validating the tree's performance with a test data set, the tree diagram displays cases from the training data set.

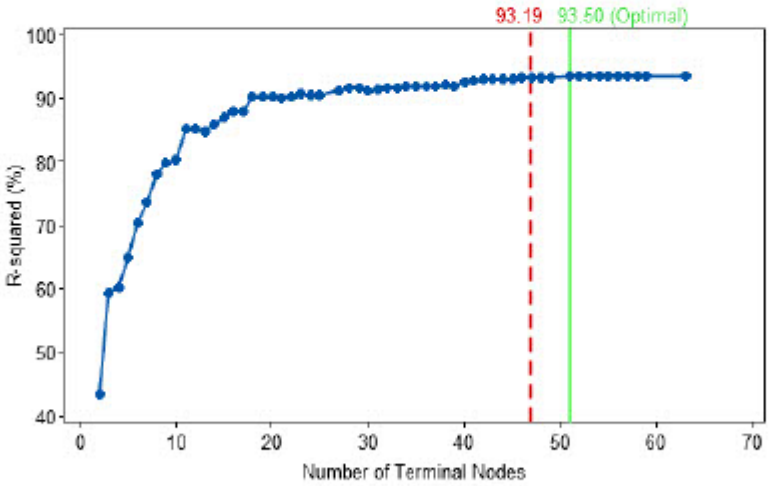


Fig. 7.3 R^2 versus Number of Terminal Nodes.

Each node presents details on the mean, standard deviation, and count. The mean represents the average response value of the cases within the node and serves as the predicted value for new data that falls into the same node. Terminal nodes with means that differ the most from other terminal nodes may be of particular interest because the predictions for cases in these nodes are the most distinct. For instance, nodes with the highest or lowest means may be of special interest. The standard deviation reflects the variability of the response values within the node. Terminal nodes with smaller standard deviations may be of particular interest because their predictions are more precise compared to the terminal nodes with larger standard deviations. The total count represents the number of cases within the node. Terminal nodes with a large number of cases may be of particular interest, as they often represent more common scenarios.

The first node is split using the variable h/h_w. Node 2 has the cases where $h/h_w \leq 0.825$. This node contains 59 cases. The mean for the node exceeds the overall mean. The standard deviation for Node 2 is approximately 0.363, which is lower than the overall standard deviation because a split creates more pure nodes. Node 11 includes cases where $h/h_w > 0.825$, with a total of 347 cases. The standard deviation for Node 11 is approximately 0.365, which is lower than the overall standard deviation. Based on different variables, these nodes are further split. This tree has 47 terminal nodes and Terminal Node 30 has the lowest standard deviation.

The number of important predictors is five. The importance order of these five variables is given in Fig. 7.2 (Relative variable importance). A terminal node is a final node that cannot be split further. RMSE, MSE, MAD, and MAPE measure the accuracy of the tree and smaller values indicate a better fit. In this study, RMSE, MSE, and MAD are unitless. The model summary is given in Table 7.3.

Table 7.3 Model Summary

Total predictors	5	
Important predictors	5	
Number of terminal nodes	47	
Minimum terminal node size	3	
Statistics	Training	Testing
R-squared (R^2)	0.9688	0.9319
Root mean square error (RMSE)	0.0780	0.1241
Mean squared error (MSE)	0.0061	0.0154
Mean absolute deviation (MAD)	0.0538	0.0913
Mean absolute percentage error (MAPE)	3.9332	4.1880

A scatterplot is used to assess the accuracy of the predictions. The calculated line signifies where the observed value matches the predicted value. Any outliers or clusters of points that deviate significantly from this line in the test data may indicate that the data points need further investigation. The scatterplot given in Fig. 7.4 displays almost similar patterns in both the training and test datasets, indicating that the performance of the tree on new data is closely identical to its performance on the training data.

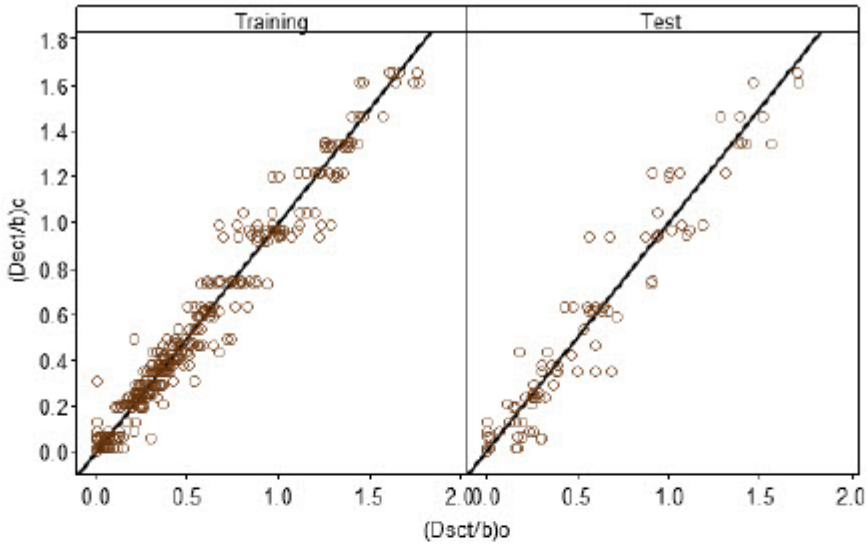


Fig. 7.4 Scatterplot of computed versus observed nondimensional temporal scour depth.

The accuracy of the fits is more reliable for nodes with lower MSE values. Figure 7.5 shows that the terminal node 28 has lower accuracy compared to the other terminal nodes. Terminal node 28 presents the greatest opportunity for improvement of the tree if the variation can be reduced.

From Fig. 7.6, it is seen that terminal node 21 exhibits the largest residual, while terminal node 45 shows a series of negative residuals. Further investigation of these points may uncover why the tree does not fit them as well as other points in the node.

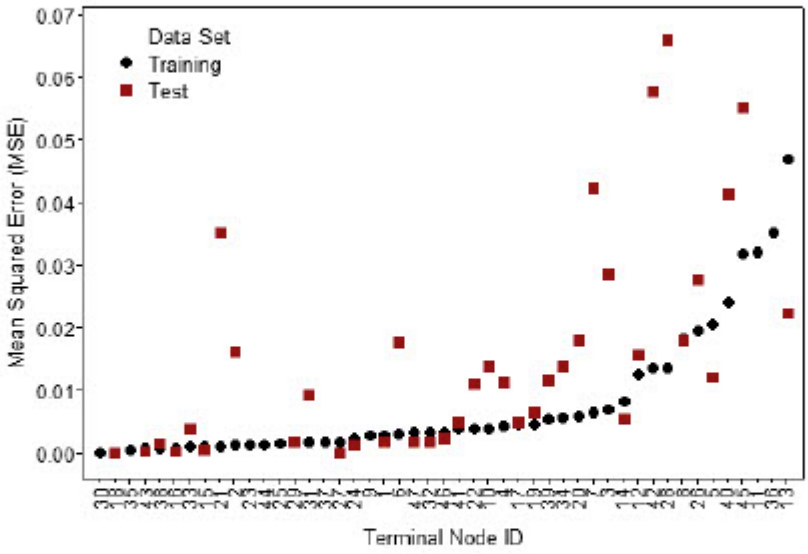


Fig. 7.5 Scatterplot showing the MSE at different Terminal Nodes.

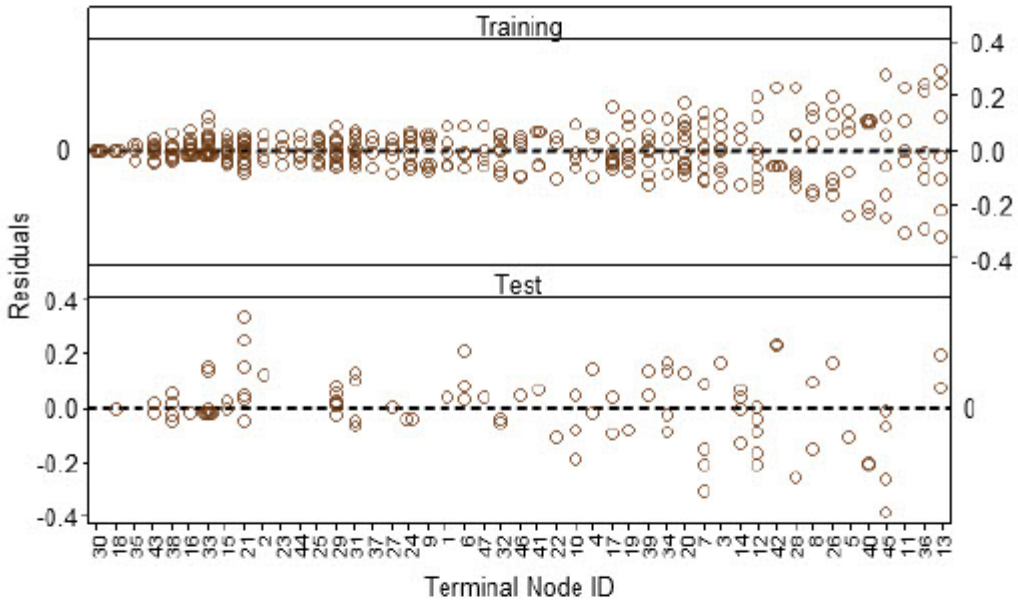


Fig. 7.6 Residual Plot training and testing data at different Terminal Nodes.

The R^2, RMSE, and MAD and percentage in (P_{in}) for 10%, 20%, and 30% error lines have been calculated for Pandey et al. (2020), Gupta et al. (2024), and the present study. These are presented in Table 7.4. The R^2 value lies between 0 to 1 or 0 to 100%. From the formulas of RMSE and MAD (given in Chapter 4), we can see that the unit of these values depends on the units of $(D_{sct}/b)_o$ and $(D_{sct}/b)_c$. As $(D_{sct}/b)_o$ and $(D_{sct}/b)_c$ are unitless, RMSE and MAD are unitless. The data in Table 7.4 shows that the predictive model of the present study performs well.

Table 7.4 Performance matrix using different statistical measures

Literature	R^2	RMSE	MAD	P_{in} (10%)	P_{in} (20%)	P_{in} (30%)
Pandey et al. (2020)	0.72	0.24	0.31	9.33	22.02	35.71
Gupta et al. (2024)	0.28	0.49	0.36	17.86	34.13	46.63
Present study	**0.96**	**0.09**	**0.36**	**39.68**	**60.91**	**70.04**

The perfect agreement line (PAL) is a reference line used in the plot to indicate where the observed values, $(D_{sct}/b)_o$ perfectly match the computed values of scour depths, $(D_{sct}/b)_c$. Figure 7.7 shows that approximately 39.68%, 60.91%, and 70.04% of the data points for the predictive model of the present study are within ±10%, ±20%, and ±30% error lines respectively.

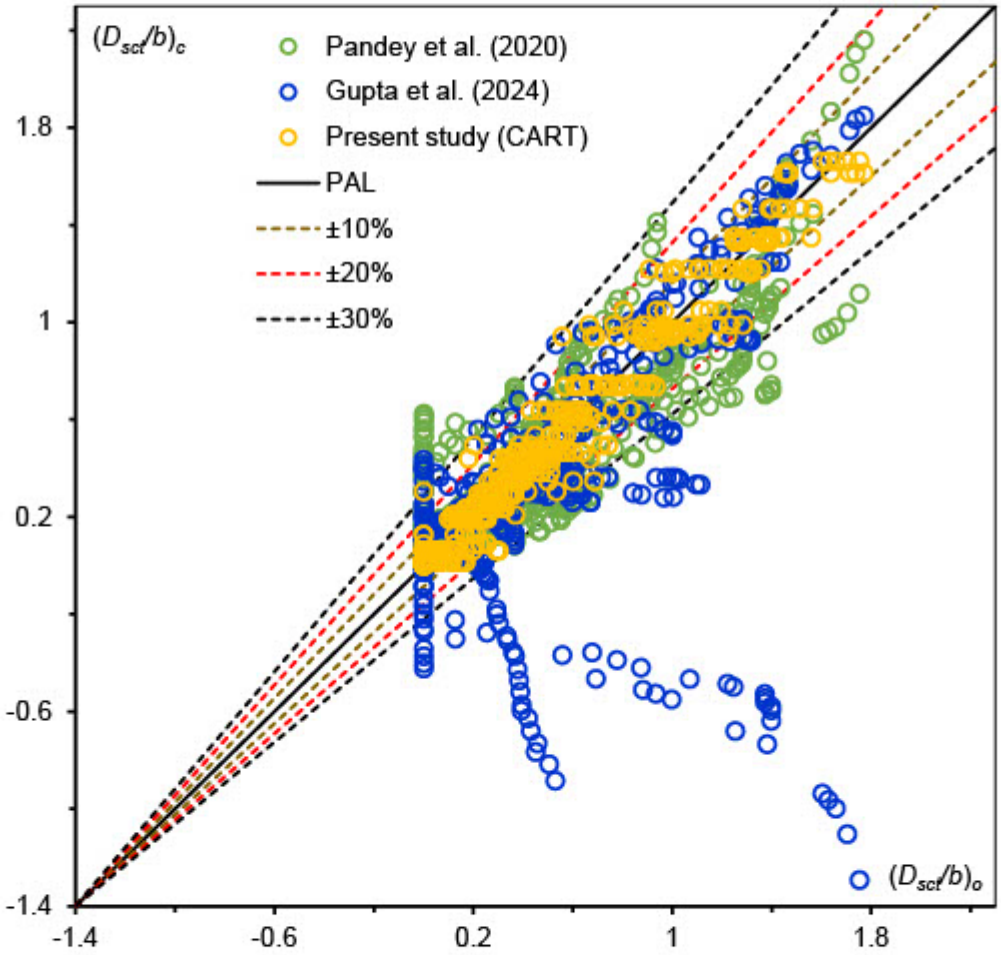


Fig. 7.7 Graphical representation of error analysis of computed and observed non-dimensional temporal scour depth around a circular pier with a circular collar for ±10%, ±20%, and ±30% error lines.

7.1.2 Modeling of Scour Depth for Pier with Airfoil Collars

By rearranging the most important parameters and using dimensional analysis, temporal scour depth around the pier in the presence of an airfoil collar can be written as (Eq. 7.2):

$$\frac{D_{scr}}{b} = f\left(\frac{b_c}{b}, \frac{l_c}{b}\frac{h}{h_w}, \frac{U}{U_c}, \frac{Ut}{b}, \frac{d_{50}}{b}, \mathrm{Re}, \mathrm{Fr}\right) \tag{7.2}$$

From the correlogram (Fig. 7.8) we can see that Fr (Froude number) and d_{50}/b have a strong relationship. Hence Fr can be eliminated. Again, Fr and Re (Reynolds number) are related and hence Re can also be eliminated. Again, b_c/b and l_c/b, have a correlation coefficient of 1, and hence l_c/b can also be eliminated. Again d_{50}/b and Re also have a correlation coefficient of 1. Hence, d_{50}/b is eliminated. The relative importance of the remaining variables is given in Fig. 7.9.

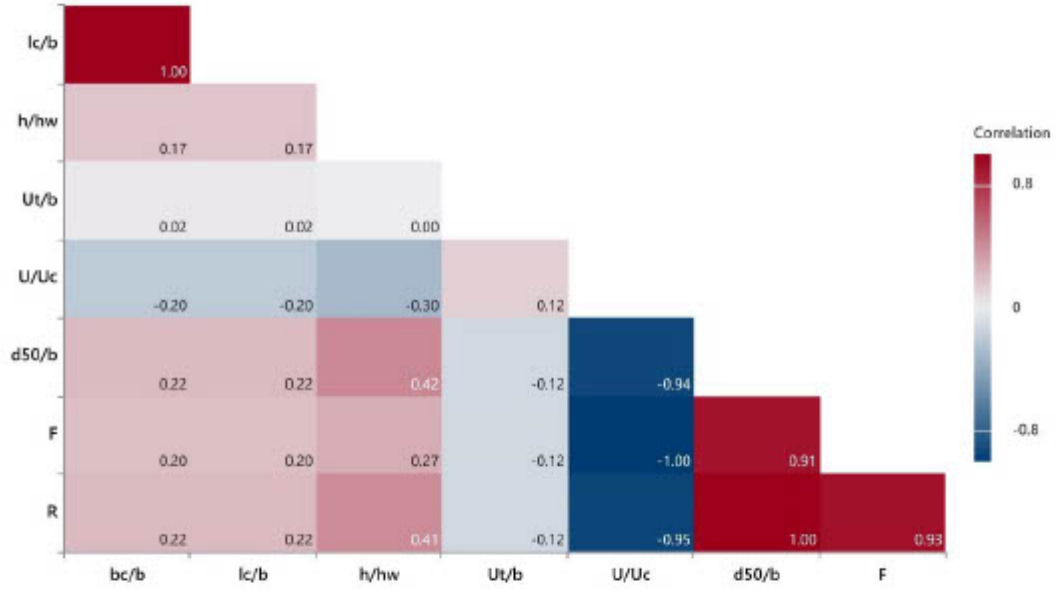


Fig. 7.8 Correlogram showing correlations between b_c/b, l_c/b, h/h_w, Ut/b, U/U_c, d_{50}/b, Fr, Re

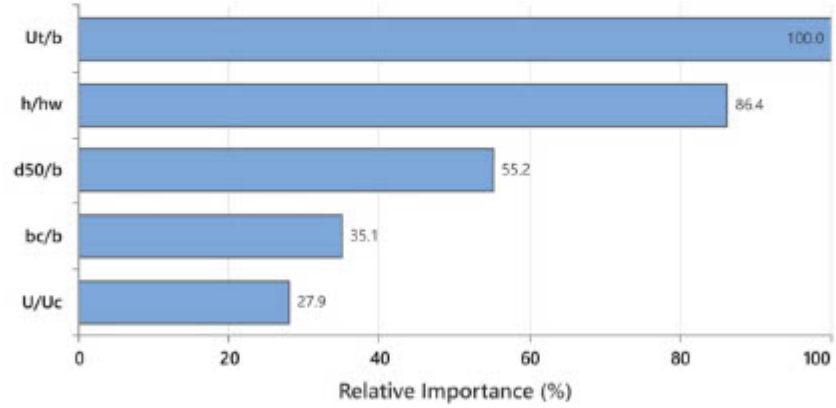


Fig. 7.9 Relative Variable Importance of five shortlisted parameters.

The method used for the modeling is given in Table 7.5. In CART regression, the 80-20% training-testing refers to the method of splitting the dataset into a training set (80% of the data for building a predictive model) and a test set (20% of the data for evaluating the model). A total of 474 data points have been used for building the CART model. The node splitting method used is the least squared error and the criterion for selecting the optimal tree is maximum R^2.

Table 7.5 Methods for building the model (Circular Collar)

Criteria	Method
Node splitting	Least squared error
Optimal tree	Maximum R-squared
Model validation	80/20% training/test sets
Data points used	474

For training 383 data points and for the test 91 data points have been used. The descriptive statistics about the response variable are given in Table 7.6. Here, mean, standard deviation, minimum, median, and maximum are unitless.

Table 7.6 Response information

Data points	N	% of N	Mean	SD	Minimum	Median	Maximum
Training	383	80.8	0.330264	0.338977	0	0.29737	1.14995
Testing	91	19.2	0.355217	0.348117	0	0.367769	1.14995

Note: SD is the standard deviation SD is the standard deviation of non-dimensional temporal scour depth (D_{scr}/b), and N is the number of data sets.

The plot given in Fig. 7.10 illustrates the R^2 value corresponding to each tree. The regression tree with 45 terminal nodes has an R^2 value of approximately 0.9759. It is labeled "Optimal" because it represents the smallest tree with an R^2 value within 1 standard deviation of the maximum R^2 value. Since the R^2 values remain relatively stable for trees with around 38 to 45 nodes (Fig. 7.10), we evaluate the performance of a smaller tree that is similar to the one in the results. The reason for choosing an alternative tree is discussed in the previous section. The regression tree with 40 terminal nodes has an R^2 value of 0.9758 (Fig. 7.10).

The detailed alternative decision tree is given in Appendix II. The tree diagram shows all 383 cases (training dataset) from the full dataset. The first node is split using the variable h/h_w. Node 2 has the cases where $h/h_w \leq 0.875$. This node contains 202 cases. The mean for the node exceeds the overall mean. The standard deviation for Node 2 is approximately 0.259, which is lower than the overall standard deviation because a split creates more pure nodes. Node 33 includes cases where $h/h_w > 0.875$, with a total of 181 cases. The mean for the node is less than the overall mean. The standard deviation for Node 33 is approximately 0.126, which is lower than the overall standard deviation. Based on different variables, these nodes are further split. This tree has 40 terminal nodes and Terminal Node 40 has the lowest standard deviation.

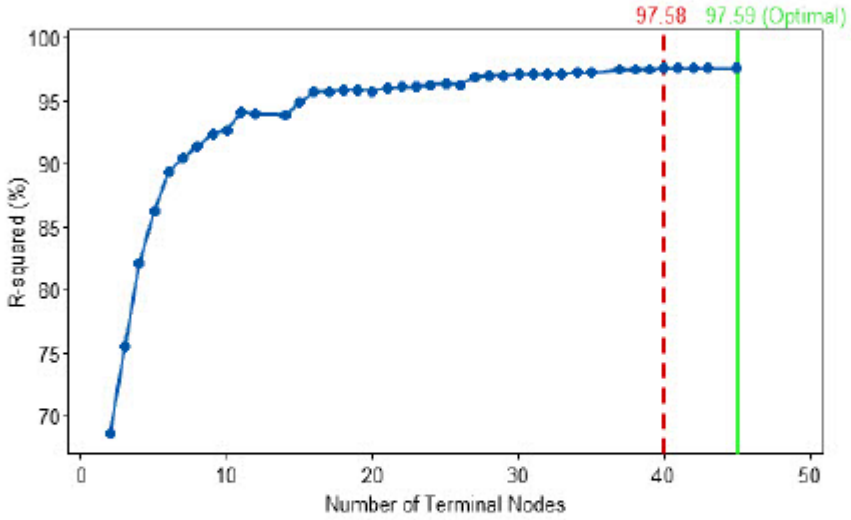


Fig. 7.10 R-squared percentages at different Terminal Nodes

The number of important predictors is 4. The importance order of these four variables is given in Fig. (Relative variable importance). The model summary is given in the Table 7.7

Table 7.7 Model Summary

Total predictors	4	
Important predictors	4	
Number of terminal nodes	40	
Minimum terminal node size	3	
Statistics	Training	Test
R-squared	0.9862	0.9758
Root mean square error (RMSE)	0.0398	0.0539
Mean squared error (MSE)	0.0016	0.0029
Mean absolute deviation (MAD)	0.0231	0.0330
Mean absolute percentage error (MAPE)	1.0165	0.1303

The scatterplot given in Fig. 7.11 displays almost similar patterns in both the training and test datasets, indicating that the tree's performance on new data is closely identical to its performance on the training data.

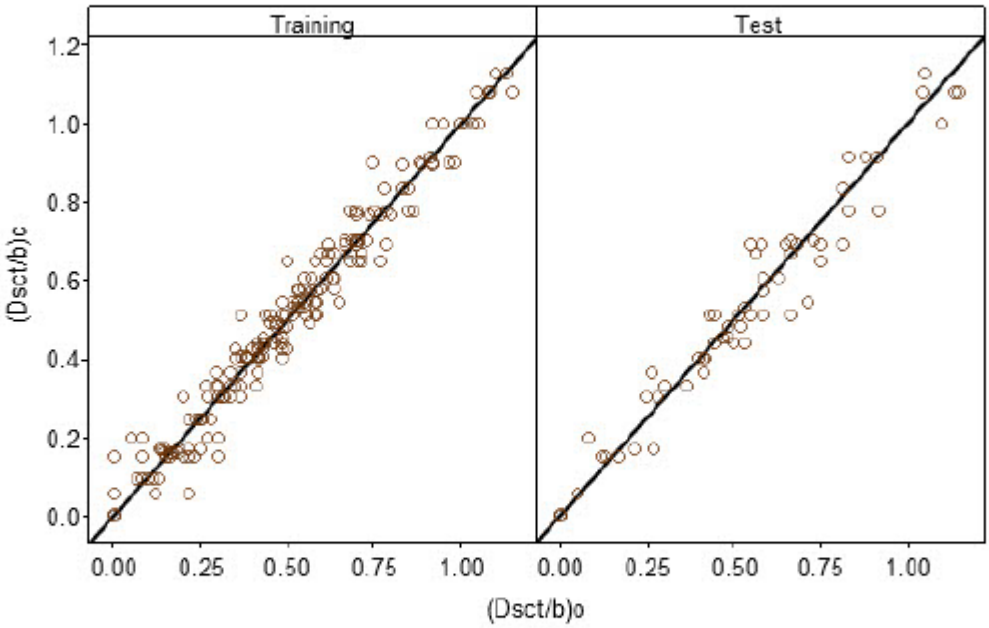


Fig. 7.11 Scatterplot of computed versus observed nondimensional temporal scour depth (airfoil collar)

The accuracy of the fits is more reliable for nodes with lower MSE values. Figure 7.12 shows that terminal node 7 has lower accuracy compared to the other terminal nodes. Terminal node 7 presents the greatest opportunity for improvement of the tree if the variation can be reduced. From Fig. 7.13, it is seen that terminal node 7 exhibits the largest residual, while terminal node 8 shows a series of negative residuals. Further investigation of these points may uncover why the tree does not fit them as well as other points in the node.

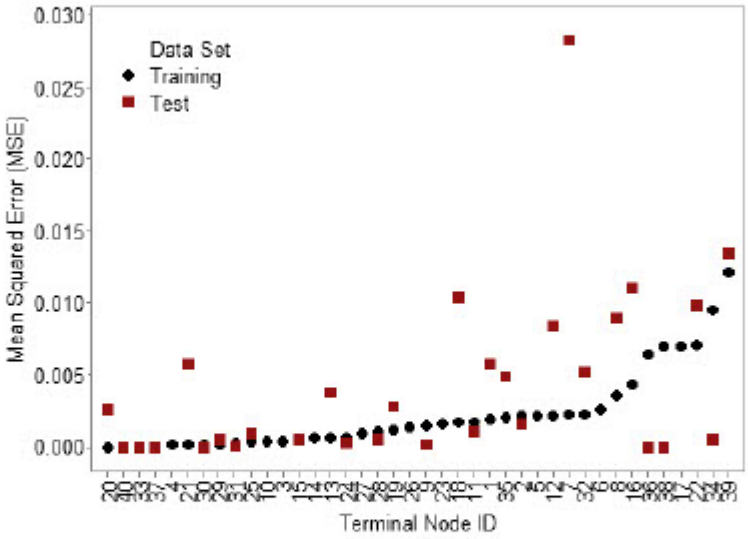


Fig. 7.12 Scatterplot of MSE at different Terminal Nodes

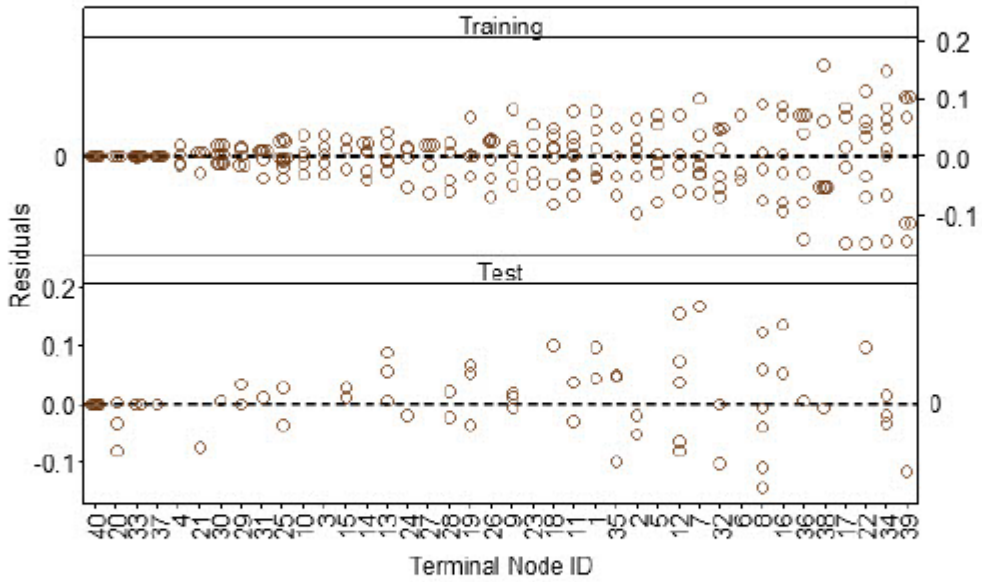


Fig. 7.13 Residual Plot by Terminal Node

The R^2, RMSE, and MAD and percentage in (P_{in}) for ±10%, ±20%, and ±30% error lines have been calculated for the present study and Gupta et al. (2023*b*) and are presented in Table 7.8. The data in Table 7.8 shows that the predictive model of the present study performs well. Here, RMSE and MAD are unitless.

Table 7.8 Performance matrix

References	R^2	RMSE	MAD	P_{in} (10%)	P_{in} (20%)	P_{in} (30%)
Gupta et al. (2023)	0.95	0.09	0.31	25.95	42.19	49.79
Present study	**0.98**	**0.04**	**0.30**	**70.25**	**81.65**	**87.55**

The perfect agreement line (PAL) is a reference line used in the plot to indicate where the observed values, $(D_{sct}/b)_o$ perfectly match the computed values of scour depths, $(D_{sct}/b)_c$. Figure 7.14 shows that approximately 70.25%, 81.65%, and 87.55% of the datasets are within ±10%, ±20%, and ±30% error lines for the present study.

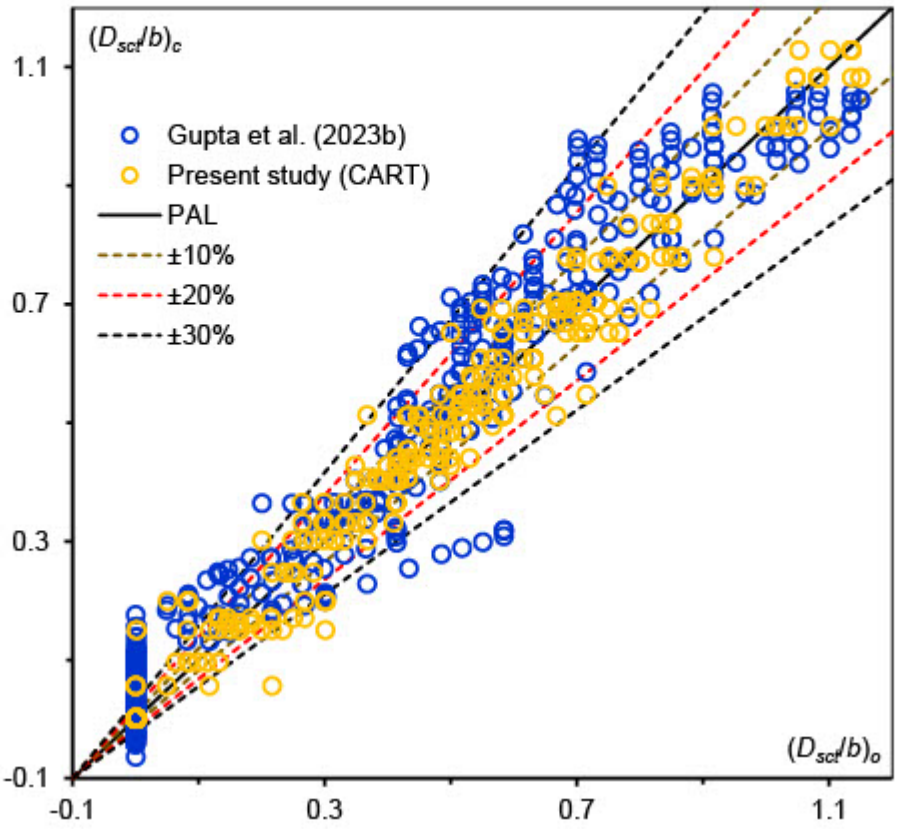


Fig. 7.14 Error analysis of computed and observed non-dimensional temporal scour depth around the pier with an airfoil collar for ±10%, ±20%, and ±30% error lines

7.2 A New Empirical Equation for Temporal Variation of Scour Depth around a Pier with Circular Collar

The temporal scour at the pier is affected by several factors as discussed in Chapter 3. A few researchers have proposed empirical equations for temporal scour depth around a pier in the presence of a collar (please see Chapter 2). However, using those equations, one can calculate the percentage reduction of scour depth at a pier with a collar compared to an unprotected pier. This means that temporal scour depth at an unprotected pier must first be known, either through experimentation or by using existing empirical equations (e.g., Melville and Chiew, 1999; Aksoy et al., 2017; Franzetti et al., 2022; etc). Then only the scour in the presence of a collar can be calculated. However, in this study, a relationship has been proposed in such a way that the temporal scour depth around a pier with a circular collar can be calculated directly, eliminating the need to first determine the scour depth at an unprotected pier.

The temporal development of scour (D_{sct}) around the pier with a circular collar can be expressed (Eq. 7.3) as follows:

$$\frac{D_{sct}}{b} = f\left(\frac{b_c}{b}, \frac{h}{h_w}, \frac{U}{U_c}, \frac{Ut}{b}, \frac{b}{d_{50}}, \sigma_g\right) \tag{7.3}$$

where, b = pier diameter, b_c = collar diameter, h = location of the collar from the water surface, h_w = flow depth, U = flow velocity, U_c = critical flow velocity, t = time, d_{50} = median diameter of particles, σ_g = geometric standard deviation.

A total of 420 datasets are used to develop the equation. The variation of the non-dimensional temporal scour depth (D_{scr}/b) with the non-dimensional parameters mentioned in Eq. 7.1 is shown in the plots below (Fig. 7.15).

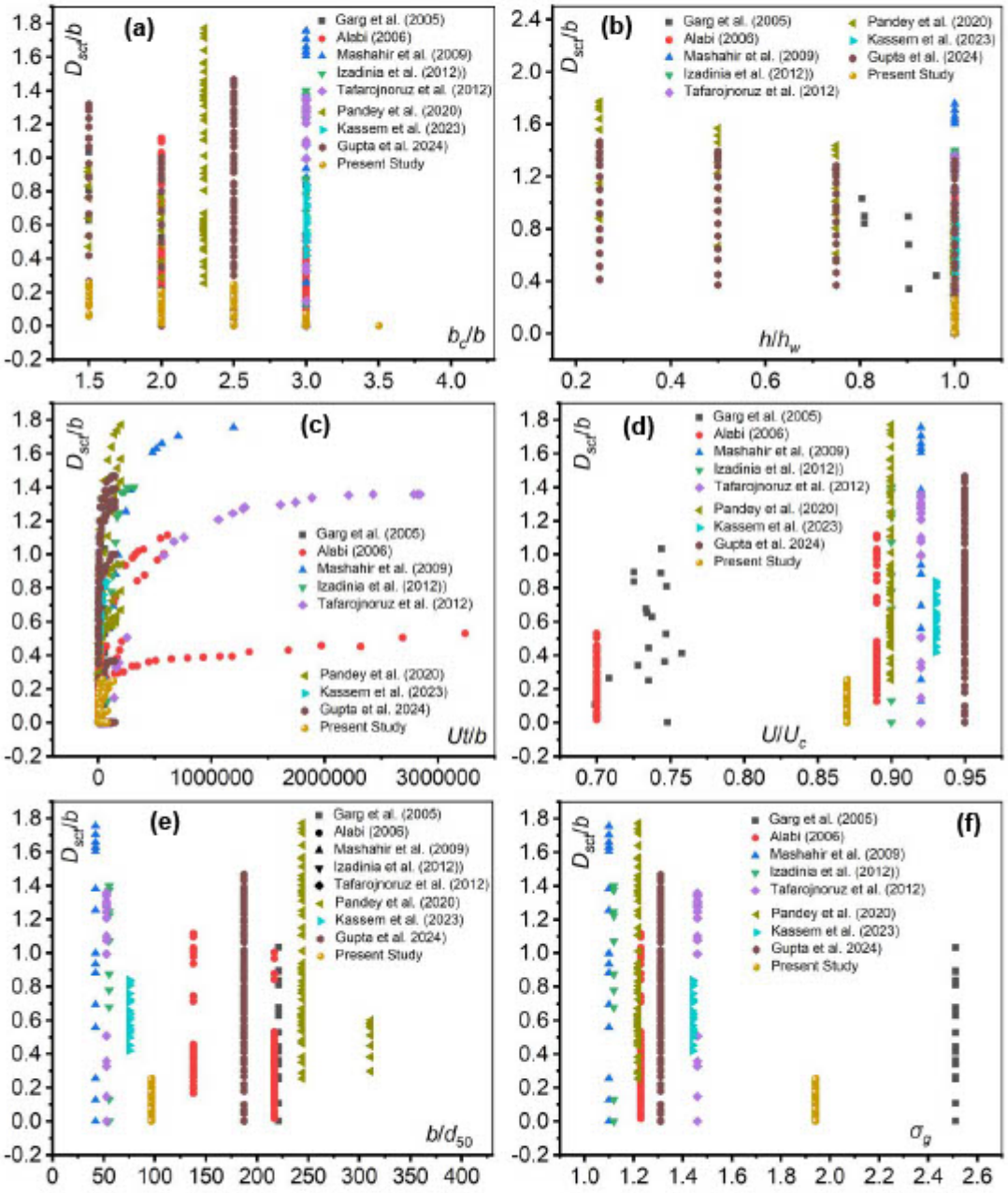


Fig. 7.15 Influence of different non-dimensional parameters: **(a)** b_c/b, **(b)** h/h_w, **(c)** Ut/b, **(d)** U/U_c, **(e)** b/d_{50}, and **(f)** σ_g on D_{scr}/b for different literature

A non-linear regression analysis is performed to derive the equation in software named "IBM SPSS (Statistical Package for the Social Sciences) Statistics" using the present experimental dataset and some previous literature datasets (Garg et al., 2005; Alabi, 2006; Mashahir et al., 2009; Izadinia et al., 2012; Tafarojnoruz et al., 2012; Pandey et al., 2020; Kassem et al., 2023; and Gupta et al., 2024).

The nonlinear regression analysis resulted in the development of a new equation (Eq. 7.4) for calculating temporal scour depth around the pier with a circular collar. By including various parameters that influence the scouring process, this equation is expected to provide a more comprehensive and accurate estimation of the time-dependent scour depth when using a circular collar around a pier.

$$\frac{D_{sct}}{b} = -0.193\left(\frac{b_c}{b}\right)^{-1.469}\left(-0.078+\frac{h}{h_w}\times 0.057\right)\left(\ln\frac{Ut}{b}\right)^{3.088}\left(1-\frac{U}{U_c}\right)^{-0.359}\left(\frac{b}{d_{50}}\right)^{-0.354}\left(\sigma_g\right)^{-1.505} \quad (7.4)$$

Each function in the above equation has been carefully chosen to represent specific aspects of the scour process. Here is an explanation of why each function is used:

- The ratio of the collar diameter to the pier diameter (b_c/b) is raised to the power of -1.469. This power-law relationship indicates that the effect of the collar diameter on the scour depth is non-linear. It agrees with the observations that larger collars reduce scour depth significantly, but the reduction effect decreases as the collar diameter increases beyond a certain point.
- The ratio of the collar location from the water surface to the flow depth (h/h_w) is significant as it demonstrates how collar elevation influences the scour process. The linear relationship simplifies the representation and effectively captures how changes in collar elevation affect scour. A collar placed on the bed is most effective and as the collar elevation from the bed surface is increased, the efficiency reduces.
- The logarithmic function is used to represent the time-dependent development of scour. Oliveto and Hager (2002) used a logarithmic profile for time scales in predicting scour depth. The natural logarithm represents the decreasing rate of scour over time.
- When flow velocity approaches critical velocity (U_c), the scour becomes more likely. The negative exponent reflects the inverse relationship, indicating that as flow intensity increases, the potential for clear water scour also increases, but not in a simple linear way.
- When $b/d_{50} > 50$, the sediments are relatively finer than the pier diameter. In such a scenario, the scour depth decreases as the ratio increases and the negative exponent in the power-law function reflects this relationship but in a non-linear manner.
- Ettema (1980) found that as the standard deviation of the particle size distribution increases, both the rate of scour hole development and the equilibrium scour depth decrease. For non-uniform sediments (i.e., higher σ_g values, $\sigma_g > 2$), armoring occurs on the approach flow bed and at the base of the scour hole around the threshold condition. This armoring significantly reduces local scour depth. The negative exponent of the power-law relationship $(\sigma_g)^{-1.505}$ reflects the inverse relationship.

The exponents and coefficients are derived from regression analysis, ensuring that the model accurately predicts observed scour depth in similar experimental conditions. This equation is a comprehensive representation of the complex relationships between different

factors influencing scour, using mathematical functions that best represent the known physical processes.

7.2.1 Error Analysis

The (D_{sct}/b) computed using the equations of Pandey et al. (2020) and Gupta et al. (2024) (mentioned in Chapter 2, Table 2.1) versus the observed (D_{sct}/b) are also plotted in Fig. 7.16(a,b). To show the goodness of fit of Eq. (7.4) to the data, the values of (D_{sct}/b), computed using Eq. (7.4) are plotted against the observed values of (D_{sct}/b) in Fig. 7.16c.

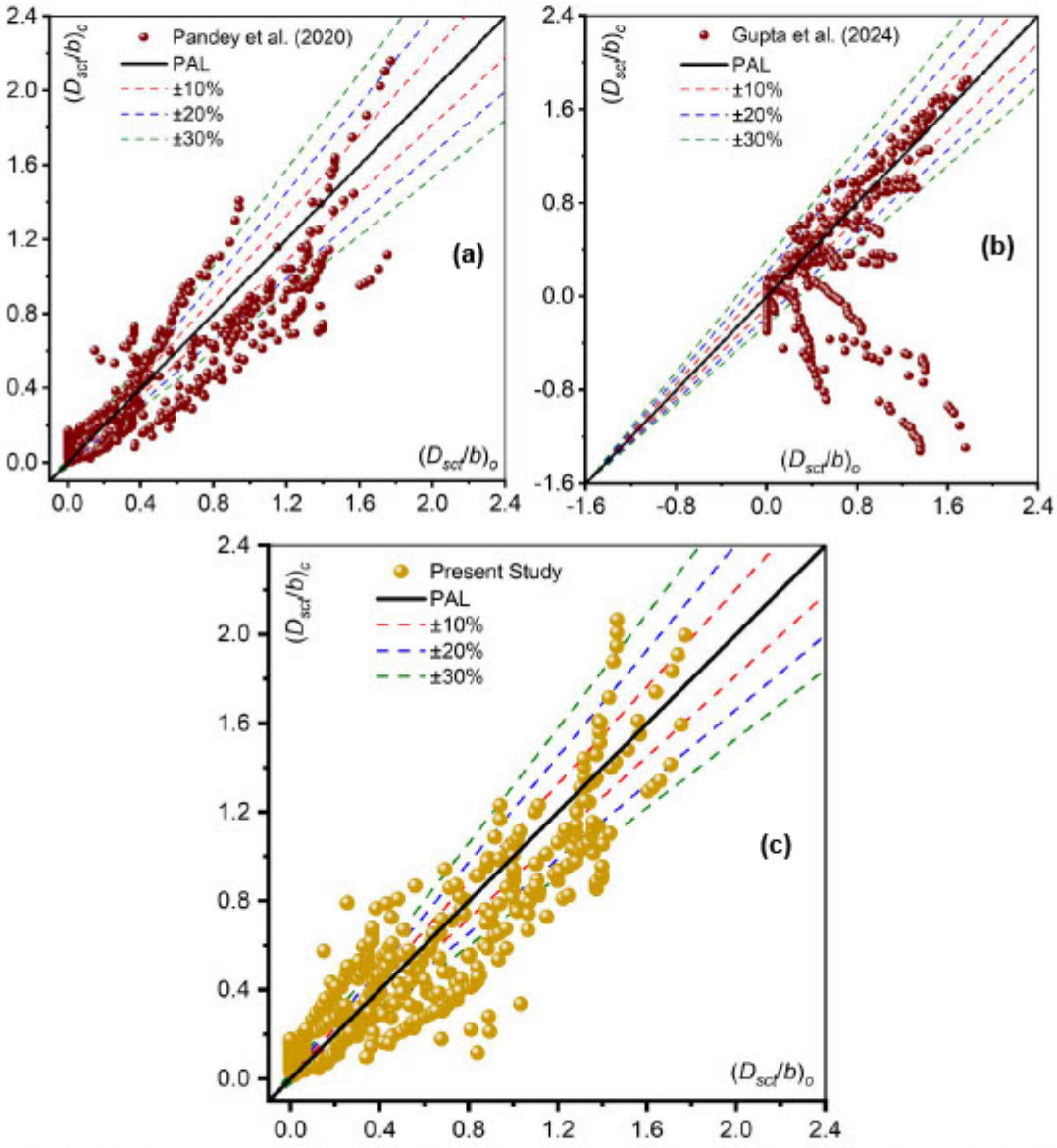


Fig. 7.16 Error analysis of computed and observed scour depths for ±10%, ±20, and ±30% error lines using **(a)** Pandey et al. (2020), **(b)** Gupta et al. (2024), and **(c)** the present study equation (Note – PAL indicates perfect agreement line)

The figure shows that approximately 9.52, 25.71, and 44.29% and 16.43, 32.38, 43.33% of the datasets are within ±10%, ±20%, and ±30% error lines when computed using Pandey et al (2020) and Gupta et al, (2024), respectively. On the other hand, the (D_{sct}/b) computed by the proposed relationship of the present study (Eq. 7.4) shows good agreement between computed and observed values as can be seen from Fig. 7.16c. Approximately 19.76, 37.38, and 51.67% of the datasets have been found within the ±10%, ±20%, and ±30% error lines when computed using Eq. 7.4 (Table 7.9).

Table 7.9 Percentage in (P_{in}) of the datasets for ±10%, ±20%, and ±30% error lines

Literature	P_{in} (10%)	P_{in} (20%)	P_{in} (30%)
Pandey et al. (2020)	9.52	25.71	44.29
Gupta et al. (2024)	16.43	32.38	43.33
Present study	**19.76**	**37.38**	**51.67**

7.2.2 Statistical Analysis

Statistical analysis is performed to assess the accuracy of Eq. 7.4. The R^2, RMSE, and MAE are common tools to check the goodness of fit of a regression model. A lower RMSE and MAE indicate greater accuracy of a regression model, whereas a higher R^2 value is more desirable. These statistical indices and their ideal fit for model evaluation are discussed in great detail in Chapter 4.

For time-dependent scour depth, the values of R^2, RMSE, and MAE, when calculated using Eq. 7.4 are 0.81, 0.21, and 0.16, respectively. These indices for the equations of Paney et al. (2020) and Gupta et al. (2024) are given in Table 7.10. The value of R^2 lies within 0-1 or 0-100%. Here, RMSE and MAE are unitless. From the formulas of RMSE and MAE (given in Chapter 4), we can see that the unit of these values depends on the units of $(D_{sct}/b)_o$ and $(D_{sct}/b)_c$. As $(D_{sct}/b)_o$ and $(D_{sct}/b)_c$ are unitless, RMSE and MAE are unitless.

Table 7.10 Statistical Indices

Literature	R^2	RMSE	MAE
Pandey et al. (2020)	0.77	0.24	0.19
Gupta et al. (2024)	0.09	0.73	0.39
Present study	**0.81**	**0.21**	**0.16**

From the error analysis and statistical analysis, we can see that the proposed equation in the present study gives more reasonable correspondence with observed data than the other two equations proposed by Pandey et al. (2020) and Gupta et al. (2024).

7.2.3 Limitations of Proposed Equation

The relationship considers several factors and appears to predict accurately, as indicated by the high conformity of the datasets to the relationship. However, this relationship (Eq. 7.4) has some limitations:

- Clear-water scour conditions should be maintained.
- The influence of the side walls should not be there.
- Steady and uniform flow should be maintained.
- The collar shape should be circular and the location of the collar should be on or above the sediment bed.

CHAPTER – 8

CONCLUSIONS AND RECOMMENDATIONS

8.1 Conclusions

The present study investigated collars as scour countermeasures around the bridge pier by conducting laboratory experiments. The influence of different collar shapes and sizes on the temporal development of scour in clear-water conditions around a pier at four different locations is examined. Time-dependent scour depth variation around an unprotected pier was also studied for comparison. Collars weaken the horseshoe vortices and downflow. As a result, the scour depth reduces in front of the pier. The current study considered two types of collars, namely circular and airfoil. A total of 11 experiments were conducted at a constant discharge of 25.5 l/s with and without collars. One experiment was without a collar and ten experiments were with collars fixed on the bed – five each with circular and airfoil collars of different sizes. The results of the present study show that the collar may significantly reduce scour depth around the pier. The following general conclusions can be drawn from this study.

- Without a collar, the scour depth was initially found to be increasing rapidly. Around 81% of the maximum scour depth was observed during the first 90 minutes (17% of the maximum time). However, the rate of scouring was observed to be decreased with time. On the other hand, for the circular collars of diameters 2.5b and 3b, 81% of the maximum scour depth was found to have reached 50% of the maximum time. It means that the rate of scour was much less for piers which were protected with collars.
- Using a collar effectively slowed down the temporal development of scour. Collar delayed the development of scour holes. As floods often last for a much shorter duration than the equilibrium time, this property of the collar becomes significant.
- For circular collars, the scour was started around 135° (either side of the collar) and with time it was extended towards 90° (sides), eventually converging at 0°. Conversely, in the case of airfoil collars, the scour was started at 90° and propagated towards 135° first and then 0°.
- The maximum scour depth was observed at the upstream face of the pier (0°) for an unprotected pier, and also with 1.5b and 2b circular collars, indicating the inefficiency of these two collars. For 1.5b and 2b airfoil collars, the maximum scour depth (D_{scm}) was seen to be protected at 90° and 0°. In the case of the 2.5b, 3b, and 3.5b collars D_{scm} was observed at 135° (downstream of the pier) which was far from the rear nose of the pier. However, for a 2.5b collar, significant scour depth was seen at 0° (circular) and 90° (airfoil). Hence, the best and most economical circular collar dimension for reducing scour was in the range of b_c = 3b-3.5b, when placed at bed level, indicating the larger the collar diameter, the smaller the scour depth. However, an important point to note here is, that the airfoil collars of all sizes protected the upstream face of the pier and none of them was undermined totally.

- The maximum scour depth reduction efficiency was found for circular collar width (b_c) of 3.5b for 0° position, and the minimum was found for b_c = 1.5b. In the case of the airfoil collar, almost 100% efficiency was found for all the b_c at the 0° position.
- It is seen that for an unprotected pier the length of scour (l_s) is 8.45% less than the width of scour (w_s). For circular collars of 1.5b diameter, l_s, and w_s are almost the same. For circular collars of diameters 2b, 2.5b, 3b, and 3.5b, the scour lengths are 54.69, 40.88, 36.54, and 49.76% more than the scour width, respectively. For airfoil collars of diameters 1.5b, 2b, 2.5b, 3b, and 3.5b, the scour lengths are 10.34, 42.62, 33.23, 53.47, and 49.37% more than the scour width, respectively.
- The protection efficiencies of circular collars compared to an unprotected pier are 32.43, 26.23, 71.39, 81.32, and 84.96% for 1.5b, 2b, 2.5b, 3b, and 3.5b collars respectively at upstream and 4.94, 66.9, 68.55, and 74.13% for 1.5b, 2.5b, 3b, and 3.5b collar at the side of the pier. On the other hand, for airfoil collar, those are 87, 83.81, 83.29, 87.32, and 89.20% for 1.5b, 2b, 2.5b, 3b, and 3.5b respectively at upstream and 32.67, 48.86, 78.95, 81.62, and 82.80% for 1.5b, 2b, 2.5b, 3b, and 3.5b at the side of the pier.
- The airfoil collar is observed to be more effective in reducing scour depth, compared to the circular collar. One of the possible reasons may be that the area covered by the airfoil collar at the upstream side of the pier is more and hence, it protected a larger area of sediment bed from the impingement of downflow and subsequently horseshoe vortex.
- The CART model developed for the present study outperforms previous literature equations (Pandey et al., 2020; Gupta et al., 2024) for both the circular and airfoil collars in terms of all the statistical influence factors. The statistical characteristics of the CART model for circular collars are calculated as R^2 = 0.96, RMSE = 0.09, and MAD = 0.36, and for airfoil collars, they are computed as R^2 = 0.98, RMSE = 0.04, and MAD = 0.30. The present model demonstrates superior performance compared to other literature formulas for both types of collars, with respect to P_{in} (%) within error bands of ±10%, ±20%, and ±30%.
- A new equation for time-dependent scour around a pier protected with a collar on bed level is developed through nonlinear regression analysis using the present experimental dataset and some previous literature datasets. This equation is verified using different statistical analyses. Based on the error and statistical analyses, the equation proposed in this study shows a better fit with the observed data than the equations from Pandey et al. (2020) and Gupta et al. (2024).

8.2 Limitations of Present Study

Limitations of the present study include the following:

- Constant flow discharge across all experiments may restrict the generalizability of findings to varying flow conditions.
- The use of fixed pier diameter limits the exploration of the influence of pier diameter on scour depth.

- Restricting the bed material to coarse sand may limit the applicability of results to different sediment types.
- Limited variability in collar shapes, with only two shapes considered, may overlook the potential effects of different collar designs on scour reduction effectiveness.
- Another limitation of this study is the utilization of a single model for predicting scour depth.
- The consideration of the clear-water scour may be the other limitation of this study.
- Each experiment could not be carried out for the same duration due to some unavoidable circumstances.

8.3 Scopes of Future Study

The scope of future endeavors is outlined below:

- The current study examines scour depth under a constant flow velocity and flow depth. Future research could explore how varying flow velocities and changing water depths affect scour depth.
- There is insufficient data on how scour depth in the presence of a collar is affected by factors such as flow intensity, sediment coarseness, flow shallowness, etc. More comprehensive research is needed to better understand the influence of these parameters.
- After running tests in this study for approximately 8-9 hours, it can be concluded that the scour did not reach the vicinity of the pier when a collar of diameter $3b$ or $3.5b$ was used. However, the scour depth continued to increase at a reduced rate. Alabi (2006) conducted an experiment for about 40 days and he also found no scour around the pier in case of a collar of diameter $3b$. For future research, extending the test duration significantly could help determine whether the scour hole will eventually reach the area around the pier.
- Given that rivers often carry debris, especially during floods, investigating the impact of debris on the performance of a collar and the temporal development of scour could provide valuable insights into the effectiveness of using a collar.
- Expanding beyond the straight flow path analyzed in the present study, future investigations could explore the ramifications of flow paths with bends.
- A prospective avenue for future research entails the theoretical development of a method for calculating scour depth based on the phenomenological theory of turbulence. This theoretical approach could then be validated against experimental results, constituting a comprehensive investigation into scour depth prediction methods.
- Investigating the influence of various pier sizes on scour depth to provide a more comprehensive understanding of pier geometry effects.
- Extending the study to encompass different types of bed materials beyond coarse sand to broaden the applicability of results to diverse sediment compositions.
- Conducting further research to assess the effectiveness of additional collar shapes in reducing scour, thereby expanding the range of potential scour countermeasure designs.
- Developing and validating multiple models for predicting scour depth to provide a more robust and comprehensive approach to scour depth estimation.

- Literatures commonly described the flow mechanisms causing local scour around an unprotected pier. However, there has not been much research on how the presence of a collar affects flow behavior. Therefore, a study investigating this aspect will address a significant gap in our understanding of the flow dynamics involved.
- Previous studies on collars as a countermeasure for local scour at piers have focused solely on cohesionless materials and clear-water flow conditions. Since local scour can occur at a bridge pier under different conditions, including live-bed scour and cohesive soils, it would be valuable to investigate the effectiveness of collars in these scenarios to gain a better understanding of their performance.
- All existing studies on the use of collars as a countermeasure for local scour at bridge piers have relied on experiments with physical hydraulic models. It would be beneficial to evaluate the practical application of collars in the field through a prototype study.

NOTATIONS

The following symbols are used in this dissertation work:

a_{pd}	Planar area of sediment deposition (L^2)
a_{ps}	Planar area of maximum scour hole (L^2)
a_{sd}	Surface area of maximum sediment deposition (L^2)
a_{ss}	Surface area of maximum scour hole (L^2)
b	Pier diameter [L]
b_c	Collar diameter [L]
B	Width of the tilting flume [L]
d_{16}	16% finer sand diameter [L]
d_{50}	Median diameter of sand (mm), [L]
d_{84}	84% finer sand diameter [L]
d_{90}	90% finer sand diameter [L]
D_{sce}	Equilibrium scour depth at the pier with collar, [L]
D_{scm}	Maximum temporal scour depth at the pier with collar, [L]
D_{sct}	Temporal scour depth at the pier with collar, [L]
D_{se}	Equilibrium scour depth at the pier without collar, [L]
D_{sm}	Maximum temporal scour depth at the pier without collar, [L]
D_{st}	Temporal scour depth at the pier without collar, [L]
Fr	Froude number of flow, [—]
g	Gravitational acceleration [LT^{-2}]
h	Location of the collar from the water surface, [L]
h_c	Collar elevation from the sediment bed [L]
h_w	Approaching flow depth [L]
l_c	Length of airfoil collar [L]
l_d	Length of sediment deposition [L]
l_s	Maximum scour hole length [L]
L	Total length of sediment transportation (cm), [L]
n	Manning's coefficient of roughness [—]
P_m	Percentage of corrected predicted data within ±error lines (%)
Q	Flow discharge [L^3T^{-1}];
Re	Flow Reynolds number, [—]
Re_p	Pier Reynolds number, [—]
S	Relative density of sand, [—]
S_0	Bed slope [—]
t	Time [T]
t_{ce}	Equilibrium time for the pier with collar [T]
t_e	Equilibrium time for pier without collar [T]
t_m	Run time for the experiments of the present study [T]
T_c	Dimensionless time, [—]

U	Approaching flow velocity [LT^{-1}]
U_c	Critical velocity [LT^{-1}]
U_*	Shear velocity [LT^{-1}]
U_{*c}	Critical shear velocity [LT^{-1}]
V_d	Volume of the deposition, [L^3]
V_s	Volume of the scour hole, [L^3]
w_d	Width of sediment deposition [L]
w_s	Maximum scour hole width [L]
ρ_s	Mass density of sand [ML^{-3}]
ρ_w	Mass density of water [ML^{-3}]
τ_0	Average bed shear stress [$ML^{-1}T^{-2}$]
τ_{0c}	Critical bed shear stress on the horizontal bed [$ML^{-1}T^{-2}$]
σ_g	Geometric standard deviation [—]
ν	Kinematic viscosity [L^2T^{-1}]

REFERENCES

Ahmed, F. and Rajaratnam, N. (1998). Flow around Bridge Piers. *Journal of Hydraulic Engineering*, Vol. 124, Issue 3, pp. 288-300. https://doi.org/10.1061/(ASCE)0733-9429(1998)124:3(288).

Aksoy, A. O., Bombar, G., Arkis, T. and Guney, M. S. (2017). Study of the time-dependent clear water scour around circular bridge piers. Journal of Hydrology and Hydromechanics, Vol. 65, Issue 1, pp. 26-34. https://doi.org/10.1515/johh-2016-0048.

Alabi, P. D. (2006): Time development of local scour at a bridge pier fitted with a collar. M.S. Thesis, University of Saskatchewan, Saskatoon, Saskatchewan, Canada.

Arneson, L. A., Zevenbergen, L. W., Lagasse, P. F. and Clopper, P. E. (2012). Evaluating Scour at Bridges - Fifth Edition. Report No. FHWA-HIF-12-003, Hydraulic Engineering Circular 18 (HEC-18), Federal Highway Administration, USA.

Bagheri, A., Bordbar, A., Heidarnejad, M. and Masjedi, A. (2024). In-depth simulation of netted collars on scour depth control using machine-learning models. *Results in Engineering*, Vol. 21, Art. No. 101820. https://doi.org/10.1016/j.rineng.2024.101820.

Breiman, L., Friedman, J., Olshen, R.A., and Stone, C.J. (1984). Classification and Regression Trees. Boca Raton, Florida: Chapman & Hall/CRC.

Breusers, H. N. C. and Raudkivi, A. J. (1991). Scouring - Hydraulic structures design manual. International Association for Hydraulic Research (IAHR), Balkema, Rotterdam. https://doi.org/10.1201/9781003079477.

Breusers, H.N.C., Nicollet, G. and Shen, H.W. (1977). Local scour around cylindrical pier. *Journal of Hydraulic Research*, Vol. 15, Issue 3, pp. 211-252. https://doi.org/10.1080/00221687709499645.

Chabert, J. and Engeldinger, P. 1956. Etude des affouillements autour des piles de ponts (Study of scour at bridge piers). Bureau central d'études pour les équipements d'outre-mer, Laboratoire National d'Hydraulique (Chatou, France), France.

Chang, F. F. M. and Karim, M. (1972). An experimental study of reducing scour around bridge piers using piles. Report No. 640 (67), South Dakota Department of Highways, Pierre, South Dakota, USA.

Chang, H.H. (1988). Fluvial processes in river engineering. John Wiley & Sons, New York.

Cheremisinoff, P. N., Cheremisinoff, N. P. and Cheng, S. L. (1988). Civil Engineering Practice: 2/Hydraulics/Mechanics, Technomic Publishing Company, Inc., Lancaster, Pennsylvania, U.S.A.

Chiew, Y. and Lim, S. (2003). Protection of bridge piers using a sacrificial sill. Proceedings of the Institution of Civil Engineers. Water And Maritime Engineering, Thomas Telford Journals, London, Vol. 156, Issue 1, pp. 53-62. March, 2004.

Chiew, Y. M. (1984): Local Scour at Bridge Piers. PhD Thesis, Department of Civil Engineering, Auckland University, Private Bag, Auckland, New Zealand.

Chiew, Y. M. (1992). Scour protection at bridge piers. *Journal of Hydraulic Engineering*, Vol. 118, Issue 9, pp. 1260-1269. https://doi.org/10.1061/(ASCE)0733-9429(1992)118:9(1260).

Chiew, Y. M. (2004). Local scour and riprap stability at bridge piers in a degrading channel. *Journal of Hydraulic Engineering*, Vol. 130, Issue 3, pp. 218-226. https://doi.org/10.1061/(ASCE)0733-9429(2004)130:3(218).

Chiew, Y. M. and Melville, B. M. (1987). Local scour around bridge piers. *Journal of Hydraulic Research*, Vol. 25, No, 1, pp. 15-26. https://doi.org/10.1080/00221688709499285.

Dargahi, B. (1990). Controlling Mechanism of Local Scouring. *Journal of Hydraulic Engineering*, Vol. 116, Issue 10, pp. 1197-1214. https://doi.org/10.1061/(ASCE)0733-9429(1990)116:10(1197).

Das, R., Das, S., Jaman, H. and Mazumdar, A. (2019). Impact of upstream bridge pier on the scouring around adjacent downstream bridge pier. *Arabian Journal for Science and Engineering*, Vol. 44, pp. 4359-4372. https://doi.org/10.1007/s13369-018-3418-5.

Das, R., Khwairakpam, P., Das, S. and Mazumdar, A. (2014). Clear-water local scour around eccentric multiple piers to shift the line of sediment deposition. *Asian Journal of Water Environment and* Pollution, Vol. 11, No. 3, pp. 47-54.

Das, S. and Mazumdar, A. (2018). Evaluation of hydrodynamic consequences for horseshoe vortex system developing around two eccentrically arranged identical piers of diverse shapes. *KSCE Journal of Civil Engineering*, Vol. 22, pp. 2300-2314. https://doi.org/10.1007/s12205-017-1842-9.

Das, S., Das R. and Mazumdar, A. (2016). Comparison of local scour characteristics around two eccentric piers of different shapes. *Arabian Journal of Science and Engineering*, Vol. 41, pp. 1199-1213. https://doi.org/10.1007/s13369-015-1817-4.

Das, S., Das, R. and Mazumdar, A. (2013). Circulation characteristics of horseshoe vortex in scour region around circular piers. *Water Science and Engineering*, Vol. 6, Issue 1, pp. 59-77. https://doi.org/10.3882/j.issn.1674-2370.2013.01.005.

Das, S., Das, R., Kuila, A. and Mazumdar, A. (2014*a*). Analysis of clear-water equilibrium scour around two eccentric circular piers to increase self-dredging. In Seminar on Dredging: Equipment and Applications, (EADA), Kolkata, India.

Das, S., Ghosh, R., Das, R. and Mazumdar, A. (2014*b*). Clear water scour geometry around circular piers. *Ecology Environment and Conservation*, Vol. 20, pp. 479-492.

Das, S., Ghosh, S. and Mazumdar, A. (2014*c*). Kinematics of horseshoe vortex in a scour hole around two eccentric triangular piers. *International Journal of Fluid Mechanics Research*, Vol. 41, Issue 4. https://doi.org/10.1615/InterJFluidMechRes.v41.i4.20.

Das, S., Jaman, H., Chatterjee, A., Das, R. and Mazumdar, A. (2017). Hydrodynamic behaviour of Flow past three typically arranged circular piers on different horizontal planes. *International Journal of Fluid Mechanics Research*, Vol. 44, Issue 5, pp. 457-468. https://doi.org/10.1615/InterJFluidMechRes.2017019421.

Das, S., Midya, R., Das, R. and Mazumdar, A. (2013). A study of wake vortex in the scour region around a circular pier. *International Journal of Fluid Mechanics Research*, Vol. 40, Issue 1, pp. 42-59. https://doi.org/10.1615/InterJFluidMechRes.v40.i1.40.

Dey, S. (1997). Local scour at piers, part 1: A review of development of research. *International Journal of Sediment Research*, Vol. 12, Issue 2, pp. 23-46.

Dey, S. and Barbhuiya, A. K. (2004). Clear-Water Scour at Abutments in Thinly Armored Beds. *Journal of Hydraulic Engineering*, Vol. 130, Issue 7, pp. 622-634. https://doi.org/10.1061/(ASCE)0733-9429(2004)130:7(622).

Dey, S., Sumer, B. M. and Fredsøe, J. (2006). Control of scour at vertical circular piles under waves and current. *Journal of Hydraulic Engineering*, Vol. 132, Issue 3, pp. 270-279. https://doi.org/10.1061/(ASCE)0733-9429(2006)132:3(270).

Ettema, R. (1976). Influence of bed material gradation on local scour. Report No. 124, School of Engineering, University of Auckland, Auckland, New Zealand. 1976.

Ettema, R. (1980): Scour at bridge piers. PhD Thesis, Civil Engineering, University of Auckland, Auckland, New Zealand.

Ettema, R., Constantinescu, G., and Melville, B. W. (2017). Flow-Field Complexity and Design Estimation of Pier-Scour Depth: Sixty Years Since Laursen and Toch. *Journal of Hydraulic Engineering*, Vol. 143, Issue 9, Art. No. 03117006. https://doi.org/10.1061/(ASCE)HY.1943-7900.0001330.

Ettema, R., Nakato, T. and Muste, M. (2006). An Illustrated Guide for Monitoring and Protecting Bridge Waterways against Scour. IIHR Technical Report No.449, Iowa Highway Research Board, Project TR-515, The University of Iowa, Iowa.

Federico, F., Silvagni, G. and Volpi, F. (2003). Scour vulnerability of river bridge piers. *Journal of Geotechnical and Geoenvironmental Engineering*, Vol. 129, Issue 10, pp. 890-899. https://doi.org/10.1061/(ASCE)1090-0241(2003)129:10(890).

Fotherby, L. M. and Jones, J. S. (1993). The influence of exposed footings on pier scour depths. Proceeding of Hydraulics Conference, New York, pp. 922-927. 1993.

Franzetti, S., Radice, A., Rebai, D. and Ballio, F. (2022). Clear water scour at circular Piers: a new formula fitting laboratory data with less than 25% deviation. Journal of Hydraulic Engineering, Vol. 148, Issue 10, pp. 1-13. https://doi.org/10.1061/(ASCE)HY.1943-7900.0002009.

Garg, V., Setia, B., and Verma, D.V.S. 2005; Scour reduction by multiple collar plates around Bridge Piers. *Journal of Hydraulic Engineering*, Vol. 11. pp. 66-81. https://doi.org/10.1080/09715010.2005.10514802.

Gosselin, M. S. and Sheppard, M. (1995). Time rate of local scour. Proceedings of the First International Conference on Water Resources Engineering, San Antonio, Texas, pp. 775-779, 14-18 Aug. 1995.

Gupta, L. K., Bharadwaj, M. R. and Pandey, M. (2024). Comparative study of reduction of pier scour using octagonal and circular collars. *Ocean Engineering*, Vol. 298, Art. No. 117169. https://doi.org/10.1016/j.oceaneng.2024.117169.

Gupta, L. K., Pandey, M. and Raj, P. A. (2023*b*). Impact of airfoil collar on scour reduction around the bridge pier. *Ocean Engineering*, Vol. 290, Art. No. 116271. https://doi.org/10.1016/j.oceaneng.2023.116271.

Gupta, L. K., Pandey, M., Raj, P. A., Pu, J. H. (2023*a*). Scour Reduction around Bridge Pier Using the Airfoil-Shaped Collar. *Hydrology*, Vol. 10, Issue 4, Art. No. 77. https://doi.org/10.3390/hydrology10040077.

Hoffmans, G. J., and Verheij, H. J. (1997). Scour manual, First Edition. Routledge, Taylor & Francis Group, UK.

Izadinia, E. and Heidarpour M. (2012). Simultaneous use of cable and collar to prevent local scouring around bridge pier. *International Journal of Sediment Research*, Vol. 27, Issue 3, pp. 394–401. https://doi.org/10.1016/S1001-6279(12)60044-4.

Jahangirzadeh, A., Basser, H., Akib, S., Karami, H., Naji, S., Shamshirband, S. (2014). Experimental and numerical investigation of the effect of different shapes of collars on the reduction of scour around a single bridge pier. *Plos One*, Vol. 9, Issue 6, Art. No. e98592. https://doi.org/10.1371/journal.pone.0098592.

Jaman, H., Das, S., Das, R., & Mazumdar, A. (2017*a*). Hydrodynamics of flow obstructed by inline and eccentrically-arranged circular piers on a horizontal bed surface. *Journal of The Institution of Engineers (India): Series A*, Vol. 98, pp. 77-83. https://doi.org/10.1007/s40030-017-0187-1

Jaman, H., Das, S., Kuila, A., & Mazumdar, A. (2017*b*). Hydrodynamic flow patterns around three inline eccentrically arranged circular piers. *Arabian Journal for Science and Engineering*, *42*, 3973-3990. https://doi.org/10.1007/s13369-017-2536-9.

Johnson, P. G. and Niezgoda, S. L. (2004). Risk-based method for selecting bridge scour countermeasures. *Journal of Hydraulic Engineering*, Vol. 130, Issue 2, pp. 121-128. https://doi.org/10.1061/(ASCE)0733-9429(2004)130:2(121).

Kassem, H., El-Masry, A. A., and Diab, R. (2023). Influence of collar's shape on scour hole geometry at circular pier. *Ocean Engineering*, Vol. 287 (Part 2), Art. No. 115791. https://doi.org/10.1016/j.oceaneng.2023.115791.

Khodashenas, S. R., Shariati, H., Esmaeeli, K. (2018). Comparison between the circular and square collar in reduction of local scouring around bridge piers. *E3S Web of Conferences*, Vol. 40, Art. No. 03002. https://doi.org/10.1051/e3sconf/20184003002.

Kothyari, U. C., Hager, W. H., Oliveto, G., (2007). Generalized approach for clear-water scour at bridge foundation elements. *Journal of Hydraulic Engineering*, Vol. 133, Issue 11, pp. 1229-1240. https://doi.org/10.1061/(ASCE)0733-9429(2007)133:11(1229).

Kumar, V., Baranwal, A. and Das, B. S. (2023). Prediction of local scour depth around bridge piers: modelling based on machine learning approaches. *Engineering Research Express*, Vol. 6, No. 1. https://doi.org/10.1088/2631-8695/ad08ff.

Kumar, V., Ranga Raju, K. G. and Vittal, N. (1999). Reduction of local scour around bridge piers using slot and collar. *Journal of Hydraulic Engineering*, Vol. 125, Issue 12, pp. 1302-1305. https://doi.org/10.1061/(ASCE)0733-9429(1999)125:12(1302).

Lagasse, P. F., Clopper, P. E., Pagan-Ortiz, J. E., Zevenbergen, L. W., Arneson, L. A., Schall, J. D. and Girard, L. G. (2009). Bridge Scour and Stream Instability Countermeasures: Experience, Selection, and Design Guidance – Third Edition (Vol. 1 and 2). Report No. FHWA-NHI-09-112, Hydraulic Engineering Circular Number 23 (HEC-23), Federal Highway Administration, USA.

Lagasse, P. F., Clopper, P. E., Zevenbergen, L. W. and Girard, L. G. (2007). Countermeasures to Protect Bridge Piers from Scour. Report No. NCHRP Report 593, Project 24-07(2), National Cooperative Highway Research Program, Washington D.C.

Lagasse, P.F. and Richardson, E.V. (2001). ASCE Compendium of Stream Stability and Bridge Scour Papers. *Journal of Hydraulic Engineering*, Vol. 127, Issue 7, pp. 531-533. https://doi.org/10.1061/(ASCE)0733-9429(2001)127:7(531).

Lagasse, P.F., Zevenbergen, L.W., Schall, J.D. and Clopper, P.E. (2001). Bridge scour and stream instability countermeasures: Experience, selection, and design guidelines – Second Edition. Report No. FHWA NHI 01-003, Federal Highway Administration, Hydraulic Engineering Circular No. 23, Department of Transportation, Washington, D.C, USA.

Lança, R., Fael, C.S., Maia, R.J., Pego, J.P. and Cardoso, A. (2013). Clear-water scour at comparatively large cylindrical piers. *Journal of Hydraulic Research*, Vol. 139, Issue 11, pp. 1117-1125. https://doi.org/10.1061/(ASCE)HY.1943-7900.0000788.

Lauchlan, C. S. (1999): Pier scour countermeasures. PhD Thesis, Department of Civil and Resources Engineering, University of Auckland, Auckland, New Zealand.

Laursen, E. M. and Toch, A. (1956). Scour around bridge piers and abutments. Iowa Highway Research Board, Bulletin No. 4, Bureau of Public Roads, Iowa. https://publications.iowa.gov/id/eprint/20237.

Loh, Y. (2011). Classification and regression trees. *Wiley Interdisciplinary Reviews: Data Mining and Knowledge Discovery*, Vol. 1, pp. 14-23. https://doi.org/10.1002/widm.8.

Marris, A. W. (1964). A Review on Vortex Streets, Periodic Wakes, and Induced Vibration Phenomena. *Journal of Basic Engineering*, Vol. 86, Issue 2, pp. 185-193. https://doi.org/10.1115/1.3653027.

Mashahir, M. B., Zarrati, A. R., Rezayi, M. J. (2004). Time Development of Scouring around a Bridge Pier Protected by Collar. In: Chiew, Yee-Meng; Lim, Siow-Yong; Cheng, Nian-Sheng (Hg.): Proceedings of the Second International Conference on "Scour and Erosion" (ICSE-2), Nanyang Technological University: Singapore, 14-17 Nov. 2004.

Mashahir, M.B., Zarrati, A.R., Rezaei, M.J. and Zokaei, M. (2009). Effect of collars and bars in reducing the local scour around cylindrical bridge piers. *International Journal of Engineering, Transactions B: Applications*, Vol. 22, No. 4, pp. 333-342.

Melville B. W. (1975). Local Scour at Bridge Sites. Report No. 117, University of Auckland, Auckland, New Zealand.

Melville, B. (2008). The physics of local scour at bridge piers. Fourth International Conference on Scour and Erosion, pp. 28-40. 2008.

Melville, B. W. and Chiew, Y. M. (1999). Time scale for local scour at bridge piers. *Journal of Hydraulic Engineering*, Vol. 125, No. 1, Art. No. 16274, pp. 59-65. https://doi.org/10.1061/(ASCE)0733-9429(1999)125:1(59).

Melville, B. W. and Hadfield, A. C. (1999). Use of sacrificial piles as pier scour countermeasures. *Journal of Hydraulic Engineering*, Vol. 125, Issue 11, pp. 1221-1224. https://doi.org/10.1061/(ASCE)0733-9429(1999)125:11(1221).

Melville, B.W. and Coleman, S.E. (2000). Bridge scour. Water Resources Publications, LLC, Colorado, U.S.A.

Moncada-M, A. T., Aguirre-Pe, J., Bolívar, J. C. and Flores, E. J. (2009). Scour protection of circular bridge piers with collars and slots. *Journal of Hydraulic Research*, Vol. 47, Issue 1, pp. 119-126. https://doi.org/10.3826/jhr.2009.3244.

Mostafa, E. A. (1994): Scour around skewed bridge piers. PhD thesis, Department of Irrigation and Hydraulics, Alexandria University, Alexandria, Egypt.

Nandi, B. (2019): Analysis of Time Variation of Scour around Three Cylindrical Tandem Piers. M.E. Thesis, School of Water Resources Engineering, Jadavpur University, Kolkata, India.

Nandi, B. and Das, S. (2023*a*). Equation for time-dependent local scour at pier-like structures with eccentric in-line arrangements. In *Proceedings of the Institution of Civil Engineers-Water Management* (pp. 1-14). https://doi.org/10.1680/jwama.23.00006.

Nandi, B., and Das, S. (2023*b*). Identify most promising temporal scour depth formula for circular piers proposed over last six decades. *Ocean Engineering*. Vol. 286, Part 2, Art. No. 115639. https://doi.org/10.1016/j.oceaneng.2023.115639.

Nandi, B., Patel, G. and Das, S. (2024*b*). Prediction of maximum scour depth at clear water conditions: Multivariate and robust comparative analysis between empirical equations and machine learning approaches using extensive reference metadata. *Journal of Environmental Management*, Vol 354, Art. No. 120349. https://doi.org/10.1016/j.jenvman.2024.120349.

Nandi, B., Sasmal, K., and Das, S. (2024*a*). Evolution of Four Formulae Derived Over Five Decades to Predict Temporal Scour at Circular Pier. In International Conference on Science, Technology, and Engineering (pp. 131-139). Singapore: Springer Nature Singapore. https://doi.org/10.1007/978-981-99-4665-5_14.

Neill, C.R. (1973). Guide to bridge hydraulics. Project Committee on Bridge Hydraulics, Roads and Transportation Association of Canada. University of Toronto Press, Toronto.

Odgaard, A. J., Wang, Y. (1991). Sediment management with submerged vanes. I: Theory. *Journal of Hydraulic Engineering*. Vol. 117, Issue 3, pp. 267-283. https://trid.trb.org/View/352549.

Oliveto, G. and Hager, W. H. (2002). Temporal evolution of clear-water pier and abutment scour. *Journal of Hydraulic Engineering*, Vol. 128, Issue 9, pp. 811-820. https://doi.org/10.1061/(ASCE)0733-9429(2002)128:9(811).

Paice, C. and Hey, R. (1993). The controlling and monitoring of local scour at bridge piers. Hydraulic Engineering Proceedings of the National Conference on Hydraulic Engineering, pp. 1061-1066, San Francisco, USA. 1993.

Pandey, M., Azamathulla, H. M., Chaudhuri, S., Pu, J. H., Pourshahbaz, H. (2020). Reduction of time-dependent scour around piers using collars. *Ocean Engineering*, Vol. 213, Art. No. 107692. https://doi.org/10.1016/j.oceaneng.2020.107692.

Pandey, M., Pu, J. H., Pourshahbaz, H., and Khan, M. A. (2022). Reduction of scour around circular piers using collars. *Journal of Flood Risk Management*, Vol. 15, Issue 3, Art. No. e12812. https://doi.org/10.1111/jfr3.12812.

Parker, G., Toro-Escobar, C. and Voigt, R. L. J. (1998). Countermeasures to Protect Bridge Piers from Scour. National Cooperative Highway Research Program (NCHRP 24-7). http://hdl.handle.net/11299/108221.

Raudkivi, A. J. (1986). Functional Trends of Scour at Bridge Piers. *Journal of Hydraulic Engineering*, Vol. 112, Issue 1, pp. 1-13. https://doi.org/10.1061/(ASCE)0733-9429(1986)112:1(1).

Raudkivi, A. J. (1998). Loose boundary hydraulics – 4th Edition. Rotterdam, Brookfield, VT, Balkema.

Raudkivi, A. J. and Ettema, R. (1977*a*). Effect of sediment gradation on clear-water scour and measurement of scour depth. Proc. 17th Congress IAHR, Baden-Baden 4, pp. 521-527.

Raudkivi, A. J. and Ettema, R. (1977*b*). Effect of sediment gradation on clear-water scour and measurement of scour depth. *Journal of the Hydraulics Division*, Vol. 103, Issue 10, pp. 1209-1213. https://doi.org/10.1061/JYCEAJ.0004853.

Raudkivi, A. J. and Ettema, R. (1983). Clear-water scour at cylindrical piers. *Journal of Hydraulic Engineering*, Vol. 109, Issue 3, pp. 338-350. https://doi.org/10.1061/(ASCE)0733-9429(1983)109:3(338).

Raudkivi, A. J. and Sutherland, A. J. (1981). Scour at bridge crossings, Road Research Unit Bulletin 54, National Roads Board, Wellington, New Zealand.

Richardson, E. V. and Davies, S. R. (1995). Evaluating scour at bridges. Rep. No. FHWAIP-90-017 (HEC 18), Federal Administration, U.S. Department of Transportation, Washington, D.C.

Rijn, L. C. V. (1984). Sediment Transport, Part I: Bed Load Transport. *Journal of Hydraulic Engineering*, Vol. 110, Issue 10, pp. 1431-1456. https://doi.org/10.1061/(ASCE)0733-9429(1984)110:10(1431).

Sargol, M., Mohammad, Z., Aliasghar, B., Majid, R., Giovanni, D.C. and Anton, J.S. (2020). Influence of collars on reduction in scour depth at two piers in a tandem configuration. *Acta Geophysics*, Vol. 68, pp. 229-242. https://doi.org/10.1007/s11600-019-00393-0.

Shen, H. W. and Schneider, V. R. (1969). Local scour around bridge piers. *Journal of the Hydraulics Division*, Vol. 95, No. 6, pp. 1919-1940. https://trid.trb.org/View/98453.

Shields, A. (1936). Application of similarity principles and turbulence research to bed-load movement. California Institute of Technology, Pasadena (Translate from German).

Singh, C. P., Setia, B. and Verma, D. V. S. (2001). Collar-sleeve combination as a scour protection device around a circular pier. Proceedings of Theme D, 29th Congress on Hydraulics of Rivers, Water Works and Machinery, Chinese Hydraulic Engineering Society, Beijing, China, pp. 202-209 16-21 September. 2001.

Stevens, M. A., Gasser, M. M. and Saad, M. B. A. M. (1991). Wake Vortex Scour at Bridge Piers. *Journal of Hydraulic Engineering*, Vol. 117, Issue 7, pp. 891-904. https://doi.org/10.1061/(ASCE)0733-9429(1991)117:7(891).

Tabarestani, M. K. and Zarrati, A. R. (2012). Effect of collar on time development and extent of scour hole around cylandrical bridge piers. *International Journal of Engineering*, Vol. 25, No. 1, pp. 11-17. https://doi.org/10.5829/idosi.ije.2012.25.01c.02.

Tafarojnoruz, A., Gaudio, R. and Calomino, F. (2012). Evaluation of Flow-Altering Countermeasures against Bridge Pier Scour. *Journal of Hydraulic Engineering*, Vol. 138, Issue 3. https://doi.org/10.1061/(ASCE)HY.1943-7900.0000512.

Tafarojnoruz, A., Gaudio, R., and Dey, S. (2010). Flow-altering countermeasures against scour at bridge piers: a review. *Journal of Hydraulic Research*, Vol. 48, No. 4, pp. 441–452. https://doi.org/10.1080/00221686.2010.491645.

Tanaka, S. and Yano, M. (1967). Local scour around a circular cylinder. Proceedings, 12th IAHR Congress, Colorado State University, Colorado, U.S.A., Published by IAHR, Delft, The Netherlands, Vol. 3, 11-14 September. 1967.

Thomas, Z. (1967). An interesting hydraulic effect occurring at local scour. Proceedings of the 12th IAHR Congress, Colorado State University, Colorado, U.S.A., Published by IAHR, Delft, The Netherlands, Vol. 3, 11-14 September. 1967.

Ting, F. C. K., Briaud, J. L., Chen, H. C., Gudavalli, R., Perugu, S. and Wei, G. (2001). Flume Tests for Scour in Clay at Circular Piers. *Journal of Hydraulic Engineering*, Vol. 127, Issue 11, pp. 969-978. https://doi.org/10.1061/(ASCE)0733-9429(2001)127:11(969).

Valela, C. (2021): Reduction of Bridge Pier Scour Through the Use of a Novel Collar Design. PhD Thesis, University of Ottawa, Ottawa, Ontario, Canada.

Vittal, N., Kothyari, U. C. and Haghighat, M. (1994). Clear-Water Scour around Bridge Pier Group. *Journal of Hydraulic Engineering*, Vol. 120, Issue 11, pp. 1309-1318. https://doi.org/10.1061/(ASCE)0733-9429(1994)120:11(1309).

Wang, S., Wei, K., Shen, Z. and Xiang, Q. (2019). Experimental Investigation of Local Scour Protection for Cylindrical Bridge Piers Using Anti-Scour Collars. Water, Vol. 11, No. 7, Art. No. 1515. https://doi.org/10.3390/w11071515.

Wardhana, K. and Hadipriono, F. C. (2003). *Journal of Performance of Constructed Facilities*, Vol. 17, Issue 3. https://doi.org/10.1061/(ASCE)0887-3828(2003)17:3(144).

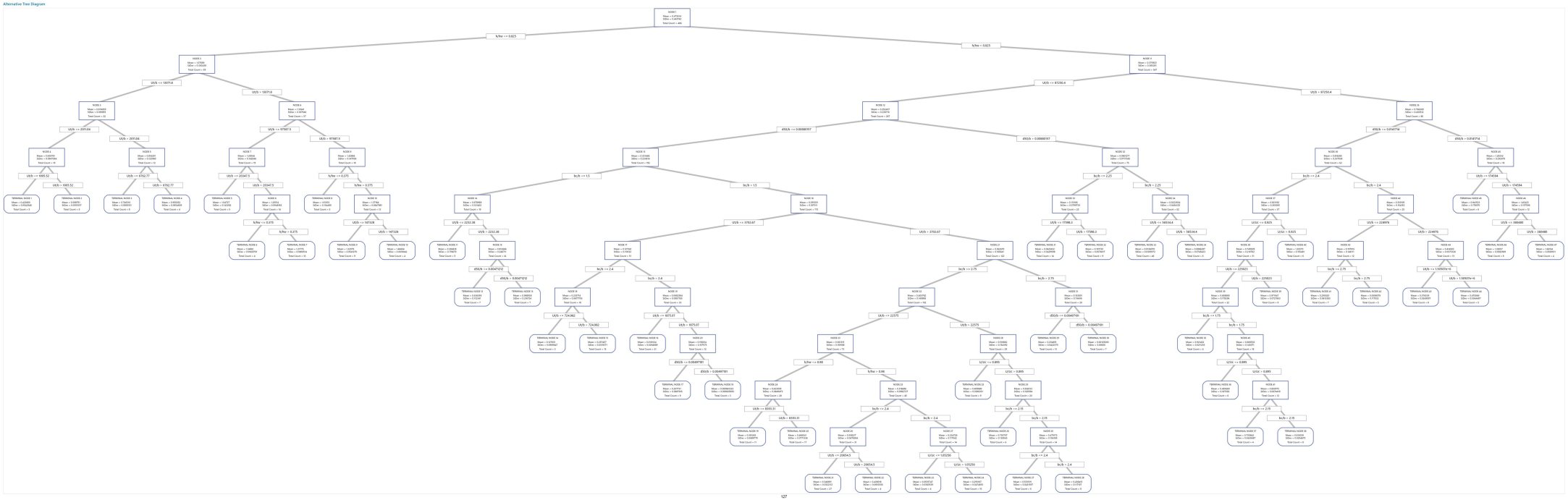
Whitehouse, R. J. S. (1998). Scour at marine structures: A manual for practical applications. Thomas Telford Publications, London, United Kingdom. http://dx.doi.org/10.1680/sams.26551.

Zarrati, A. R., Chamani, M. R., Shafaie, A. and Latifi M. (2010). Scour countermeasures for cylindrical piers using riprap and combination of collar and riprap. *International Journal of Sediment Research*, Vol. 25, Issue 3, pp. 313-322. https://doi.org/10.1016/S1001-6279(10)60048-0.

Zarrati, A. R., Gholami, H. and Mashahir, M. B. (2004). Application of Collar to Control Scouring around Rectangular Bridge Piers. *Journal of Hydraulic Research*, Vol. 42, Issue 1, pp. 97-103. https://doi.org/10.1080/00221686.2004.9641188.

Zarrati, A. R., Nazariha, M. and Mashahir, M. B. (2006). Reduction of Local Scour in the Vicinity of Bridge Pier Groups Using Collars and Riprap. *Journal of Hydraulic Engineering*, Vol. 132, Issue 2. https://doi.org/10.1061/(ASCE)0733-9429(2006)132:2(154).

Alternative Tree Diagram



Alternative Tree Diagram

Appendix II
Alternative decision tree for a circular pier with airfoil collars

